A Major-II Project Report

On

Modal analysis of LP-1 IN738 Gas Turbine Blade

Submitted
In partial fulfilment for the award of the degree

Of

Masters of Technology

In

Mechanical Engineering

With specialisation in

Computational Design

By

AMARDEEP
(2K13/CDN/03)

Under the guidance of

Mrs. Shushila Rani
(Assistant Professor)

Department of Mechanical Engineering

Delhi Technological University, Delhi

2014-15

CERTIFICATE

This is to certify that the Major-II Project Report entitled “Modal analysis of LP-1 IN738 Gas Turbine Blade” is a bonafide work carried out by Mr. Amar Deep (2K13/CDN/03) of M.Tech (Computational Design) and submitted to Department of Mechanical Engineering, Delhi Technological University, Bawana Road, Delhi in partial fulfilment of the requirement for the award of the Degree of the Masters of Technology under specialization in Computational Design under our supervision. It is further certified that the embodied work has not been submitted to any other institution for the award of other degree or certificate.

Mrs. Sushila Rani
Assistant Professor
Department of Mechanical Engg.
Delhi Technological University

DECLARATION

I, Amar Deep, hereby declare that this submission is my own work and that, to the best of my knowledge and belief, it contains no material previously published or written by another neither person nor material which to a substantial extent has been accepted for the award of any other degree or diploma of the university or other institute of higher learning except where do acknowledgement and references has made in the text.

Signature:
Amar Deep
(2K13/CDN/03)

ACKNOWLEDGEMENT

First and foremost, I would like to thank the Almighty God for giving me the strength and wisdom to carry out this work.

I would also like to express my sincere gratitude to our branch coordinator **Prof. Vikas Rastogi** and my supervisor, **Mrs. Sushila Rani,** Assistant Professor, Delhi Technological University, New Delhi, for his continuous support, creativity, his excellent skill, patience, motivation, enthusiasm, and immense knowledge which have always been a constant source of motivation for me. His excellent guidance, perseverance, invaluable suggestions made this work possible and complete.

My profound gratitude to **Prof R. S. Mishra,** Head of Mechanical Department, Delhi Technological University, New Delhi, for providing effective management, necessary facilities and valuable suggestions for success of this work.

I humbly pay my sincere thanks to the entire fraternity of Mechanical Department, Delhi Technological University, New Delhi, for their kind cooperation throughout the project work.

I owe my success to my loving parents for their abundant blessings and unconditional support and my siblings for being my source of strength throughout my life.

Last but not the least, I would like to express my heartfelt gratitude to all my friends and well-wishers without whose support and best wishes it could not have been possible to complete a task of this magnitude.

Amar Deep

ABSTRACT

As gas turbines become the integral part of the current power plant, automobile, medical, aerospace, defense, space craft, ships, submarines, missiles etc. hence the need of their care arises, as they drive these costlier systems very effectively. Here in this work we discussed the various causes of failure of gas turbine blade due to various reasons and found that most of the gas turbine failure associated with turbine blade which further associated with fatigue failure of the turbine blade. As these fatigue failure generally causes by vibration of the system components and specifically turbine blade, hence here we are concerned about determining the modal parameters for gas turbine blade and also the damping factor of blade by experimental modal analysis and computational modal analysis. But first we validated our experimental modal analysis results with computational modal analysis results with the help of a cantilever beam and determining the variation, on the basis of that we doing the same analysis on gas turbine blade and will be able to evaluating the modal parameters of gas turbine blade. Modal parameters of turbine blade are required because the vibration of the blade can be reduced by adding damper to the blade with appropriate damping so that the system remains in underdamping situation and life of the blade can be improved. If time permits we will apply damper coating to the blade then evaluating its modal parameters, else we will add this for future work.

In order to evaluate all modal parameters of gas turbine blade and damping factor we have to use NV Gate 8.30 with OROS 36 vibration analyser for experimental modal analysis and ANSYS 15.0 version for computational modal analysis.

LIST OF CONTENTS

LIST OF FIGURES

CHAPTER-1

INTRODUCTION

1.1. About Gas Turbine:

The gas turbine has become an important, well-known, and reliable device in the area of transportation, power generation and other applications. A gas turbine is an internal combustion engine; it can burn a variety of fuels to drive the engine as well as to generate power in industrial applications.

Gas turbine works on Brayton Cycle consist of the following four processes:

a) Adiabatic, quasi-static compression at the inlet of compressor.
b) Constant pressure fuel ignition (or constant pressure heat addition).
c) Adiabatic, quasi-static expansion in the turbine and exhaust nozzle.
d) Constant pressure heat rejection.

*In actual, processes a) & c) are not completely isentropic.

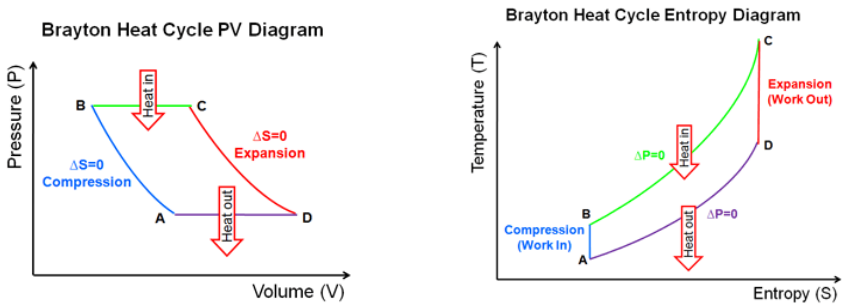

Fig.1.1. Brayton Cycle P-V and T-s diagram for ideal condition.

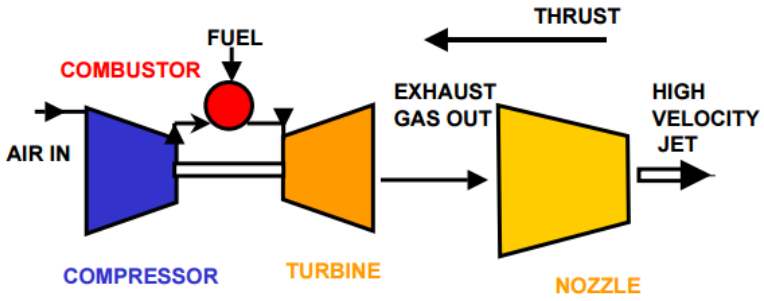

Fig.1.2. Gas Turbine as Aircraft Engine

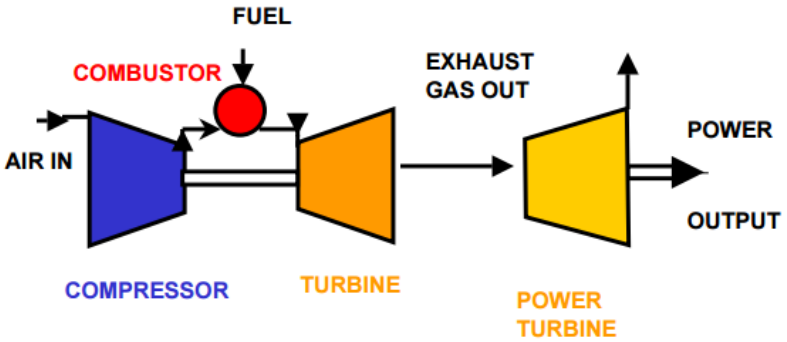

Fig.1.3. Gas Turbine as prime mover in power generation units

Types of Gas Turbine:

I. Open cycle gas turbine

Same fluid is not circulated throughout the cycle, means exhaust air is released into the environment.

II. Closed cycle gas turbine

Same fluid is circulated throughout the cycle i.e. steam gas turbine.

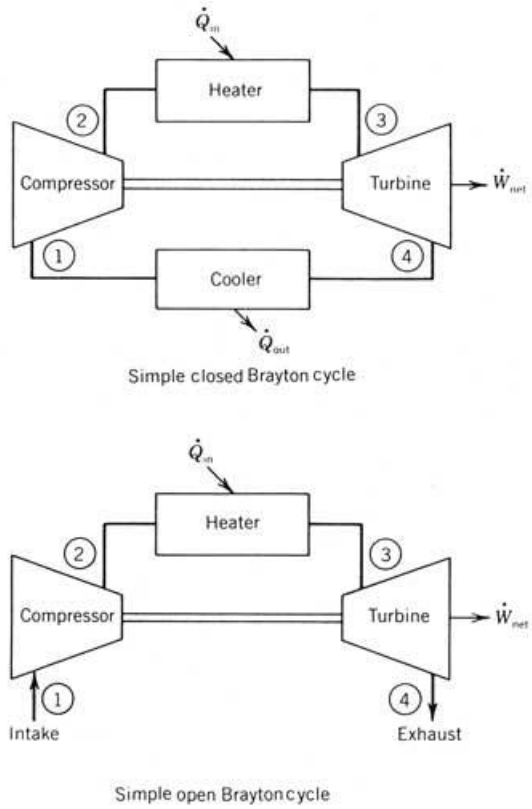

Fig.1.4. Closed and Open gas turbine cycles.

Advantages of closed cycle gas turbine over open cycle gas turbine:

- Higher thermal efficiency
- Reduced size
- No contamination
- Improved heat transmission
- Lesser fluid friction
- No loss of working medium
- Greater output and
- Inexpensive fuel.

Disadvantages of closed cycle:

- Complexity
- Large amount of cooling water is required.
- Dependent system
- More power to weight ratio.
- Requires the use of a very large air heater.

Parts of a Gas turbine:

- *Inlet duct:* The purpose of the air inlet duct is to provide clean and unrestricted airflow to the engine. Uncontaminated and undisturbed inlet airflow extends engine life by inhibiting erosion, corrosion, and foreign object damage (FOD).
- *Compressor:* Generally axial flow compressors are used. The main function of the compressor is to provide compressed air at high static pressure to the turbine. It contains 14 stages of fixed and moving blades in diverging manner. Apart from that it also contains guide vane blades at inlet and outlet of compressor; so that air is compressed at each stage and mechanical energy is converted into pressure energy. The air temperature is also increased about 550^{o} C.
- *Diffuser:* After exiting from the compressor through the guide vanes, the air enters the diffuser section of the engine. Diffuser is a very divergent duct and its primary function structure is aerodynamic. Most of the air's velocity is transformed into static pressure by the divergent duct's shape . Apart from that it provides structural support to the complete engine and rear compressor bearings.
- *Combustor:* Compressed air from diffuser enters into the combustion chamber where heat is added to the air with minimum pressure loss and maximum heat release to the air. Hence flames are given to air through converging liners which add heat to the compressed air and push into the turbine.
- *Turbine:* The energy produced by burning air- fuel mixture is transformed into mechanical energy by the turbine. The energy thus converted is used to drive the compressor. The conversion of energy occurs by, expanding the high temperature high-pressure gases to a lower temperature and pressure. This phenomenon is the reverse of the order as in the compressor. In the compressor, rotor blades add energy to the gas and stator vanes converts it into static pressure. On the other hand in case of turbine, the stator vanes increase gas velocity, and then the rotor blades extract energy.
- *Exhaust:* The gases from the turbine are discharged to the atmosphere through the exhaust. The turbine converts most of the gaseous energy into mechanical energy. But even after that a considerable amount of power remains in the exhaust gas. To increase the usefulness of this energy so that it can be used as a jet thrust the gas is accelerated by the convergent duct shape of the exhaust, which drives the airplane forward.

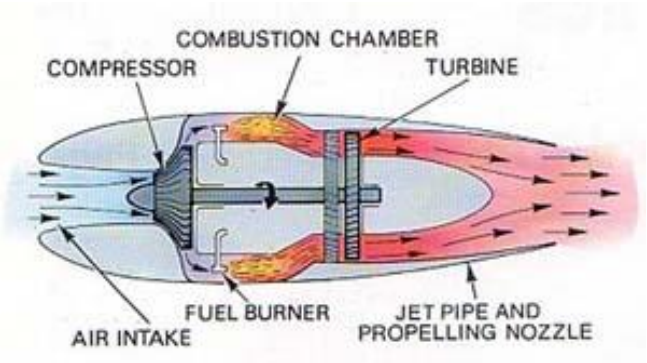

Fig.1.5. Components of Gas Turbine blade

Gas turbine applications:

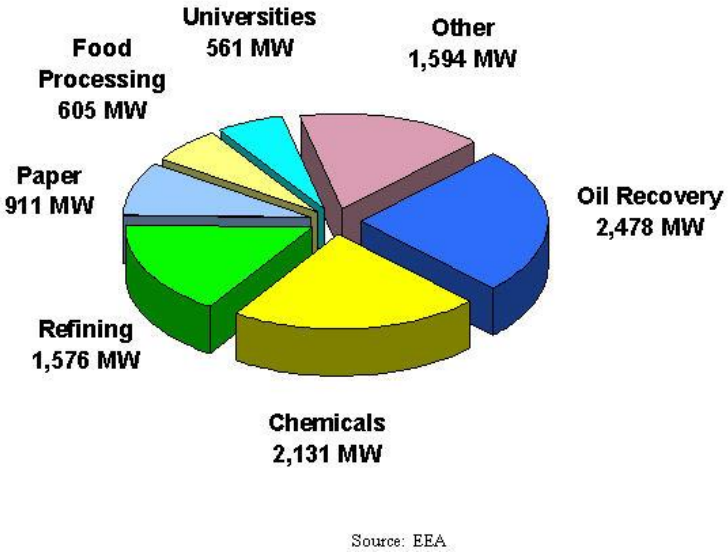

Fig.1.6.Applications of Gas turbine engine

Some major zones where gas turbine plays very important role:

- Marine Ships
- Aircraft or Jet Engines
- Space ships
- Vehicles
- Missiles
- Mining
- Power plants
- Micro-turbines

Benefits of Gas Turbine:

- Very high power-to-weight ratio, related to reciprocating engines.
- Smaller compared to most reciprocating engines of the same power rating.
- Moving parts are lesser than the reciprocating engines.
- Operative pressure is low.
- Operating speed is high.

- Low consumption and low cost of lubricating oil
- High reliability.

Drawbacks of Gas Turbine:

- Much costlier than a similar-sized reciprocating engine because of a stronger and more heat resistant material.
- Complexity in machining operations.
- Usually less efficient than reciprocating engines.
- Delayed response to changes in power settings, that's why gas turbine is less suitable for road transport and helicopters.

Gas Turbine OEMs:

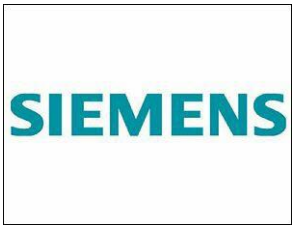

1.2. Failure in turbine blades: (causes and reasons)

Causes for gas turbine failure:

- Low cycle fatigue failure (compressor and turbine disks).
- High cycle fatigue failure (compressor and turbine blades, disks, compressor stator vanes).
- Thermal fatigue failure (nozzles, combustor components).
- Thermal aging: material degradation over time due to temperature.
- Damage due to creep (hot section nozzles and blades).
- Failure due to erosion and wear.
- Damage due to impact overload (due to foreign object damage (FOD), domestic object damage (DOD) or clash/clang of compressor blades due to surge).
- Combined failure mechanisms (creep/fatigue, corrosion/fatigue, oxidation/erosion, etc.)
- Environmental effect: oxidation, sulphidation, hot corrosion, standby corrosion (hot section blades and stators, transition pieces, and combustors).

Blade problems are of much concern to designers and users, in both the industrial and aircraft gas turbine industries,. There are various causes of blade failure which are vibration, fatigue, foreign object damage, corrosion, erosion, sulphidation, and creep. Although we have various sophisticated design tools available today, in spite of that, blade failure occurs in both compressors and turbines, the reasons for which are:

- Combined failure modes and unavoidable excitations of both aerodynamic and mechanical origin
- Deviation of analytical predictions from the actual operating condition due to much complex vibration characteristics of blades. They differ because of the intricate blade geometry. This also makes advanced finite element modelling difficult. The problem becomes more complicated because of the interaction between the vibration of blades, disks, shrouds, snubbers, and the presence of "assembly modes".
- Non-uniformity in blades and quality control problems.
- Operational environment of turbine air foils which include creep, oxidation, hot corrosion, and thermal fatigue leading to compound failure modes.
- The rapid rate of progression of high frequency fatigue failures.

Failure associated with different components of gas turbine:

Table 1.1. Failure associated with compressor in gas turbine

Component	Failure Mode	Cause
Rotor & stator blades	High Cycle Fatigue, Erosion, FOD, Corrosion clash, Fretting	Vibration, Flutter, Air flow distortion, Surge, Stall dust in air
Disc	Fatigue- Creep, Wear, Rubbing	Centrifugal loads temperature effect.
Compressor tie bolts	Mechanical fatigue, wear, fretting, and rubbing	Start-up, cycling, vibration

Table 1.2. Failure associated with combustor in gas turbine

Component	Failure Mode	Cause
Liner	Mechanical fatigue, fretting buckling, wears, thermal fatigue, yield slip, thermal distortion and corrosion.	Hot spots, temperature gradients, vibrations, excessive dynamic pressure, pulsations
Casing	Fatigue	Pressure Cycles
Cross fire tubes	Wear, rubbing fretting, corrosion thermal fatigue.	Pulsations and vibrations.
Transition piece	Thermal fatigue, wear, rubbing, fretting	Dynamic pulsations and vibrations.

Table 1.3. Failure associated with turbine section in gas turbine

Component	Failure Mode	Cause
Turbine rotor blades	High cycle fatigue, creep, corrosion, erosion, sulphidation.	Centrifugal and temperature stresses, vibratory stresses, environment, fuel problems, excessive temperature spreads, cooling problems
Turbine stator blades	Creeps rupture erosion, sulphidation, bowing fatigue, thermal fatigue.	Cooling problems, improper temperature profile
Turbine rotor disc	Creep-rupture, low cycle fatigue	Thermal stresses, improper wheel space cooling

FATIGUE

A significant number of turbine and compressor blade failures are caused by fatigue itself. The reason for this type of failure is the repeated application of fluctuating stresses. The levels of stress are much lower than the tensile stress of the material. The vibration in compressor blades is commonly caused by stator passing frequency wakes, rotating stall, surge, choke, distortions in the inlet, and blade flutter. In the turbine section, air foils are subjected to the environmental conditions which include severe vibration, high temperature, corrosion, creep, and thermomechanical fatigue.

HIGH CYCLE FATIGUE

When a periodic force acts at a frequency corresponding to a blade natural frequency, there occurs a phenomenon known as resonant fatigue which is an important failure mode. If there is not enough damping provided for absorption of the periodic input energy, then stress amplitudes grows until failure. The reason for this is overstress or propagation of a fatigue crack.

High cycle fatigue (HCF) is typically caused by aerodynamic excitations (i.e., nozzle and vane passing frequencies, strut pass frequency) or by self-excited vibration and flutter. The maximum stress at resonance can increase dramatically where the fluctuating stresses are not very high. When the stress levels goes beyond the fatigue strength, there will be a high cycle fatigue failure. The stress versus number of cycles (S-N) curve loses its validity in the corrosive environment, which greatly affects the fatigue strength.

At resonance the vibration growth is governed by:

- Resonant response factor: a measure of the ability of the blade (or blade packet) to accept energy from the stimulus.
- Magnitude of the force of excitation: operating condition like airflow or temperature distortion can be a function of the force impact.
- Damping occurring in the blade material: coulomb damping in the fir tree and shroud and hysteresis damping in the blade

EFFECT OF DAMPING

An increase occurs by a factor of four in the vibratory stresses because of the loss of damping causes by the breakage of a lacing wire. This situation arises due to elongation in the lashing wire holes in blade with wear.

Modern engines which utilize integrally bladed disks do not have the friction damping associated with the dovetails and, therefore, dynamic magnification factors can often be two to five times those found in older engines. As these blades do not have platforms, the use of under-platform dampers is not possible. Consequently, blade designs have evolved that utilize insert dampers that are placed within the airfoil. These fit inside the blade cavities and produce frictional damping.

LOW CYCLE FATIGUE

Low cycle fatigue (LCF) occurs as a result of turbine start/stop cycles and is predominant in the bores and bolt whole areas of compressor and turbine disks that operate under centrifugal stresses. It is typically a problem associated with machines that have been in operation for several years. In this situation, minute flaws grow into cracks that, upon attaining critical size, rupture. Cracks also develop in the nozzle sections to some extent, this is to be expected under normal operation and cycling service.

THERMOCHEMICAL FATIGUE

Thermo mechanical fatigue (TMF) is associated with thermal stresses, e.g., differential expansion of hot section components during start-up and shutdown, and is particularly severe during rapid starts and full load emergency trips. Crack initiation may occur if the level of induced stresses exceeds the material yield stress. Generally in hot section blading temperature variations as high as 360°F (200°C) per minute are experienced. This is the reason why full load trips are so harmful in terms of life reduction, consuming as much as 200 equivalent hours per trip.

ENVIRONMENTAL PROBLEMS

The factor of environment must be considered while evaluating blade failure. The catastrophic failure do not occurs due to environmental problems generally, instead these problems works with the other failure modes simultaneously. Apart from fouling the blade integrity is affected by other mechanisms also. Particularly oxidation, corrosion, and sulphidation attacks hot section components. Corrosion and pitting frequently affects the compressor blades and their impact will be more if there is presence of salt or other contaminants in the ambient air. Therefore environment has a great influence on the failures in the turbine blades.

HIGH TEMPERATURE OXIDATION

This phenomenon occurs when nickel based super-alloys are exposed to temperatures greater than 1000°F (538°C). A nickel-oxide layer is formed on the air foil surface when oxygen which is present in the gas stream reacts with the nickel alloy. There will be cracking and spalling of nickel oxide layer during operation because of the vibration and start stop thermal cycles. This phenomenon may also occur on the inner surfaces of blade cooling passages and result in blade failure. To diminish this effect coatings are available which can be applied to both the blade surface and internal cooling holes.

SULPHIDATION

When sulphur (from the fuel) reacts with the protective oxide layer and attacks the base metal, then there occurs a process known as sulphidation. The air taken by the gas turbine can contain impurities such as sulphur di-oxide, sulphur tri-oxide, sodium chloride (salt), and chlorine. These impurities when passes over the air foil, droplets (slag) of liquid sodium sulphate are formed. The protective oxide layer is broken down under this slag thereby permitting attack of the parent super alloy which causes very serious damage. Sodium sulfate is highly corrosive in nature which results in deep stress riser pits in the airfoil. It is of major concern when it is found in the blade root region, or along the leading or trailing edges, or under the blade shroud.

HOT CORROSION

A combined oxidation-sulphidation phenomenon which usually occurs in the hot section parts is referred to as hot corrosion. There are two types of hot corrosion have been identified so far:

- Type 1 hot corrosion (high temperature): This occurs at temperatures between 1517°F to 1742°F (825°C to 950°C) approximately. Usually a base metal denuded zone is found along with intergranular attack and sulphide spikes.
- Type 2 hot corrosion (low temperature): This occurs at between 1292°F to 1472°F (700°C to 800°C). No intergranular attack or denuded zone of the base metal is found.

Coatings are commonly used to reduce hot corrosion problems. The figure shows the turbine blades from an aero-derivative gas turbine that experienced hot corrosion.

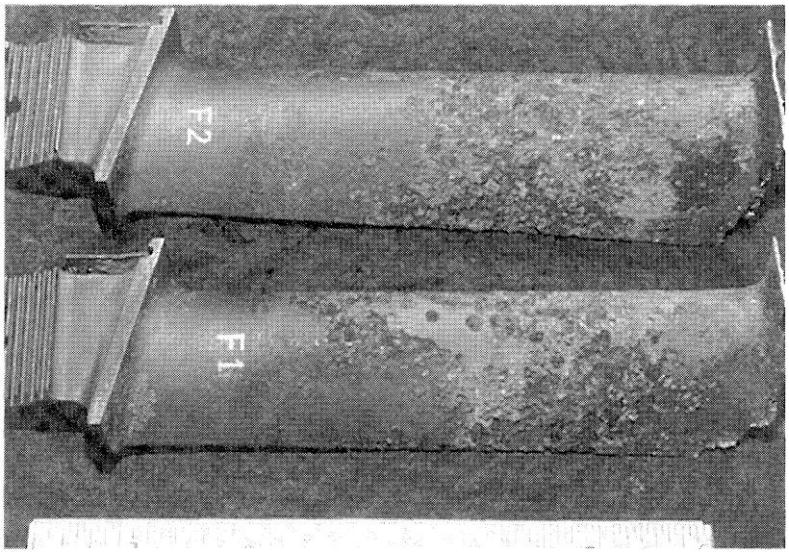

Fig.1.7. Turbine blades with Hot Corrosion

STANDBY CORROSION

Peaking gas turbines are most commonly affected by this problem only. It occurs during a turbine shutdown. The main reason behind this problem is the moisture in the air and corrosives present in the machine. The blade attachment areas are accumulated by the corrosion products which act as abrasives and increase clearances thereby results in crevice corrosion. There will be frequent development of corrosion pits in the uncoated air foils due to the presence of corrosives (possibly from airborne salt), which may then develop into cracks. Corrosion reduces the blade fatigue strength considerably. The main effect of the blade failures caused by crevice corrosion is stress corrosion fatigue or stress corrosion.

CREEP

When components operate under high stresses and temperature over a span of time, then there occurs a phenomenon known as creep. A typical creep deformation curve is shown in the figure below. Roughly speaking, an increase of l5°C in blade metal temperature reduces creep life by 50 percent. This tells us about the importance of effective cooling. Creep affects hot section parts and the final stages of high pressure ratio compressors. The mid span region of the airfoil, which experiences the highest temperature, is more prone to this phenomenon. It will lead to progressive reduction of rotor tip clearances that's why it is of greater interest. It can also occur in the disk rim region where high stresses and temperatures can cause time dependent plastic deformation. Creep behaviour is commonly modelled by use of the Larson-Miller Parameter. Exposure to creep can be detected by metallurgical tests, common

indicators being the coarsening of the gamma prime precipitates and the formation of void cavities at grain boundaries.

Often creep failures can be associated with a loss of cooling. This loss can be due to a quality control problem (such as blocked cooling passages) or due to a blockage or malfunction of the cooling airflow.

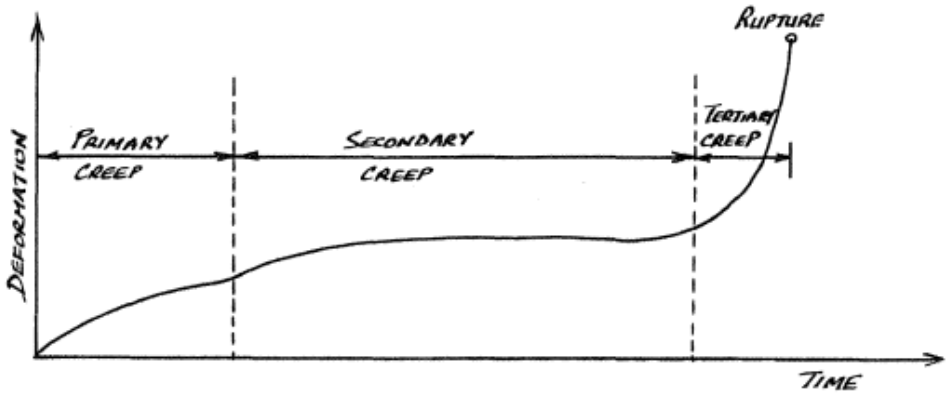

Fig.1.8. Creep Curve

EROSION/WEAR

These mechanisms rarely cause catastrophic blade failures, but contribute to other failure modes and can be of considerable economic significance, as blade replacement may be necessary. Erosion and wear can occur in both compressor and turbine components. Particles causing erosion in axial flow compressor blades are five to 10 microns or greater in size. In addition to the primary damage caused by erosion, a reduction in the surge margin can occur if the tips get severely eroded. Fretting wear occurs in the blade attachment areas (dovetails) and is often associated with standby corrosion. A considerable amount of dovetail wear (causing bucket rock) occurs during turning gear operation when the blades are not centrifugally loaded. Corrosion in the dovetail region will, of course, accelerate the process, with the corrosives acting as an abrasive.

HOT GAS CORROSION

Apart from particulate erosion, there also exists the important phenomenon of hot gas erosion. Modem air cooled gas turbine components operate at metal temperatures, hundreds of degrees lower than the gas path temperatures. The metal surface is protected by means of the natural boundary layer or by a cooling air film. If this cooling layer of air breaks down even for short periods of time, or cooling effectiveness drops, then the surface asperities (roughness) of the blade contacted by the hot gas are subjected to high thermal stress cycles. Damage takes place after several cycles and the problem become worse due to increased

roughness (erosion). The most severely affected parts are those in the hottest gas path (e.g., central to the transition piece exit). This problem can occur in the first stage nozzle segments at the platforms and may reflect inappropriate cooling.

EMBRITTLEMENT

A form of microstructure degradation which results in a loss of impact strength is known as embrittlement. It increases the material's susceptibility to foreign object damage (FOD), because of which it becomes particularly serious problem relating to blade alloys. Due to this phenomenon brittle intermetallic compounds precipitate in plate morphology and continuous carbide films form along grain boundaries.

COMBINATION MECHANISMS

Multiple failure mechanisms causes a commonly occurring problem i.e. blade failures. For example, corrosion which can reduce blade section size and drop the fatigue strength. Increased vibration amplitudes and alternating stresses is a consequence of the reduced damping, which is caused by fretting wear, occurring in the blade attachment regions. Nicks and cracks caused by the foreign object damage can then be propagated by low or high cycle fatigue. Therefore failure analysis must investigate all engineering causes including design issues, environmental factors, cleanliness of the fuel, air quality, material, and gas turbine operating and maintenance history. The problems stated above are quite common and often create significant disputes between the OEMs and the user as to how the damage is to be resolved commercially. A turbine rotor from an aero-derivative gas turbine that experienced a fatigue failure combined with hot corrosion is shown in Fig.1.9. In this case, severe tip rubs accentuated the problem.

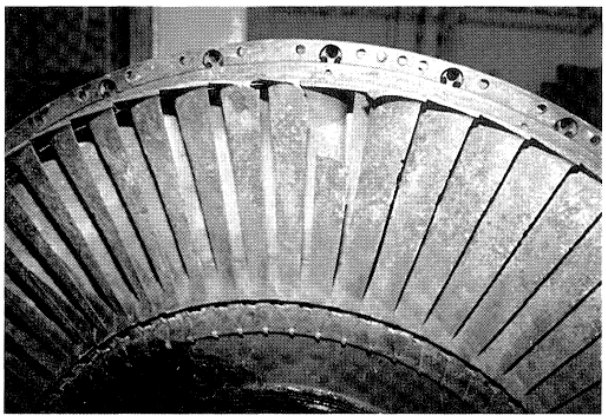

Fig.1.9. Combined Failure Mode Showing Both Tip Rub, Hot Corrosion, and a Fatigue Failure

1.3.Motivation and Background

Now a day's gas turbine almost becomes the integral part in each and every field of engineering application which require continuous power throughout the life of the system. Hence continuous monitoring of gas turbine is mandatory in order to avoid failure and prevent shut-down of the system. As gas turbine has various applications in the field of continuous power generation, driving aircrafts and jet engines, submarines, ships, medical science, robotics, missiles, tankers, gas turbine based vehicles etc. which make it superior over the other engines.

So it's troubleshooting is the prime concern in order to enhance its efficiency and life of the turbine so that continuous supply we get for long duration from it. As most of the issues in gas turbine generated from blade failure, rotor disc failure and vibrations of the system. Cost analysis shown in Table 1.4.

Table 1.4. Causes of Losses in Gas Turbines and Percentages of Damage Cost

Cause of Loss	Damage Cost % of total heavy duty gas turbines	Damage Cost % of total aero-derivative gas turbines
Turbine blade cooling air loss	14	-
High Cycle Fatigue of turbine blades	12	2
Creep in rotating parts	19	-
Compressor surge	5	24
High Cycle Fatigue of compressor blades	12	7.5
Turbine disc failure	-	7.5
Thermal cracking	-	11
Internal Overheating	-	12.5
Internal fire or explosion	5	-

From this analysis it is confirm that if the blade life increased in the turbine or compressor then it will contribute towards enhanced efficiency of the system. Now problem arises is that how we will be able to enhance the life of turbine blade, then we focused on causes of failure. Hence if cause of failures being removed from the system then it might be possible that blade life increases. Here we concentrate on one of major failure due to vibration of the blade,

which can be removed by providing appropriate damping to the turbine blade. Before which modal analysis of gas turbine blade is done using experimental analysis and computational modal analysis in which the results are verified for cantilever beam which confirm that the results obtained from computational analysis are validated.

In this way we will be able to determine natural frequency for gas turbine blade with damper and without damper. As damper reduces the amplitude of vibration hence it will be either employed between two blades or can be applied to individual blade in the form of coating.

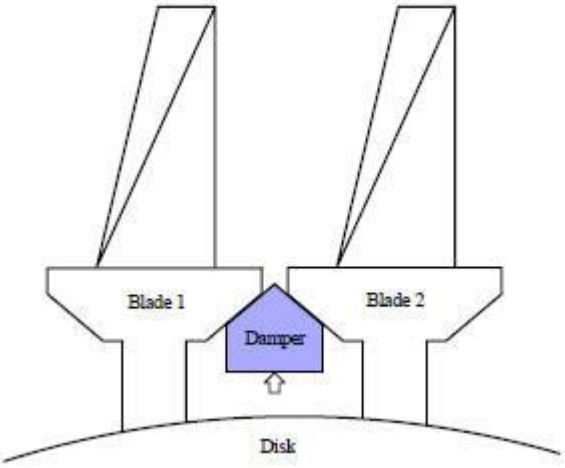

Fig.1.10. Damper applied between two consecutive turbine blades.

Hence by applying damper to the turbine blade we reduce the blade vibration and also reduce their chances of failure of gas turbine. In this work modal analysis of gas cantilever beam is done to validate the experimental and analytical results and modal analysis of gas turbine blade is done using analytical approach to determine the natural frequencies for gas turbine blade in order to apply damper coating which is recognized as future work.

Coating damper material supposed to be best as it can also provide protective shield to the blade to avoid corrosive environment, high temperature corrosion, oxidation etc. which really leads to a great research work. This inspirational project gives the zeal to researcher to perform well under worst conditions.

This project motivates me towards design and development approach to rectify fault in any system and make more reliable, susceptible and economical for use. It also optimizes the cost of production, running and maintenance of the gas turbine, so the overhauling is required at optimum interval of time and minimum shut down takes place during the running condition of gas turbine. The various applications of gas turbine also attract the researchers to modify their design in order to fetch them in maximum applications with minimum fuel requirement.

1.4. Methodology

In this work we examined the cause of failure of gas turbine blade by SEM techniques and analysed the failure modes of turbine blade using modal analysis. But here we mainly focused over the modal analysis of gas turbine blade using experimental modal analysis (EMA) and computational modal analysis (CMA) and then correlating their results in order to identify the percentage variation of the EMA with CMA. Before working on the blade directly we first did with a cantilever beam of mild steel, then verifying the results of EMA and CMA for validation and then switching over turbine blade.

In this way we will be able to rely on computational method for modal analysis of gas turbine blade and can say that this result is true upto maximum extent as per the applied boundary conditions.

1.4.1. Scanning Electron Microscopy (SEM):

This technique is used by various researchers to identify the failure cause and mode of failure from the failed specimen. Here specimen of fractured portions was taken and then fractographic analysis of the fractured region has been done. This shows the region of high cycle fatigue, corrosive fatigue, crack propagation and generation, thermal corrosive fatigue failure etc.

Fig.1.11. SEM of a failed gas turbine blade

Crystallographic view of the fracture portion depicts that from where the crack generates and how long it propagates due to slip or any other reasons. From the pattern of fracture it also depicts the material behaviour and environmental condition effect on the blade, this suggest that this is very good technique to identify the cause of failure in our own component.

1.4.2. Modal Analysis

Modal analysis is a process in which we describe structures in terms of its natural characteristics like frequency, damping and mode shape. These are called dynamic properties of the structure. In order to design structure for noise and vibration applications, understanding of both natural frequency and mode shapes are necessary. Modal analysis is helpful in designing of all types of structures including automotive structure, spacecraft, aircraft structures, turbine blades, computers, tennis rackets etc. In case of both compressor and turbine blades are subjected to vibrations due uneven loading and system imbalance.

Fig.1.12. Experimental Modal Testing of gas turbine blade.

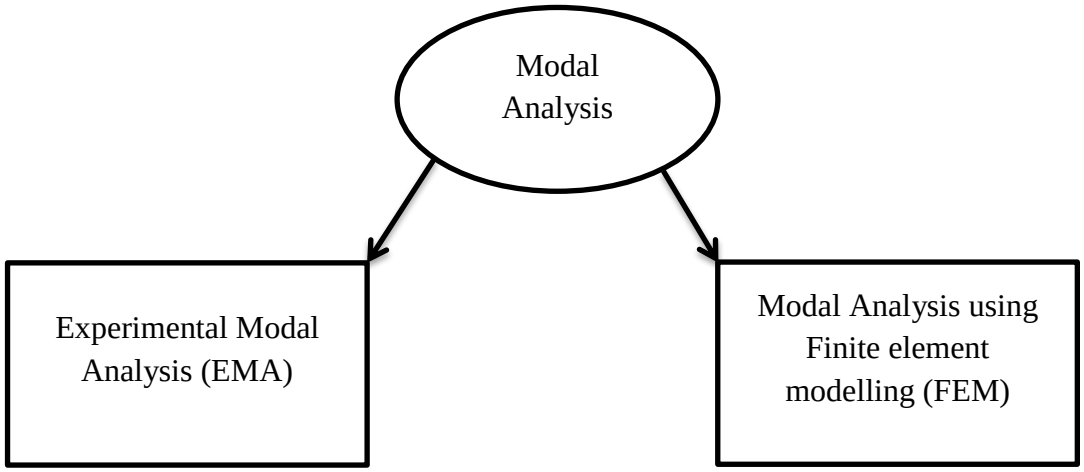

Fig. 1.13. Modal Analysis Methods

1.5. Objectives

Based upon the availability of equipment, software, and essential resources we have identified the problem of gas turbine blade which can be analysed experimentally and analytically both. Hence for analysis of our LP stage -1 gas turbine blade we set our following objectives which will help to identify the required result:

A. Study of Fractographic analysis and SEM of failed gas turbine blade.
B. Design of fixture for fitree part of LP-1 IN738 gas turbine blade
C. Experimental modal analysis (EMA) of cantilever beam using vibration analyser (OROS).
D. Computational modal analysis (CMA) of cantilever beam using FEM (ANSYS 15.0).
E. Validate results of EMA with CMA for cantilever beam.
F. Experimental modal analysis (EMA) of LP-1 IN738 gas turbine blade using vibration analyser (OROS).
G. Computational modal analysis and Structural analysis of LP-1 IN738 gas turbine blade using FEM (ANSYS 15.0).
H. Validate results of EMA with CMA for LP-1 IN738 gas turbine blade.

CHAPTER-2

LITERATURE SURVEY

In this chapter lots of literature survey has been done in the area of gas turbine blade failure, modal analysis of structures, vibration analysis, cause of blade failure, coating of blade, damped modal analysis etc. from these studies we will be able to identify the type of failure in our gas turbine blade and able to determine the cause of failure and based upon that modify the existing model for long life. This literature survey also helps to find the appropriate methodology like SEM (Scanning Electron Microscopy), Experimental modal analysis, Analytical modal analysis, Chemical analysis etc. to analyse the failure happens in the turbine blade and how to overcome these remedies in order to enhance the life of gas turbine blade.

2.1. Fractographic Analysis, Visual Examination and Metallographic Investigation of turbine blade:

Hassan Farhangi et al [1] investigated the 2nd stage turbine blade in a 32MW thermal power plant. The premature failure of the blades, made of nickel based superalloy Udimet 500, occurred after a service life of 50000 hours. They investigated the fractured blade by visual examination, SEM fractography, chemical analysis, hardness measurement, and microstructural characterization techniques and found that the fracture of the turbine blade happens at firtree root due to slow stable crack growth by crystallographic faceted cracking which leads to HCF (high cycle fatigue) fracture mechanism.

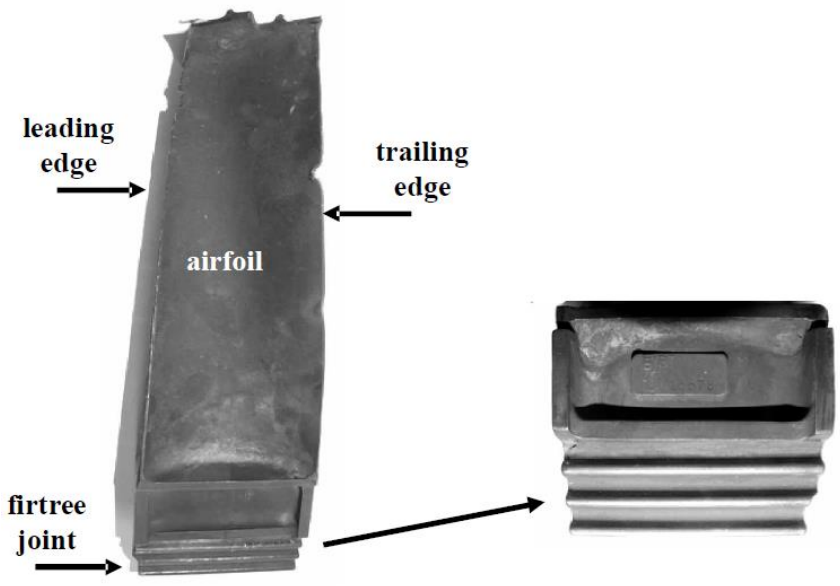

Fig.2.1. Blade geometry and the firtree joint of a damaged turbine blade

Metallographic observations were carried on transverse and longitudinal sections prepared from the firtree root region of the turbine blade in which Distribution of fine gamma prime particles and interdendritic carbides in the matrix can be seen in a higher magnification SEM micrograph in Fig. 2.2.(b).

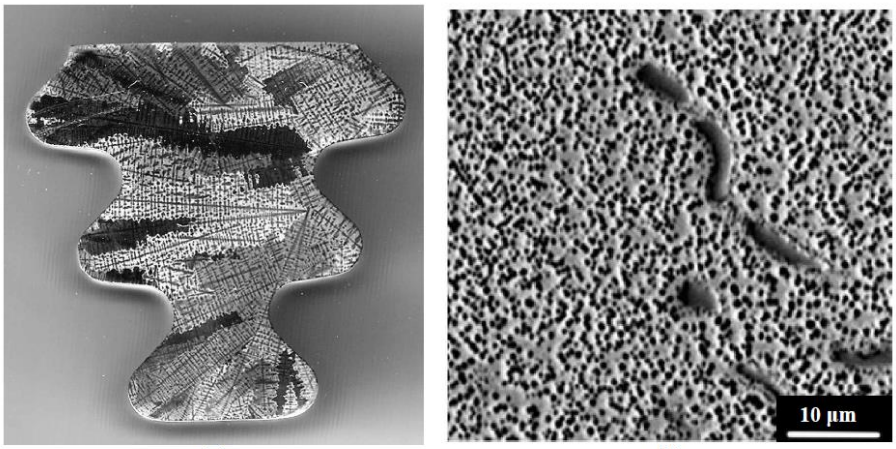

Fig. 2.2.(a) Macroetched section of the firtree root, (b) SEM micrograph representing gamma prime particles and interdendiritic carbides.

By the fractographic analysis of the fractured region in is found that the change in fracture mode from transdendritic to interdendiritic is considered as one of the typical cause of fracture of cast materials by a fatigue mechanism. Formation of wear products on the touching base surfaces of firtree root, occurrence of wear tracks, crack initiation in area of wear tracks and the slant alignment of crack in the nucleation region are indicative of fretting fatigue mechanism to the failure process of the blade.

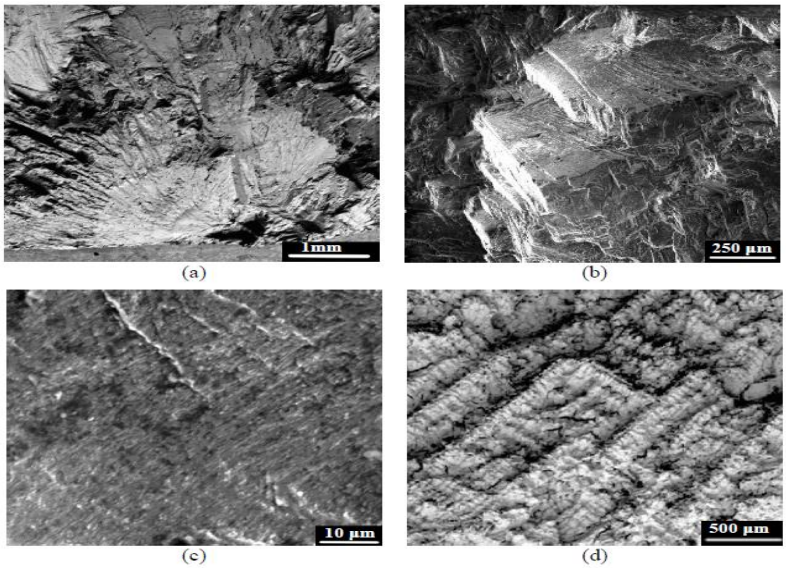

Fig.2.3. SEM fractography displaying (a) semi-elliptical crack in the initiation region (b) crystallographic fatigue crack propagation, (c) characteristic fatigue striations and (d) interdendritic fracture phenomenon in the final fracture region.

Loveleen Kumar Bhagi et al [2] discussed fracture investigations of low pressure (LP) steam turbine blade of a 110 MW thermal power plant in Punjab. They analysed one of the fractured blade made of chrome alloy steel X20Cr13 (Tempered martensitic stainless steel). One of the fractured blade of L-1 row of LP stage was collected from the unit to identify the cause of failure. The fracture took place at the aerofoil region, 203 mm from the root as shown in Fig. 2.4. Material composition analysis (EDS Analysis), energy dispersive X-ray (EDX) analysis, scanning electron microscopy (SEM), hardness measurement and microstructure analysis were performed for this study.

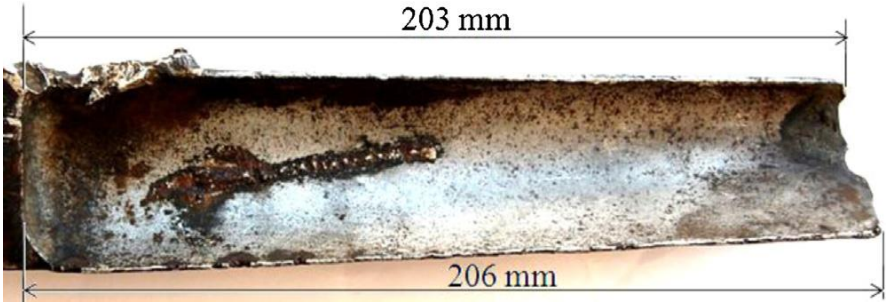

Fig. 2.4. The distance of fracture surface from the platform at blade edges.

Metallurgical analysis of blade indicates homogeneity of microstructure and hence uniform hardness throughout the blade. Fractographic analysis of blade is done using SEM (Scanning Electron Microscopy) and also EDS (Energy Dispersive Spectroscopy) is done to determine the origin of fracture. Fractured blade was cut from three positions as marked in Fig. 2.5.

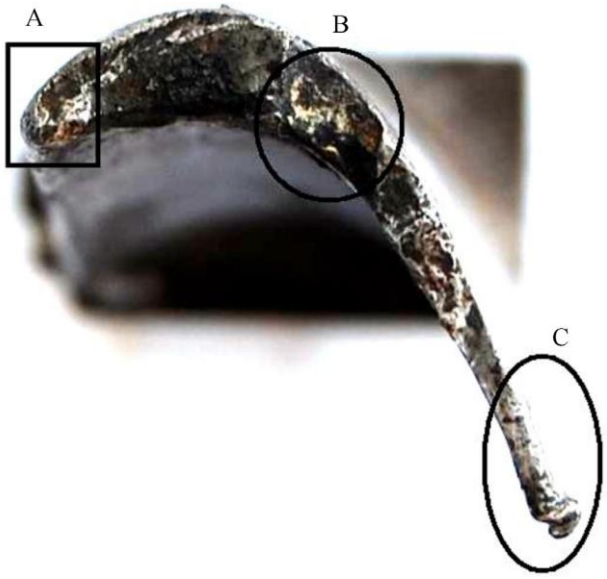

Fig. 2.5. Positions marked for Fractographic Analysis.

EDS analysis at the fractured part of the blade detected ample amount of Si along with O, K, Al, Na and S. The presence of these non-metallic inclusions at the fractured surface indicates long term exposure in the atmosphere or the reaction of blades with steam. The fractographic study of these three regions namely A, B and C of the fractured blade along with the EDS analysis reveal that the main cause of blade failure could be corrosion fatigue.

M. Attarian et al [3] discussed the failure of gas turbine blade made of IN-738LC due to metallurgical reasons. They found that dynamic embrittlement and grain boundary oxidation are two significant damage mechanisms in nickel based alloys. Once grain boundaries are lay into by these mechanisms, the situation changes from bulk dependent creep damage to localized time-cycle dependent creep damage in the notch root produced by grain boundaries oxidation. They also found that Cobalt based 40 MW gas turbine blades were replaced by those made of IN-738LC. The cobalt based superalloy had a life span of 50,000 h before much damage. The new blades made of IN-738LC failed in service after only 1500 h.
Chemical analysis, Fractography, EDS Analysis and Hardness testing of the failed blade is done from different transverse sections from root, mid-height and top of the fractured surface of the blade.

Table 2.1. Chemical Composition of IN-738LC

Element	Wt. %	Element	Wt. %
Si	0.003	C	0.08
Cr	16.47	S	0.01
Mo	1.7	Zr	0.06
Co	8.81	B	-
Ti	3.24	Ta	1.5
Al	3.24	Al+Ti	6.48
Nb	0.85	Ni	Base
W	2.6		

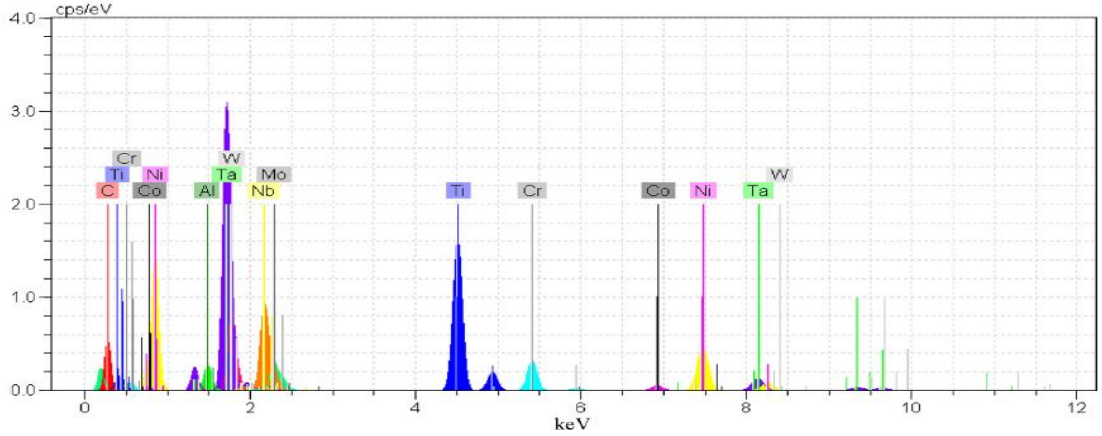

Fig.2.6. EDS Analysis of root tip

It was found that most of the fracture surfaces were trans-granular. The result shows that the blade was exposed to high temperature before fracture. It seems that with dissolving the gamma phase in medium because of high temperature exposure, oxidation and dynamic embrittlement mechanisms leads in failure of the presented blade.

2.2. Coatings and friction damper:

J. R. Nicholls et al [4] discussed the smart coating technique to save the blade from thermal oxidation as well as corrosive oxidation by automatic switching action of coating layer. In this technique the smart coat design consists of a MCrAlY base, enriched first in chromium and aluminium to provide a chemically graded structure. High purity alumina scales gives the best protection under high temperature oxidation conditions, and thus it has been a major drive behind the development of platinum aluminide coating technology. Chromia scales form more readily at low to intermediate temperatures, are more resistant to salt fluxing and thus provide a rapid repair route under hot corrosion conditions. Conventional commercial MCrAlY coatings have compositions containing: 18-30wt%Cr, plus 5-14wt%Al and so are a compromise between optimal protection for Type-I corrosion and high temperature oxidation. The best corrosion performance at each of the test temperatures was obtained with alloy compositions in the following ranges:

650^{o}C: alloys rich in chromium, with Cr > 40wt% and Al levels between 5-10wt%.

700^{o}C: alloys rich in chromium, with Cr > 40wt%, but containing 20-40wt% aluminium.

750^{o}C and 800^{o}C: alloys contain 24-40wt%Cr and 27-37wt% Al: the optimum being 33wt%Cr, 33wt%Al

950^{o}C: alloys with 16-24wt%Cr and 13-18wt%Al

1093^{o}C +: alloys centred on 25wt%Cr and 14wt%Al

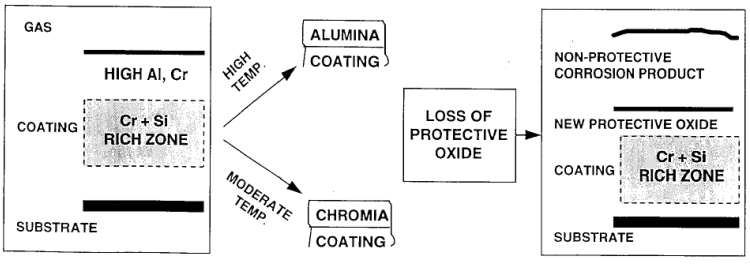

Fig.2.7. Smart Coating Concept

Bruce M. Warnes et al [5] discussed diffusion coating impurities introduced by standard aluminizing processes and their effect on oxidation resistance behaviour of coating. In this work they taken IN-738 tabs and foils were platinum electroplated, and then aluminized using three different processes:

- High-activity pack cementation
- High-activity CVD and
- Low-activity CVD.

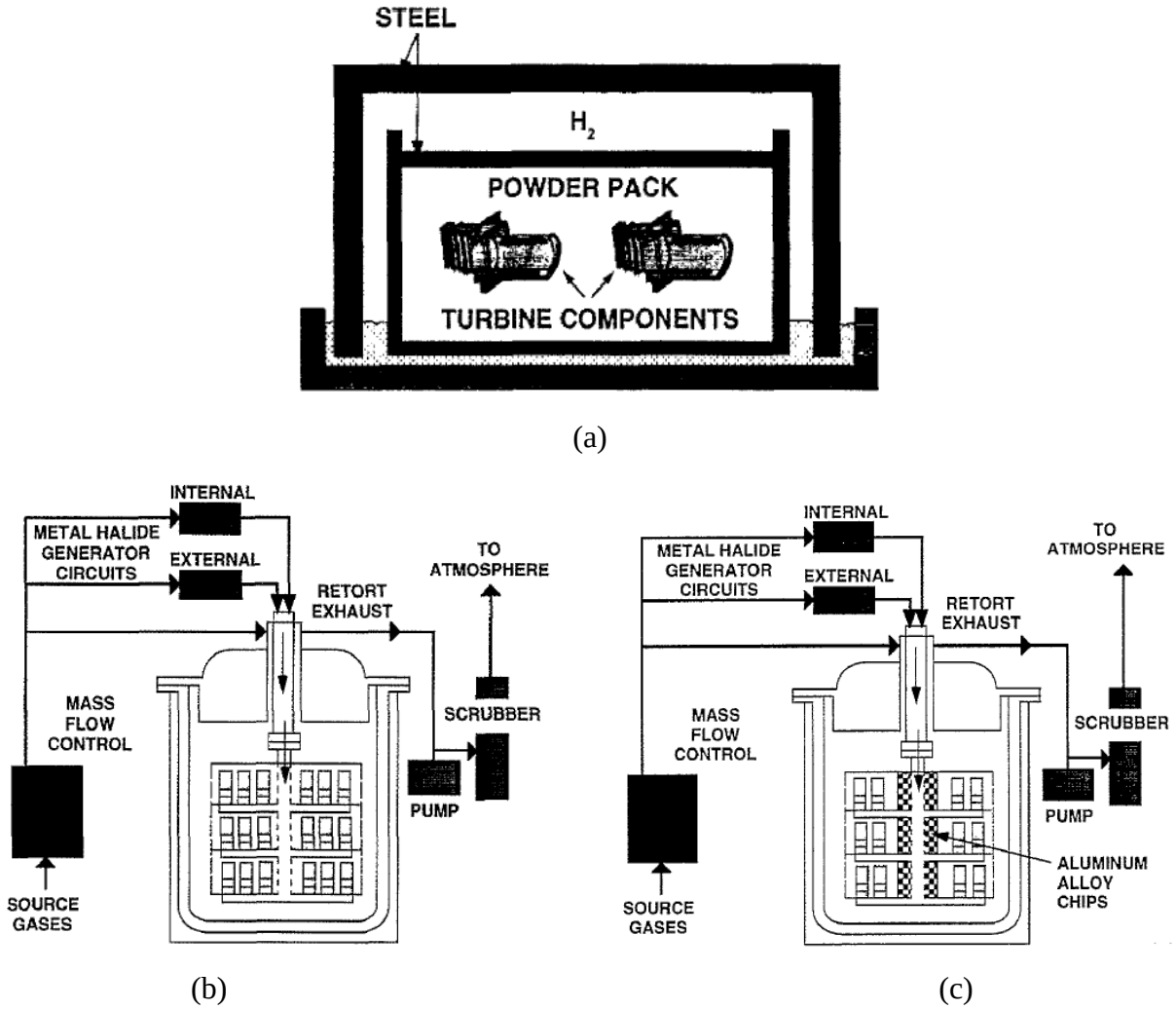

Fig.2.8. Schematic diagram (a) pack cementation aluminizing process (b) the CVD low-activity aluminizing apparatus (c) the CVD high-activity aluminizing apparatus.

From the above analysis it was found that the transport of impurities to or away from coatings during standard aluminizing processes is possible. High-temperature aluminium sources inside the coating chamber are also a significant source of coating impurities during aluminizing. CVD low-activity aluminizing purifies the (Ni, Pt) Al additive layer during growth. The purity of (Ni, Pt)Al is directly proportional to its oxidation resistance.

2.3. Fatigue failure and Vibration of gas turbine blade:

N. S. Vyas & J. S. Rao [6] analysed the resonant stresses through which a blade passes during start-up and shut-down operations whereas blade is designed for constant speed running conditions. In this literature they identified the loading biography of gas turbine blade. A blade designed for safe operation at constant rotor speeds may get damaged during transient operations. In this study blade stresses during constant and variable speed operations have been analyzed. Non-linear damping is used to increase the fatigue life of the turbine blade at different rotor speed.

J. A. Loya et al [7] discussed the natural frequencies of bending vibrations of a cracked Timoshenko beam and applied the boundary conditions at both ends of the beam as simply supported beam. He compares the result of natural frequency obtained by solving the differential equations obtained from the equations of vibration of Timoshenko beam with the frequencies obtained from the perturbative method.

Craig P. Lawson et al [8] discussed the effect of tip clearance on the turbine blade efficiency and how to maintain it for maximum efficiency and minimum chances of failure. They used capacitive probe on the tip of the blade which monitors the tip gap, as efficiency of the system have inverse relation with the tip gap of the blade. In capacitive probe measurement technique we correlating capacitance probe tip timing results with simultaneously measured blade-mounted strain gauge vibration results and precise rotational speeds. Blade tip vibration amplitudes are measured using capacitance probes and compared to strain derived vibration levels, which measure the vibration characteristics and monitor it.
Blade vibration was investigated using blade mounted strain gauges. A low stiffness quasi blade was mounted on the compressor rotor. It was found that this blade could be resonated in vibration mode one at a rotor speed of 938 rpm. This is due to the 16 engine order coinciding with the blade's first natural frequency of vibration. Blade tip vibration amplitudes of up to 1.2mm were measured. The vibration was successfully detected through dual capacitance probe tip timing, which was used to measure blade vibration amplitude. This was done with the instrumented blade vibrating in mode one. Two capacitance probes were mounted over the blade tip mid chord paths at different circumferential positions. Capacitance probe tip timing was used to measure instantaneous tip deflections at both capacitance probes. The frequency of blade vibration was obtained from spectral analysis of

the blade mounted strain gauges' signals. This frequency information was used in conjunction with the measured capacitance probe separation to curve fit a sine wave to the two tip timing measured tip deflections. In this way the blade tip deflection amplitude was calculated. This amplitude was compared to the tip vibration amplitude calculated from the blade mounted strain gauge signals. The vibration amplitudes measured through capacitance probe tip timing agreed with those derived from the blade mounted strain gauges within the associated error bands.

2.4. Experimental and Analytical modal testing:

S. Zucca et al [9] discussed experimental study of the effect of under platform dampers on the dynamics of blade disks. The work has been produced using an experimental rotating test rig equipped with non-contact excitation and measurement systems, this being important for preventing additional and unpredictable mistuning cause by the transducers. Scanning Laser Doppler Vibrometer is used to measuring vibrations of rotating structure such as bladed discs is of invaluable importance to succeed in such experimental studies. The effects of under platform dampers on the first bending vibration mode of the blades have been investigated for different levels of the excitation force and for different engine order values. Then on-linear relationship between the force and the vibration amplitude has been observed and measured experimentally so as to identify arrange of excitation forces within which a robust design of the damper worked efficiently. The effects of the number of engine order excitation on the damper performances has been systematically measured.
These showed that dampers are effective in reducing vibrations of blades in a range of excitation force levels, which increases as much as the number of nodal diameter associated to the excited mode shapes becomes larger.

S. Narasimha et al [10] discussed the effect of introducing cottage-roof friction damper between two turbine blades. They investigated the turbine blades with and without damper using ANSYS software by FEM and found that friction damper increases the modal frequencies of the turbine blade and push the blade towards extended life. As shown in figure 2.9.

Table 2.2. Natural frequencies with and without damper

Mode No	Natural frequencies of blade (Hz)	
	without damper	with damper
1	828.83	1337.2
2	829.02	2264.5
3	4671.1	4087.5
4	4673.2	6131.6
5	7105.8	7125.9
6	7114	8658.3
7	11472	10671
8	11483	11196
9	19415	13844
10	19476	15540

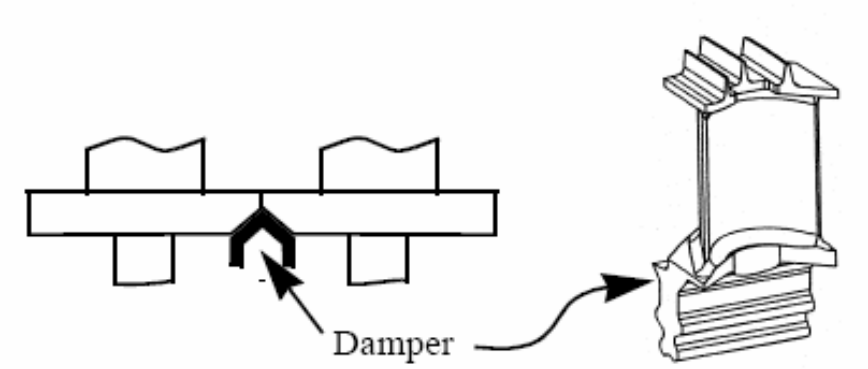

Fig.2.9. Cottage-roof friction damper

CHAPTER – 3

DESIGN OF FIXTURE

3.1. Need for fixture:

As gas turbine blade is not uniform throughout its cross-section and have different portions at different orientation, hence it is very difficult to make experiment without stability of the system where impact testing is to be done. Further in order to get original result we have to provide same boundary conditions as per in the gas turbine rotor disc.

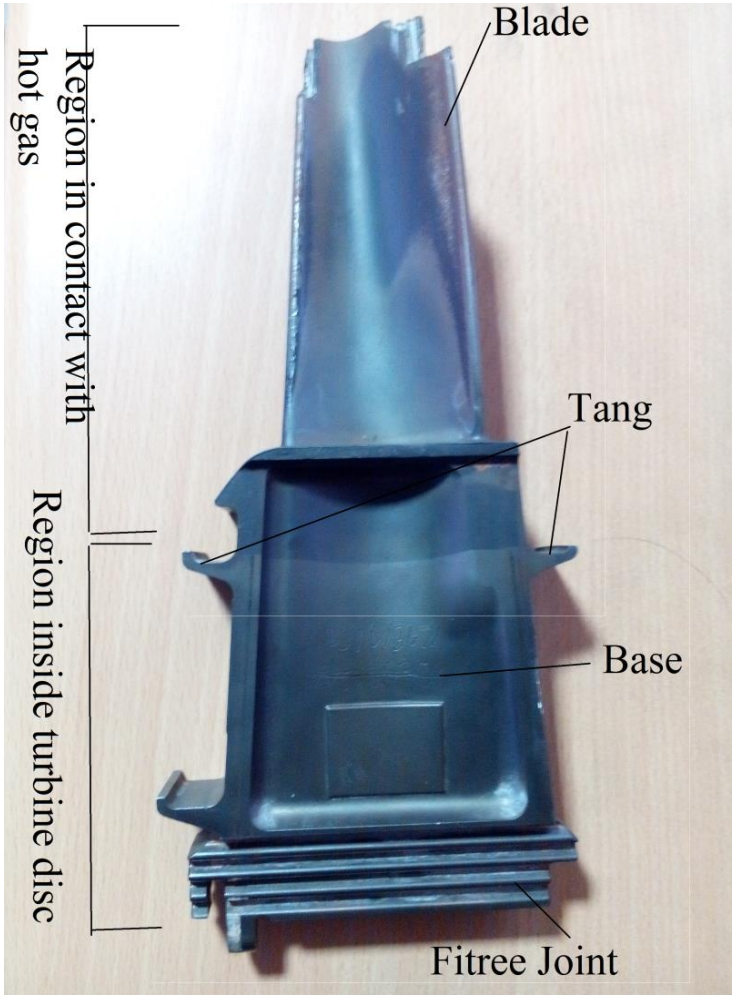

Fig.3.1. Nomenclature of IN738 LP-1 gas turbine blade

To provide same boundary conditions and physical similarity as in turbine rotor disc we decided to make a fixture which fixes the turbine blade from the fitree joint. Hence we required a fixture which has same profile as fitree joint and which fixes into it perfectly also proper tightening force is to be given to fitree joint.

3.2. Design procedure:

- To make fixture for fitree joint of gas turbine blade we need such an arrangement that the joint can be opened easily and tight properly as required. For this reason we decided to make fixture using two similar block of cast iron with dimensions 6×6×12 cm.
- Then these blocks placed side by side with the help of C-clamp on the lathe bed to make the fixed. After that packing material is applied to them to get the profile impression of fitree joint on the blocks, and then the profile of the fitree joint is to be drawn on the blocks with the help of scriber.

Fig.3.2. Geometry of fixture

- Two lines are drawn on the profile of fitree joint called as minor diameter and major diameter. Then a wedge is created on the both blocks with minor diameter and after that the angle is measured to be 11.5^{o} with bevel protector.
- Then the block is fixed over UNIVERSAL MILING MACHINE with bevel protector at an angle of 11.5^{o} and an up-milling cutter is mounted in the arbor with wedge face perpendicular to it.
- After subsequent alignment of block *gashing* is done on one block with 16 DP (Diametral Pitch). Gashing is termed as the rough cutting made on work piece approximately to the profile required.

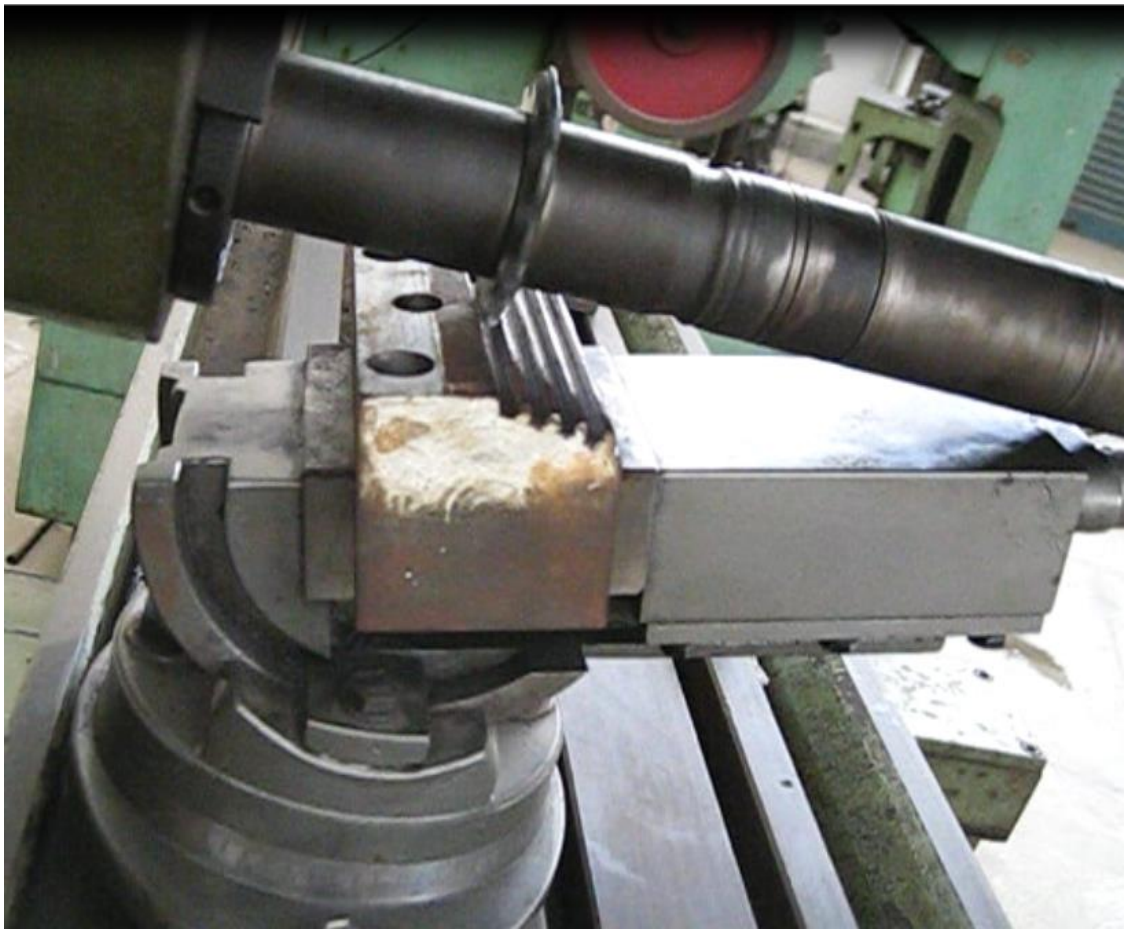

Fig.3.3. Machining over fixture blocks

- After this cut a 14 DP finishing cutter is used to make accurate profile for the teeth of the block same as fitree joint.
- Similarly another block is finished by changing arbor by 180^{o} so that same profile can be generated on another half of the fixture block.
- Now fitree profile created on the both the blocks and to make them tight and fit joint three holes of 16mm diameter has been created in the block to make tighten by nut-bolt.

Table.3.1. Fixture Parameters

Rough cutting	16 DP
Finishing	14 DP
Depth of cut	4.35 mm
Gap between blocks	6 mm
Wedge angle	11.5^{o}

Fig.3.4. Final fixture formed

Fixture is made of cast iron and it has very good damping properties hence it can be employed with blade to testing and give positive results.

CHAPTER-4

EXPERIMENTAL MODAL ANALYSIS

4.1. Introduction

In this work vibration analyses of components had been done using Vibration Analyser OROS 36, which operates with NV Gate 8.30 version software, and record the signals of component in the form of acceleration, velocity and displacement.

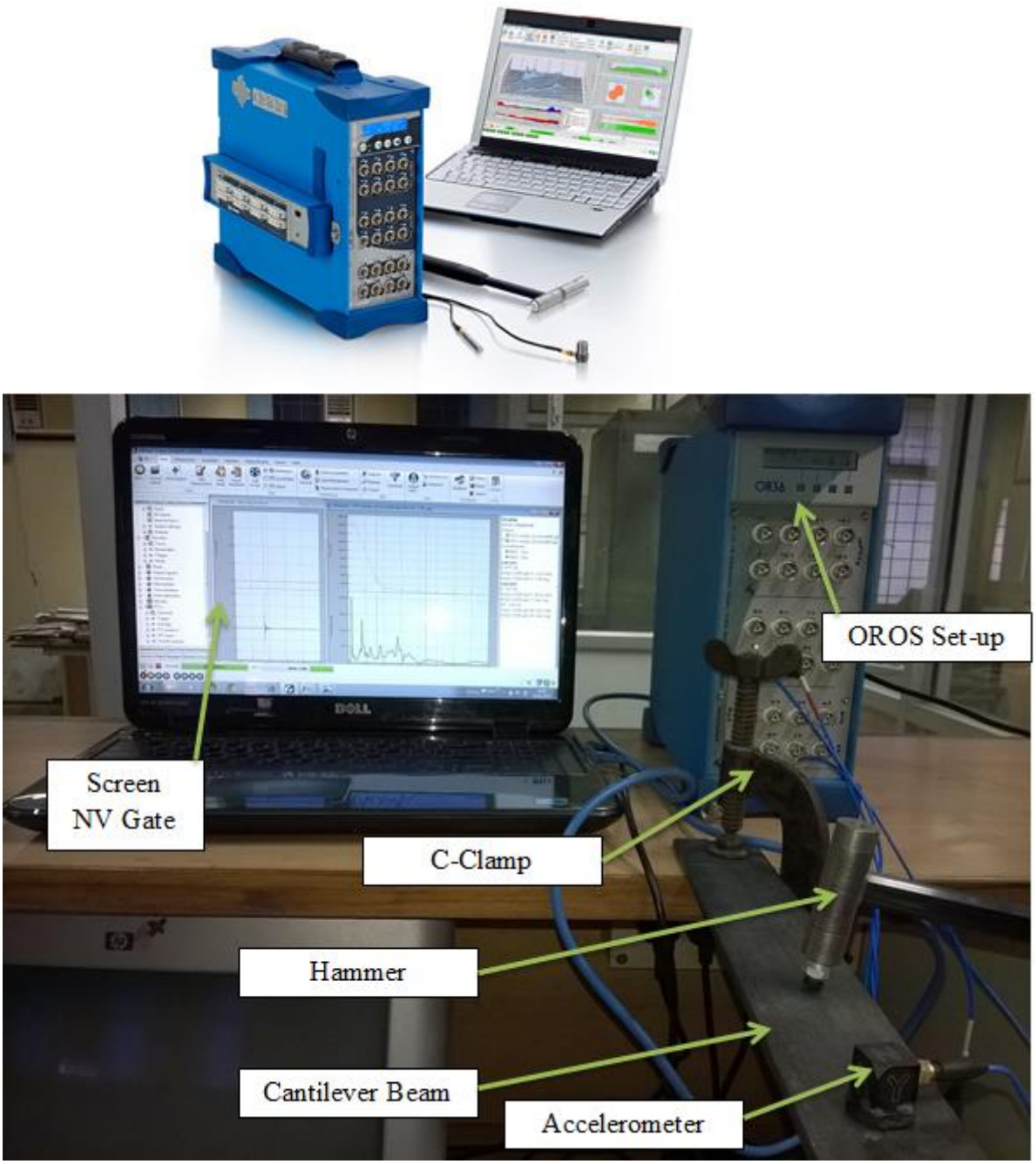

Fig.4.1. Experimental set-up for vibration analysis.

4.1.1. About OROS & NV Gate 8.30:

OR36/OR38 is designed for high channel count capacity without comprising the analyzer geographies. All the channels are handled in real-time whatever the analysis mode: FFT, 1/3rd Octave, CPB or Synchronous order analysis. OR36 & OR38 keep these real-time capabilities up to 20 kHz. There are LCD screen controls on the OR36 and OR38 hardware that allow you to run, stop the analyzer, change the fan speed etc.

Basic procedures of NV Gate follow a simple sequence:

- Input connection to the plug-in analyzers.
- Format of Front-end and plug-in analyzers.
- Range of results to be displayed and/or saved.
- Result management (manager) and report generation.

NV Gate platform offer a comprehensive sets of tools for noise and vibration acquisition, recording and analysis.

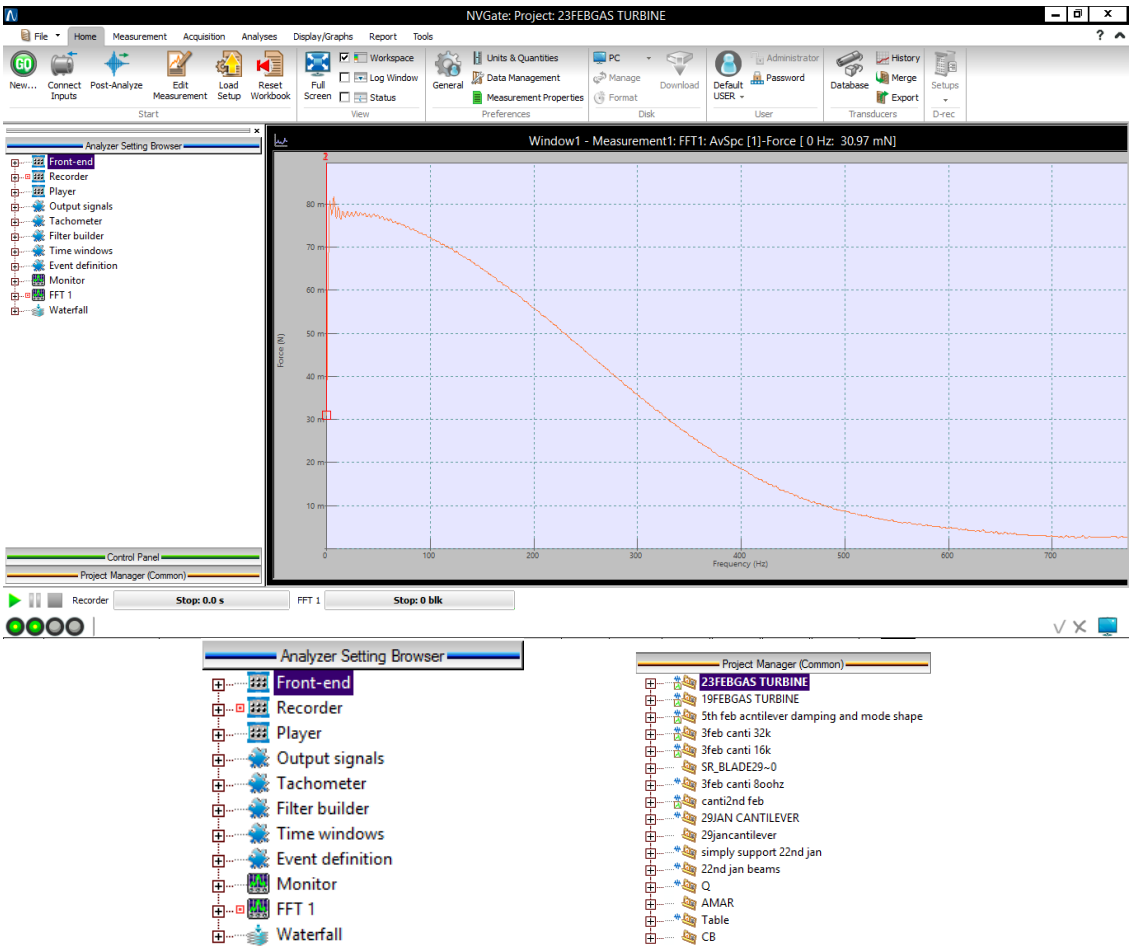

Fig.4.2. GUI of NV Gate 8.30

4.1.2. Specifications

4.1.2.1. OROS Hardware

Table 4.1. OROS Hardware Specification

Inputs	1 to 16 Dynamic Inputs DC Inputs	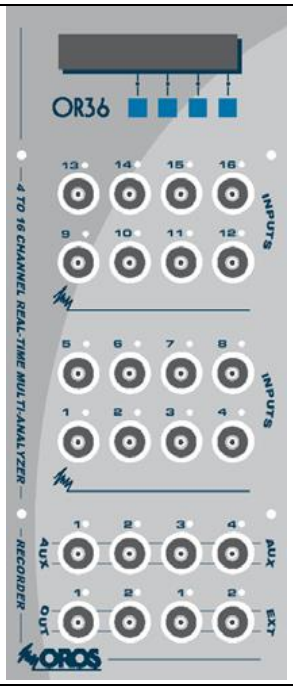
Out.	Generators 1 & 2	
Ext.	External Sync.1 & 2	
Aux.	Auxiliary connectors 1 to 4	

4.1.2.2. Transducers

Table 4.2. Accelerometer Specification

Transducer Type	Acceleration Sensor
Unit/ Magnitude	Acceleration (m/s^2)
Identifier	PCB-78534
Model	356A16
Coupling	ICP
Sensitivity	1×10^{-2} V/g or V/(m/s^2)

Table 4.3. Hammer Specification

Transducer Type	Force Sensor
Unit/ Magnitude	Force (N)
Identifier	PCB
Model	SN-25679
Coupling	ICP
Sensitivity	2.25×10^{-3} V/N

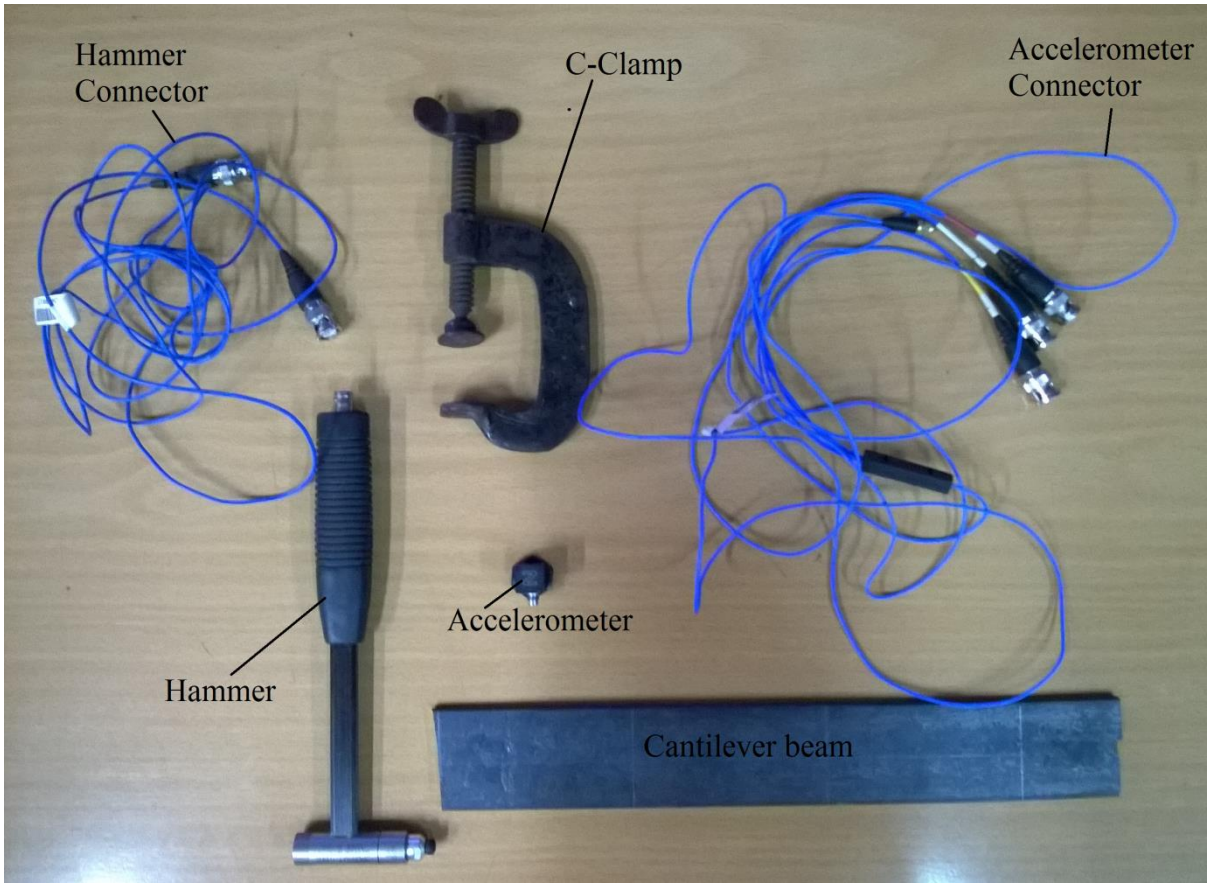

Fig.4.3 Nomenclature of Components

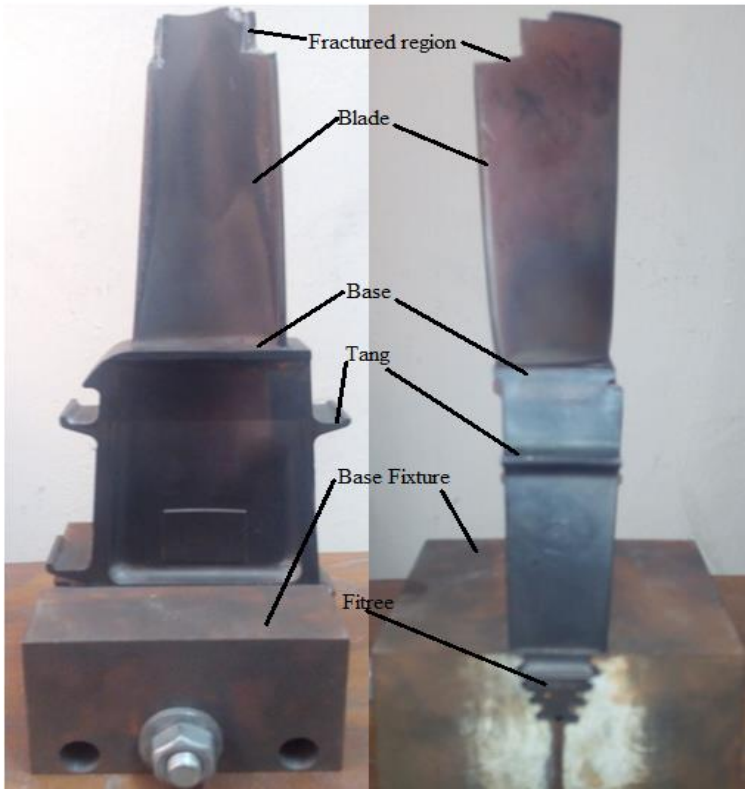

Fig. 4.4. Gas turbine blade Nomenclature

4.2. Modal Analysis using OROS & NV Gate:

Modal analysis is a process where we describe a structure in terms of its natural characteristics which are the frequency, damping and mode shapes i.e. its dynamic properties. FRF based modal testing started in the early 1970's with the commercial availability of the digital FFT analyzer, and has grown steadily in popularity since then.

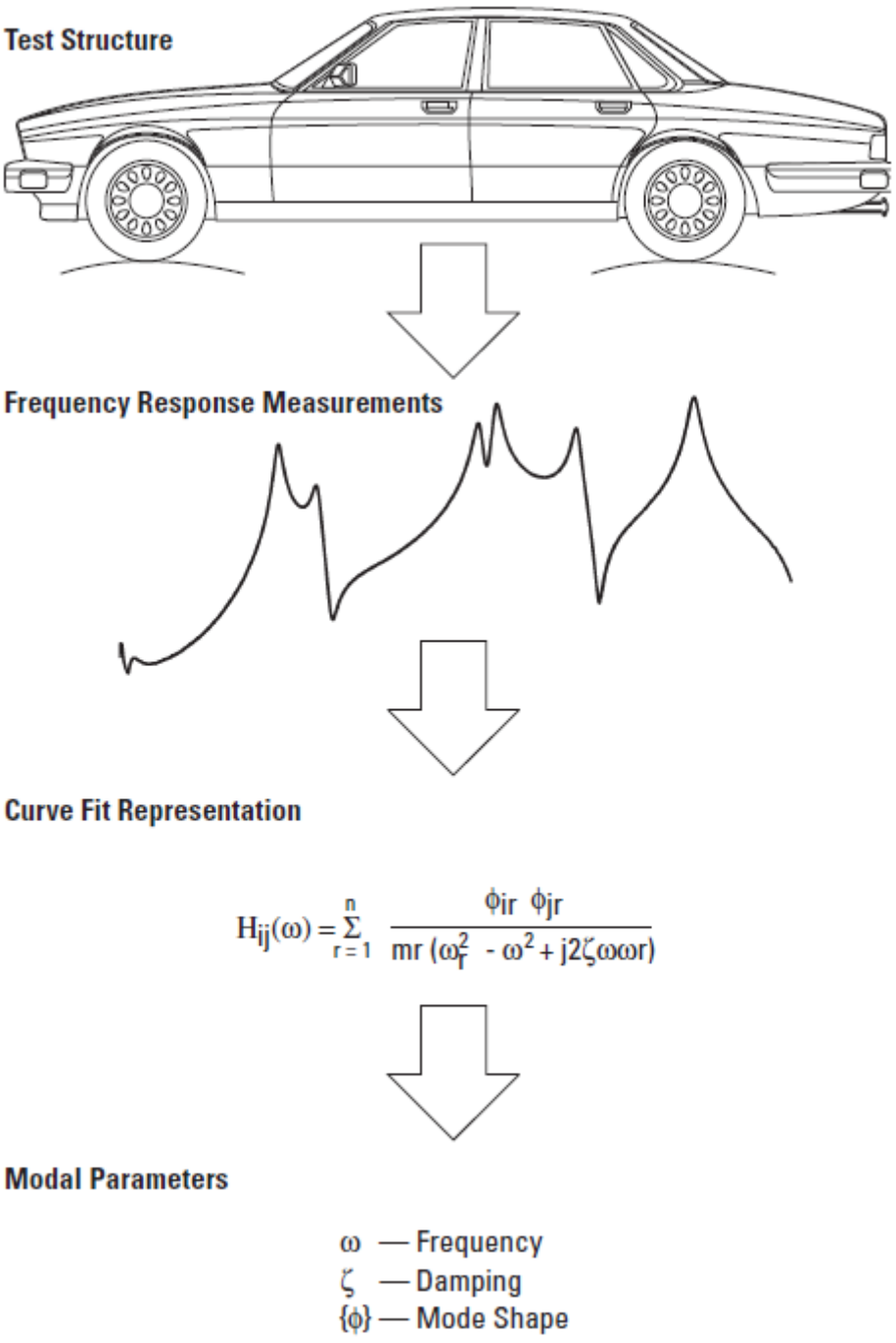

Fig4.5. Phases of Modal Test

Modal analysis is a method to explain any structure in the form of its natural characteristics like frequency, damping and mode shapes which are its dynamic properties. Modal analysis used to find the modal parameters of any structure to build a modal model for the response.

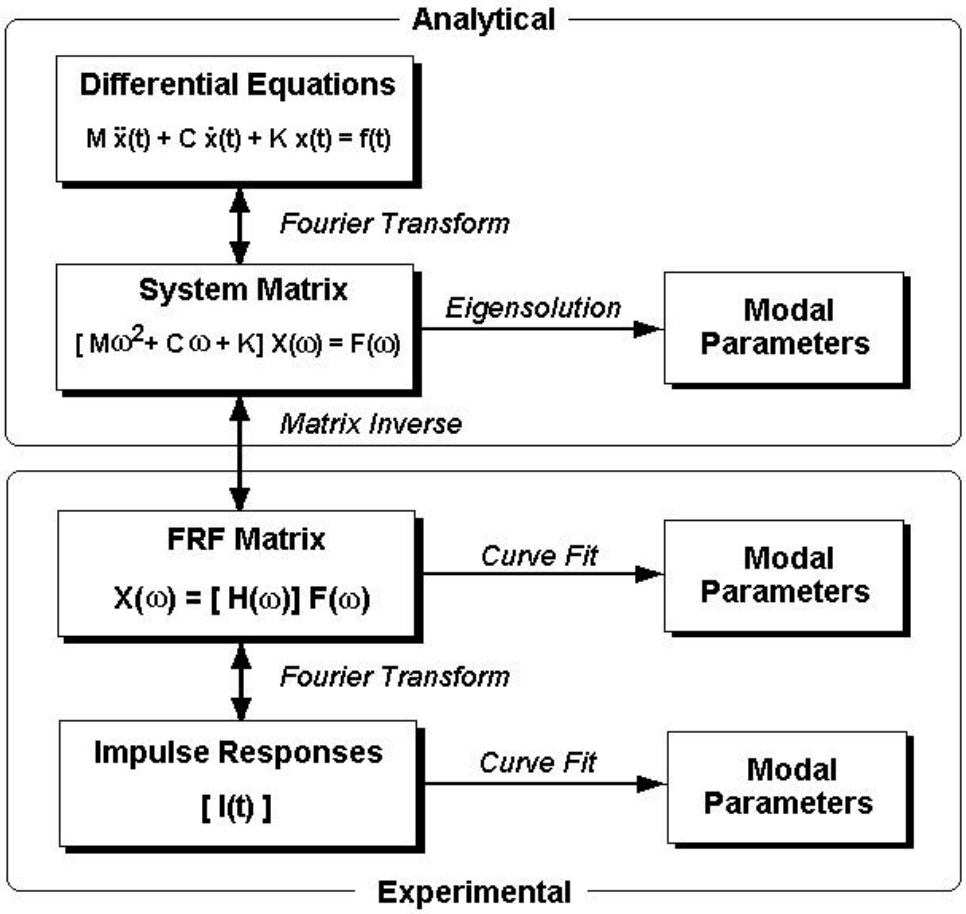

Fig 4.6. Analytical and Experimental procedure to determine modal parameters

- Modal parameters determined by analytical techniques such as FEA and also by EMA, which is the verification of the results of FEA with EMA.
- As analytical model does not exist for long time hence the modal parameters obtained experimentally serve the model for future reference.
- Hence mostly experimental modal analysis is used to explain the dynamics of the structure, vibration or acoustics, analytical models etc.
- Models of the vibrational structures:
    a) Spatial Model
    b) Modal Model
    c) Response Model

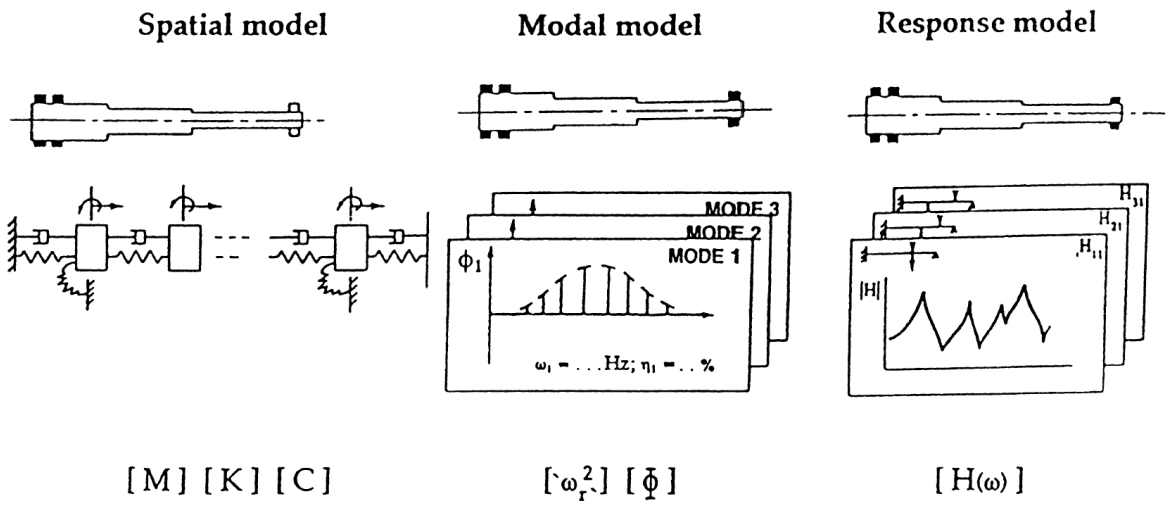

Fig.4.7. Models of Vibratory Structure

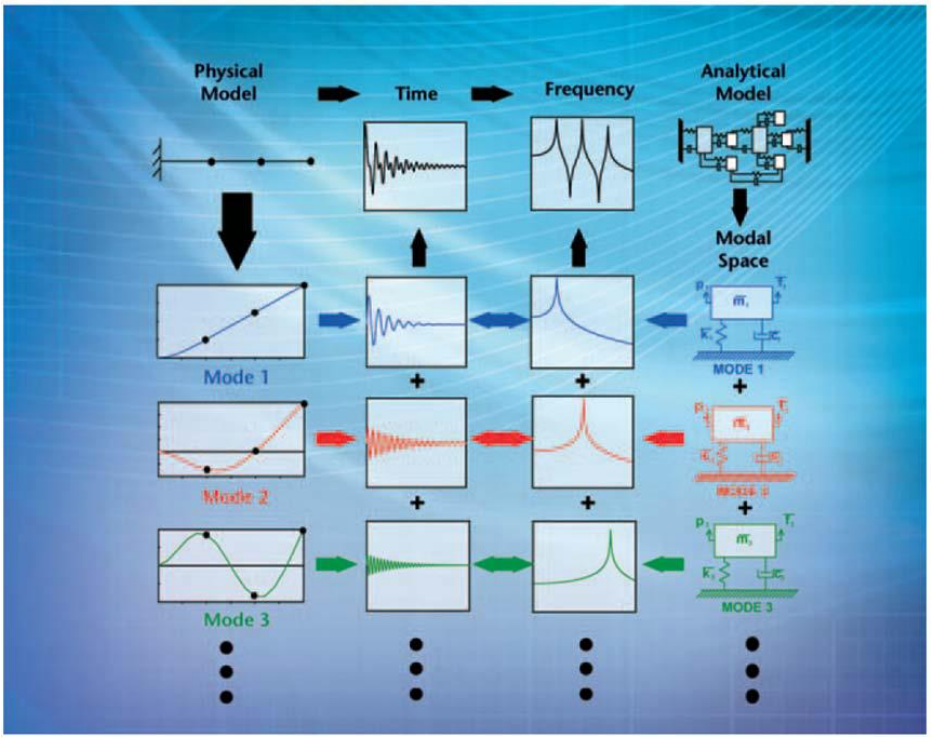

Fig.4.8. An overview of EMA of a cantilever beam

4.2.1. Operating deflection shape (ODS)

An operating deflection shape (ODS) is termed as any forced motion of two or extra points at a structure. Stipulating the motion of two or more points expresses a shape. Stated in a different way, a shape is the movement of one point relative to all others. Motion is a vector quantity, which means that it has both a position and a direction associated with it. Motion at a point in a direction is also called a Degree Of Freedom, or DOF. All experimental modal constraints are obtained from dignified ODS's.

4.2.2. FRF (Frequency Response Function):

FRF is defined as the ratio of the Fourier transform of an output response signal (X(w)) divided by the Fourier transform of the input force signal (F(w)) that produced the output. Depending on whether the response motion is dignified as displacement, velocity, or acceleration, the FRF and its reverse can have a variety of names,

- Compliance (displacement / force)
- Mobility (velocity / force)
- Inertance or Receptance (acceleration / force)
- Dynamic Stiffness (1 / Compliance)
- Impedance (1 / Mobility)
- Dynamic Mass (1 / Inertance)

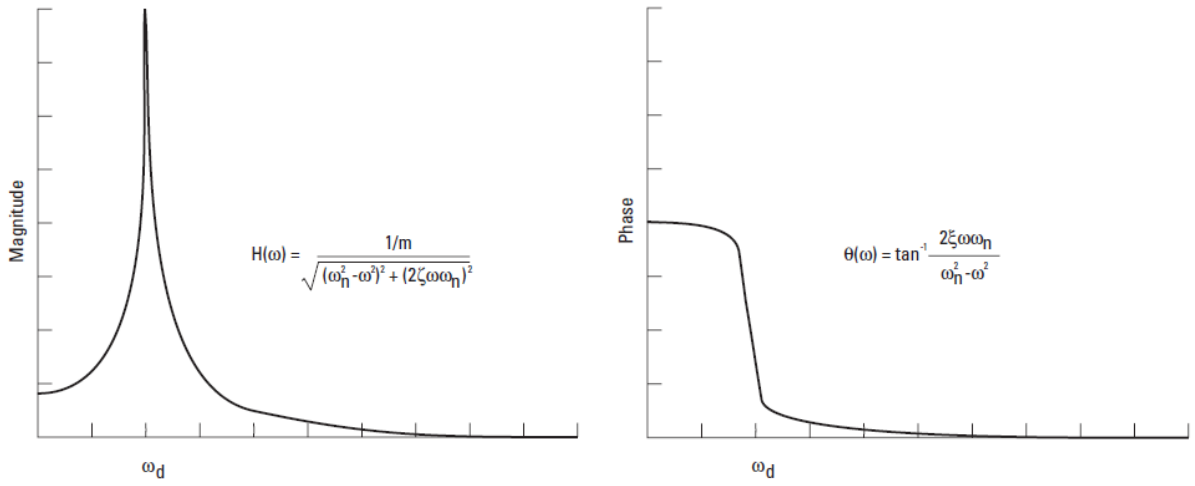

Fig.4.9. Frequency Response Polar Coordinates for SDOF

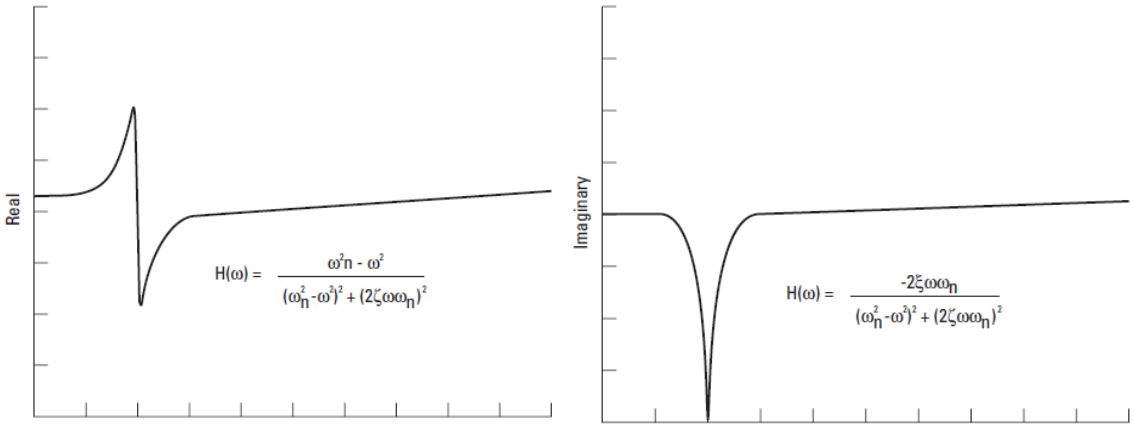

Fig.4.10. Frequency Response Rectangular Coordinates of SDOF

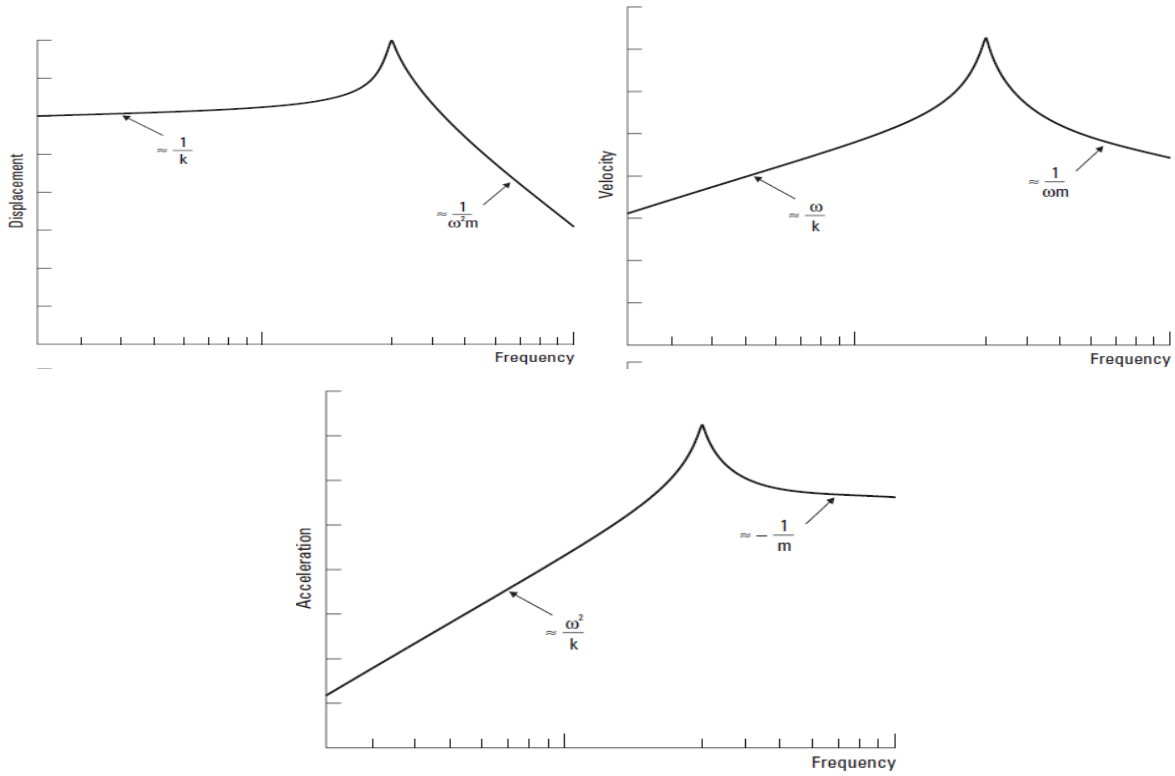

Fig.4.11. Different forms of frequency response

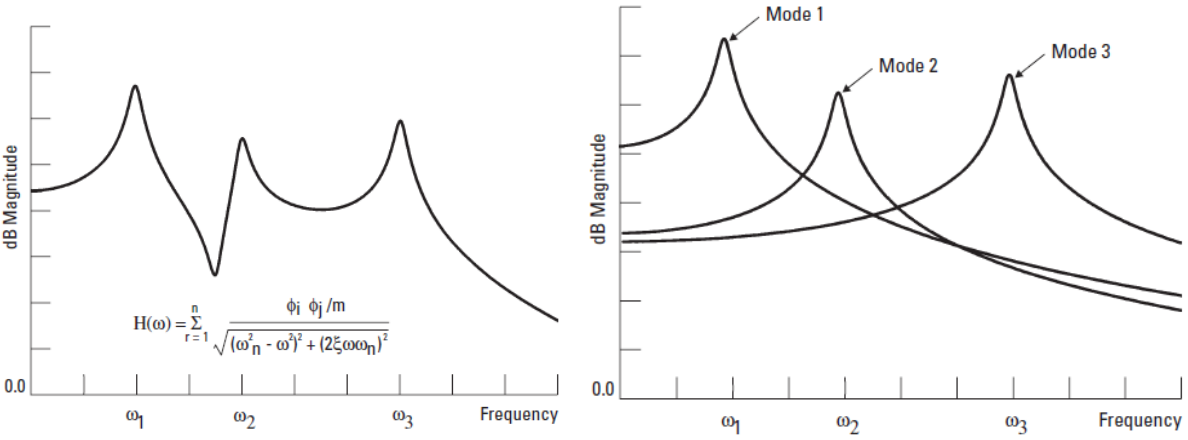

MDOF Frequency Response *SDOF Frequency Response*

Fig.4.12. SDOF modal contribution to MDOF

4.2.3. Single Input (or SIMO) Testing

The most mutual type of modal testing is completed with either a single static input or a single static output. A moving hammer impact test using a single static motion transducer is a mutual example of single reference testing. The single static output is called the allusion in this case. When a single static input (such as a shaker) is used, this is termed SIMO (Single Input Multiple Output) analysis. In this case, the single static input is called the reference.

4.2.4. Multiple Input (or MIMO) Testing

When two or more static inputs are used, and FRFs are considered between each of the inputs and multiple outputs, then FRFs as of multiple columns of the FRF matrix are found. This is termed Multiple Reference or MIMO (Multiple Input Multiple Output) analysis. In this case, the inputs are the references.

4.3. Experimental Procedure:

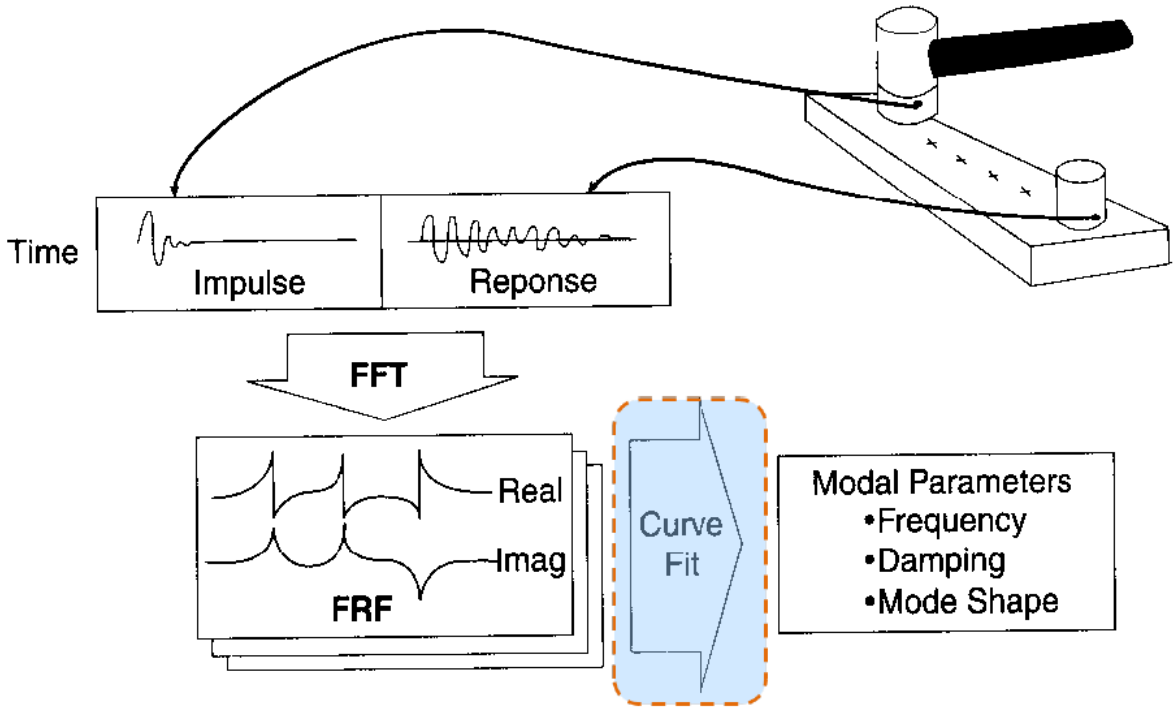

Fig.4.13. Impact testing

The following equipment is required to perform an impact test:

- An impact hammer with a load cell attached to its head to measure the input force.
- An accelerometer to measure the response acceleration at a fixed point & direction.
- A two or four channel FFT analyzer to compute FRFs.
- Post-processing modal software for identifying modal parameters and displaying the mode shapes in animation.

4.3.1. Impact Testing Requirements:

Even though impact testing is fast and convenient, there are several important considerations that must be taken into account in order to obtain accurate results. They include, pre-trigger delay, force and exponential windowing, and accept/reject capability.

4.3.1.1. Pre-Trigger Delay:

Because the impulse signal exists for such a short period of time, it is important to capture all of it in the sampling window of the FFT analyzer. To insure that the entire signal is captured, the analyzer must be able to capture the impulse and impulse response signals prior to the occurrence of the impulse. In other words, the analyzer must begin sampling data before the trigger point occurs, which is usually set to a small percentage of the peak value of the impulse. This is called a pre-trigger delay.

4.3.1.2. Force & Exponential Windows:

Two common time domain windows that are used in impact testing are the force and exponential windows. These windows are applied to the signals after they are sampled, but before the FFT is applied to them in the analyzer. The force window is used to remove noise from the impulse (force) signal. The exponential window is used to reduce leakage in the spectrum of the response.

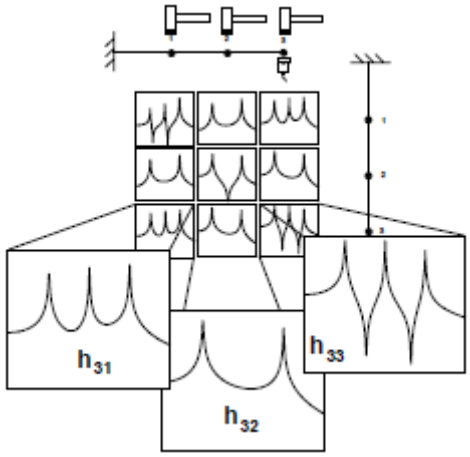

Fig.4.14. Response of hammer impact from different position hitting

An impact test generally results in measuring one of the rows of the frequency response function matrix whereas the shaker test generally results in measuring one of the columns of the frequency response function matrix.

In impact testing method when the FRF is obtained once from the magnitude vs frequency and phase vs frequency graph, then this is converted into real and imaginary parts to obtain the mode shapes of the structure. Hence steps involved to obtain the mode shapes from the FRF given as follows:

- Obtain the FRF from recorded signal.
- Convert Magnitude vs Frequency graph to Real and Imaginary parts.

- Identify the peaks where phase change of 180^o occurs.
- Take the readings for hitting at different positions of equal intervals.
- Mark the positions of peak for different positions and same frequencies.

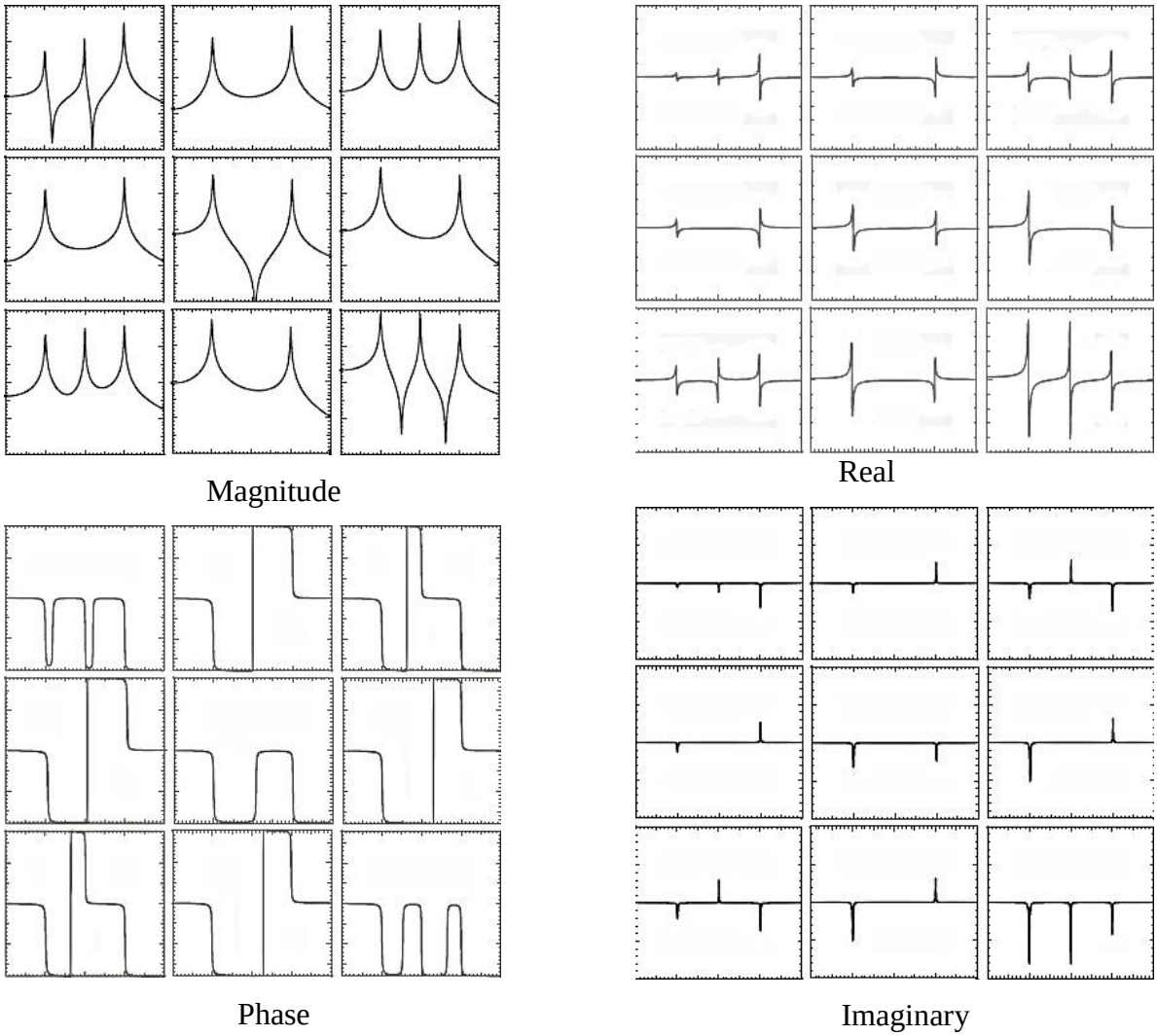

Fig.4.15.Response measurements of a 3 DOF model of a cantilever beam

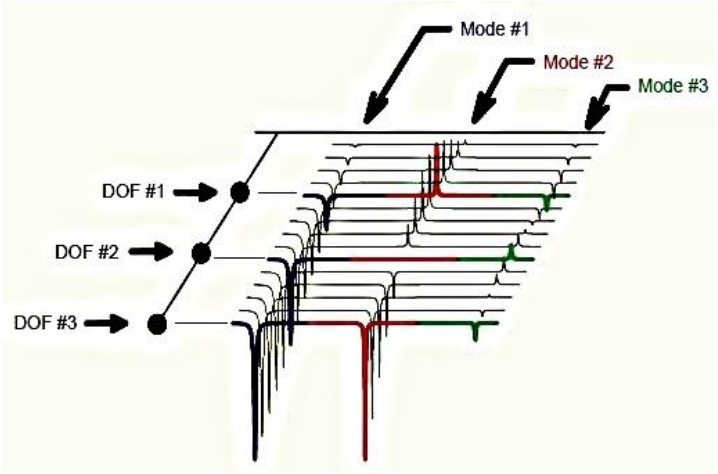

Fig.4.16. Mode shapes obtained from the imaginary part of FRF

4.3.2. Curve fitting:

Curve fitting method is employed here to obtain the value damping factor and mode shapes from the sharp peaks obtained by curve fitting technique of FRF obtained. Here peak to peak method is to be employed to determine the damping factor value and obtaining the mode shapes.

4.3.2.1. Determination of modal damping: (Half Power Method)

Here width of the resonance peak is the measure of modal damping factor and resonance peak with will remain same for all FRF measurements. Actually width of the resonance peak is twice the damping factor hence it is termed as half power method.

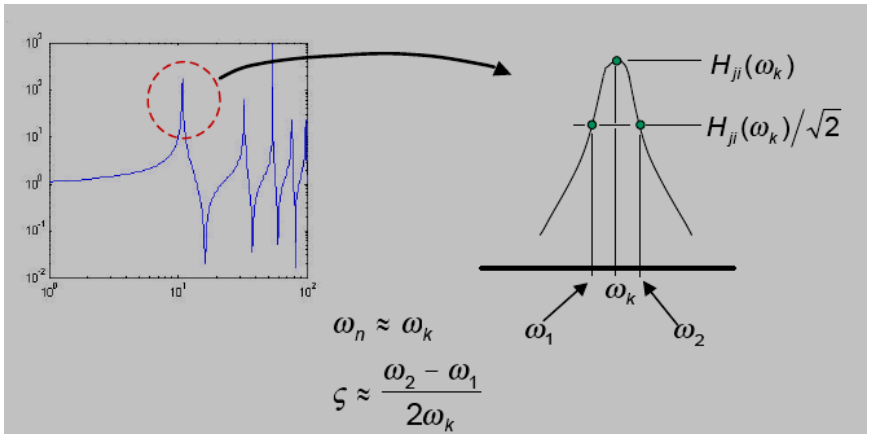

Fig.4.17. Damping factor calculation from half power method

4.3.2.2. Determination of mode shapes: (Quadrature Method)

The FRF obtained from the imaginary part of the acceleration/force vs frequency graph the peak values obtained from the appropriate phase change of the imaginary part of FRFs are considered for the component of mode shapes which on joining give the mode shapes of the cantilever beam, this method is called as Quadrature method of curve fitting.

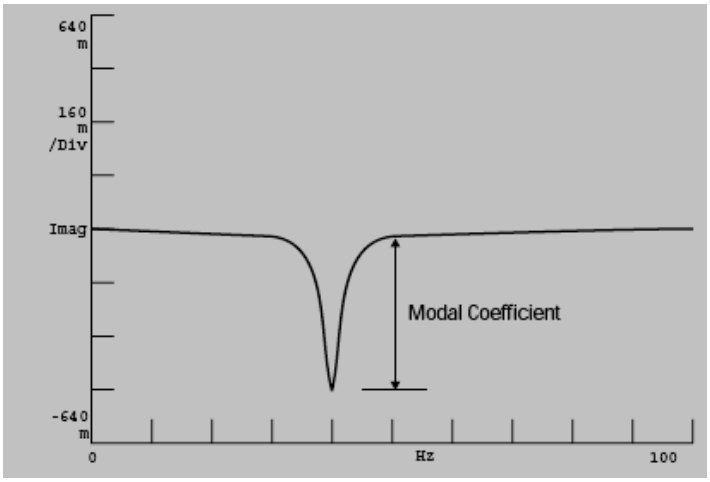

Fig.4.18. Quadrature method of curve fitting

4.3.2.3. FFT Analysis:

FFT analysis of recorded signals is to be done separately for each window i.e. weighted, triggered, average spectral etc. the overall FFT analysis procedure discussed in the below figure, that how recorded input signal results into desired output signals.

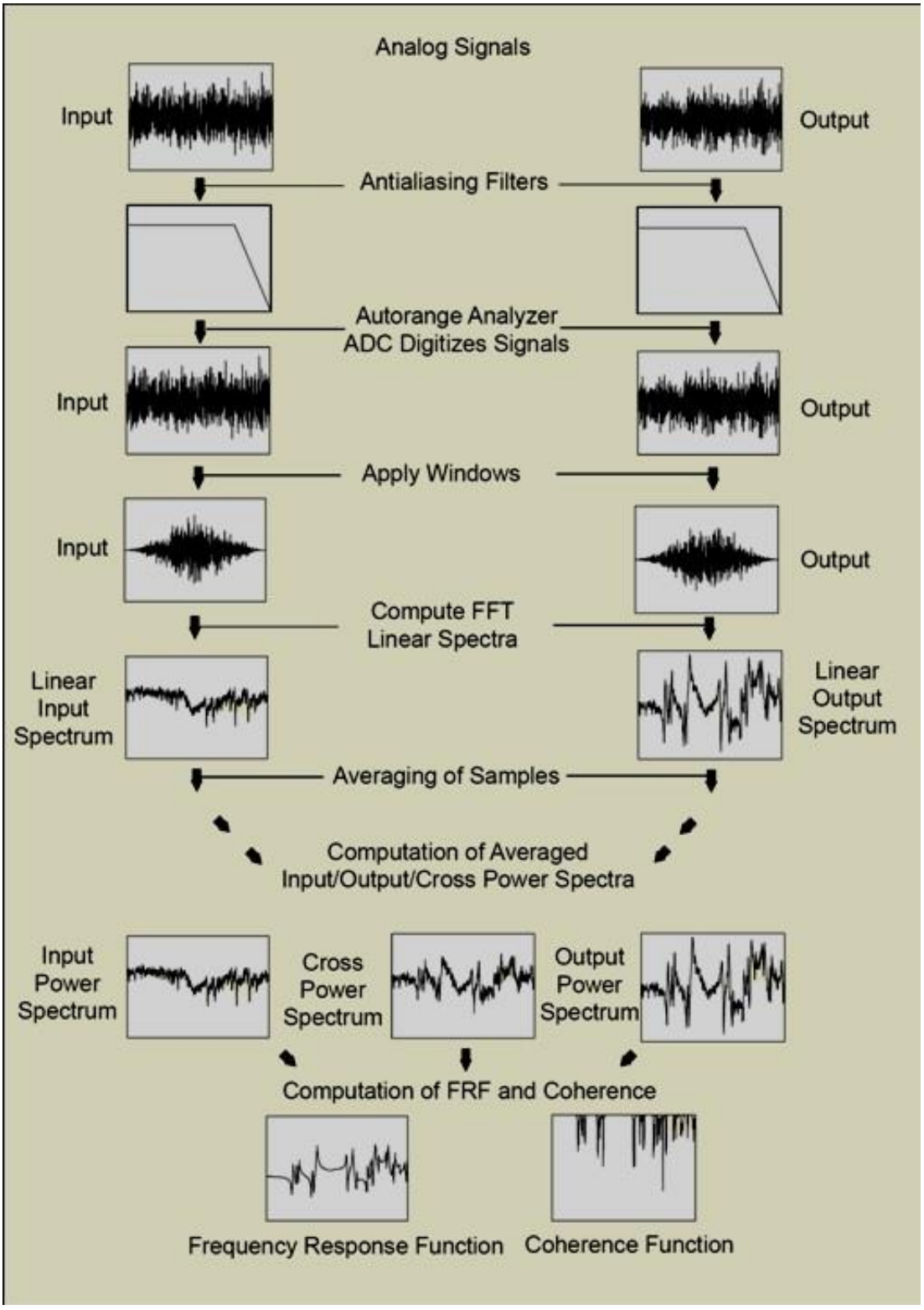

Fig.4.19. Flow diagram showing FFT analysis

4.3.2.4. Assumptions:

Three assumptions have been made in order to get appropriate results for EMA of cantilever beam and gas turbine blade as follows:

A. Superimposition: According to the principle of superimposition if two FRF can be evaluated as combined. This assumption is used in the conversion of single degree of freedom FRF to multi degree of freedom FRF.
B. Homogeneity: According to this assumption the position of the accelerometer does not change from its mounted location during vibration analysis.
C. Reciprocity: According to this assumption the positions of hammer sensor and accelerometer are interchangeable and no variation occurs in FRF obtained.

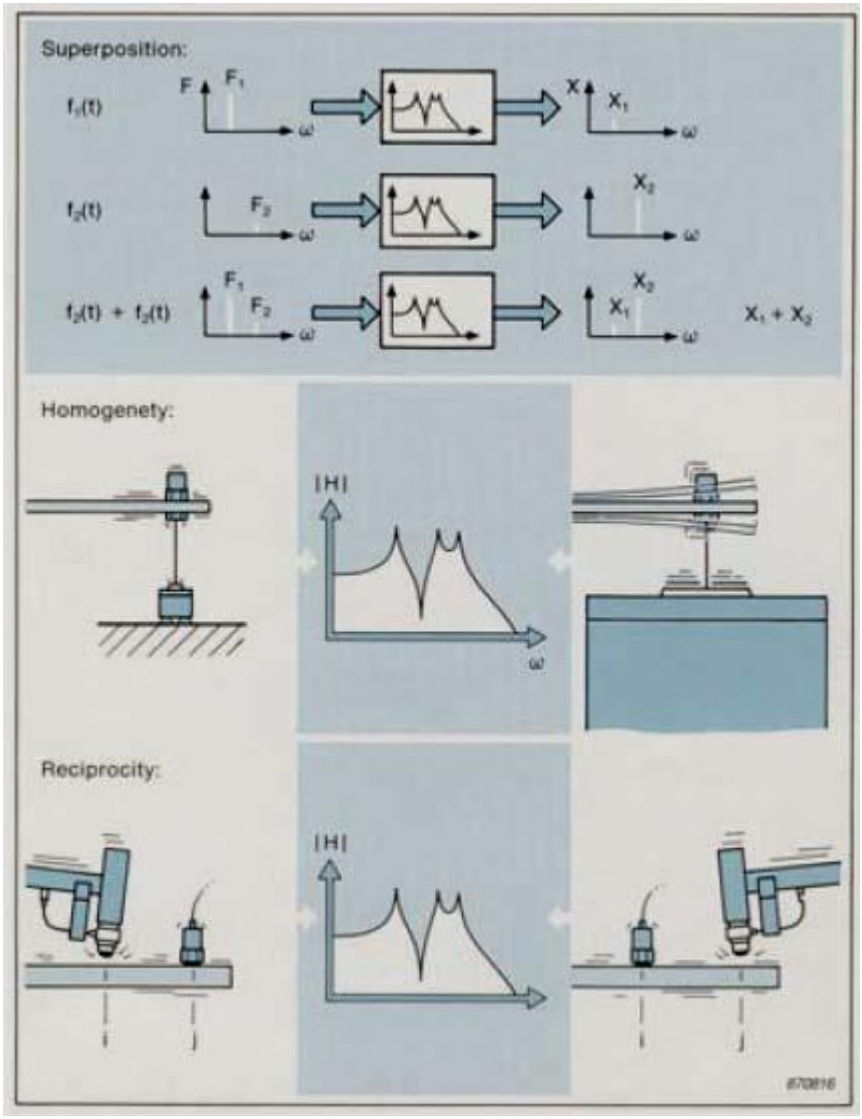

Fig.4.20.Assumptions taken during EMA

Experimental procedure flow chart:

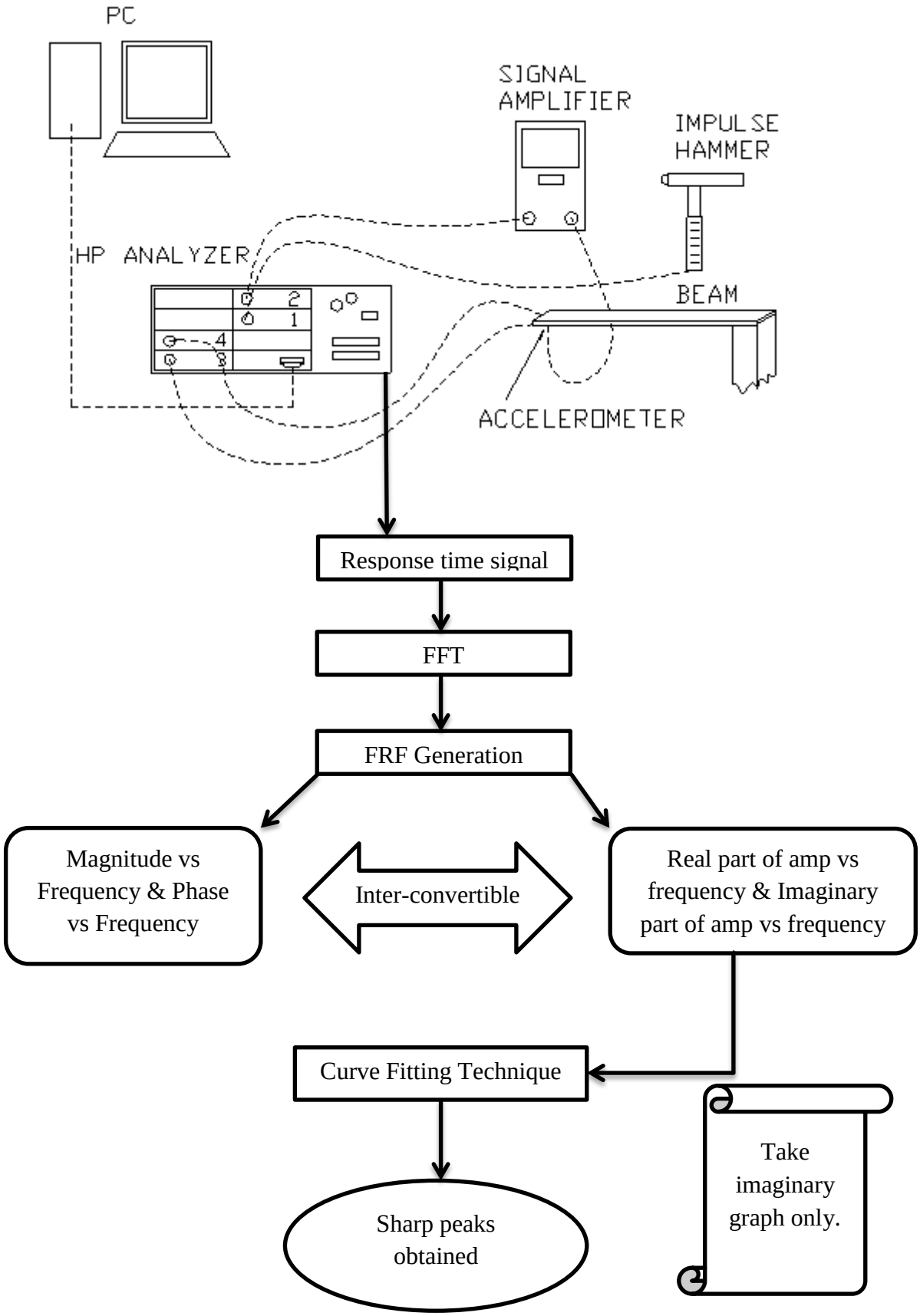

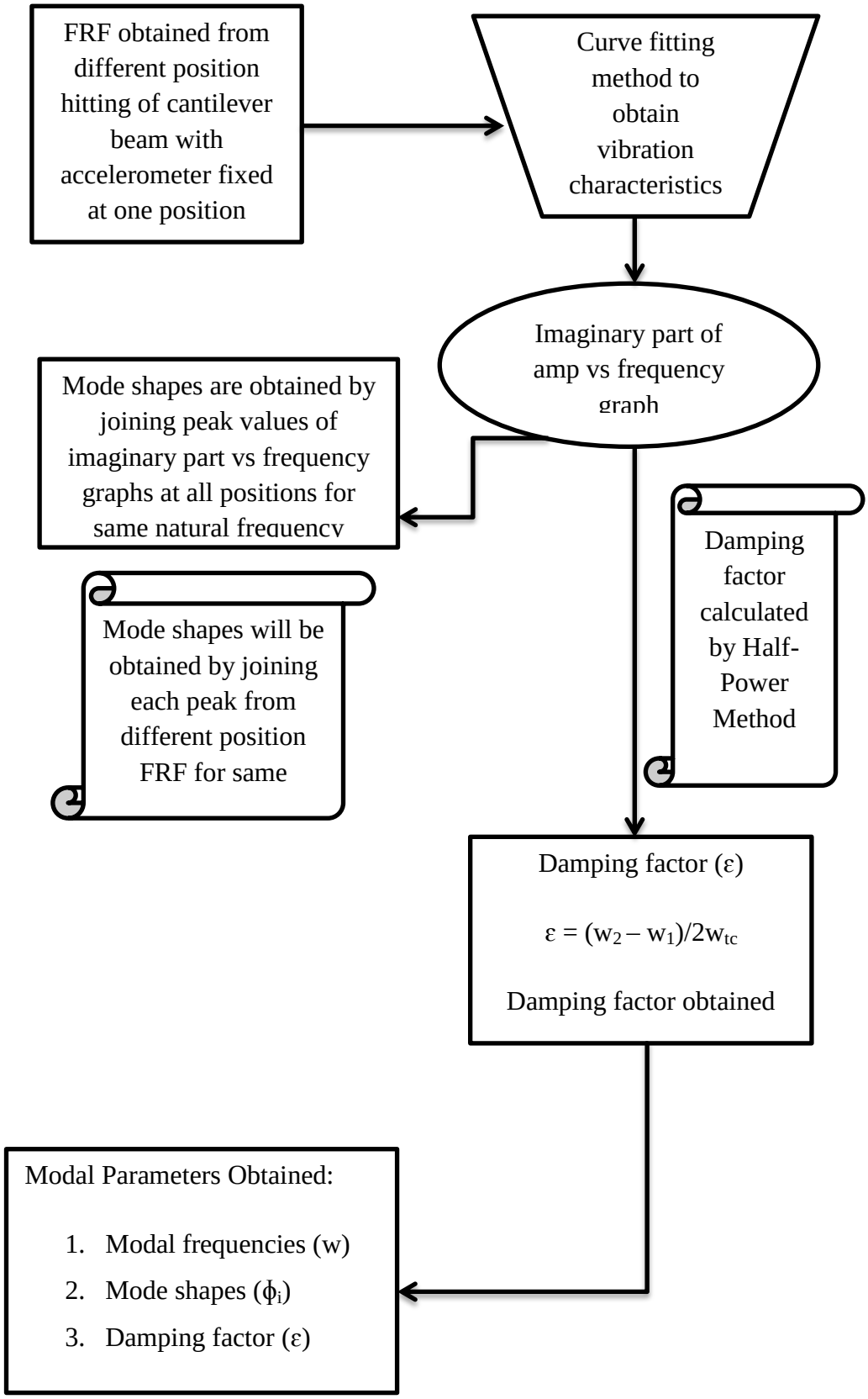

Fig.4.21.Flow chart to obtain the modal parameters.

4.4. EMA of Cantilever Beam

Here we determined the natural frequency and damping factor for a mild steel cantilever beam to make sure that the results we finding from computational analysis are correct or not, also the variation from the analytical result.

Different observations has been taken at different frequency band and using different tip of hammer by hitting at different location on the component.

This experimental analysis is done for frequency of 800 Hz, 16 KHz, 32 KHz with different tips of hammer like rubber tip, plastic tip and metallic tip.

Following measurements has been taken on mild steel cantilever beam by hitting four different positions and mounting accelerometer at the tip of the cantilever beam.

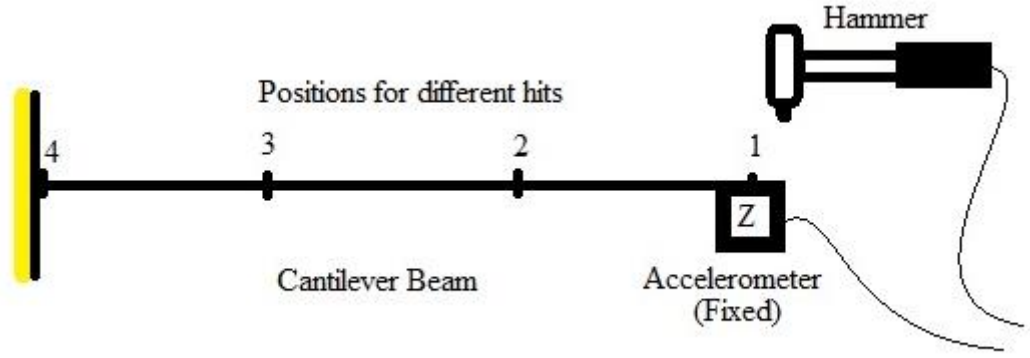

Fig.4.22. EMA of cantilever beam at different position

In the experimental modal analysis of cantilever beam four positions were marked with scriber with equal distance from the fixed position and the tip of cantilever beam. And accelerometer is fixed at the tip of the cantilever beam and different observations have been obtained by hitting the beam with hammer at different marked positions as per MIMO technique. This will results into four recording signals for four different positions as marked on the cantilever beam and then the FFT for all four observations will be obtained which will further converted into FRF (Real & Imaginary parts).

After obtaining FRF for four different positions we will focus on those regions where phase difference of 180^{o} or approx. seen in the FRF, then these frequencies marked and peaks of 180^{o} phase difference are matched which will give the mode shapes for cantilever beam only for bending frequencies.

4.4.1. Hit at position 1 of cantilever beam:

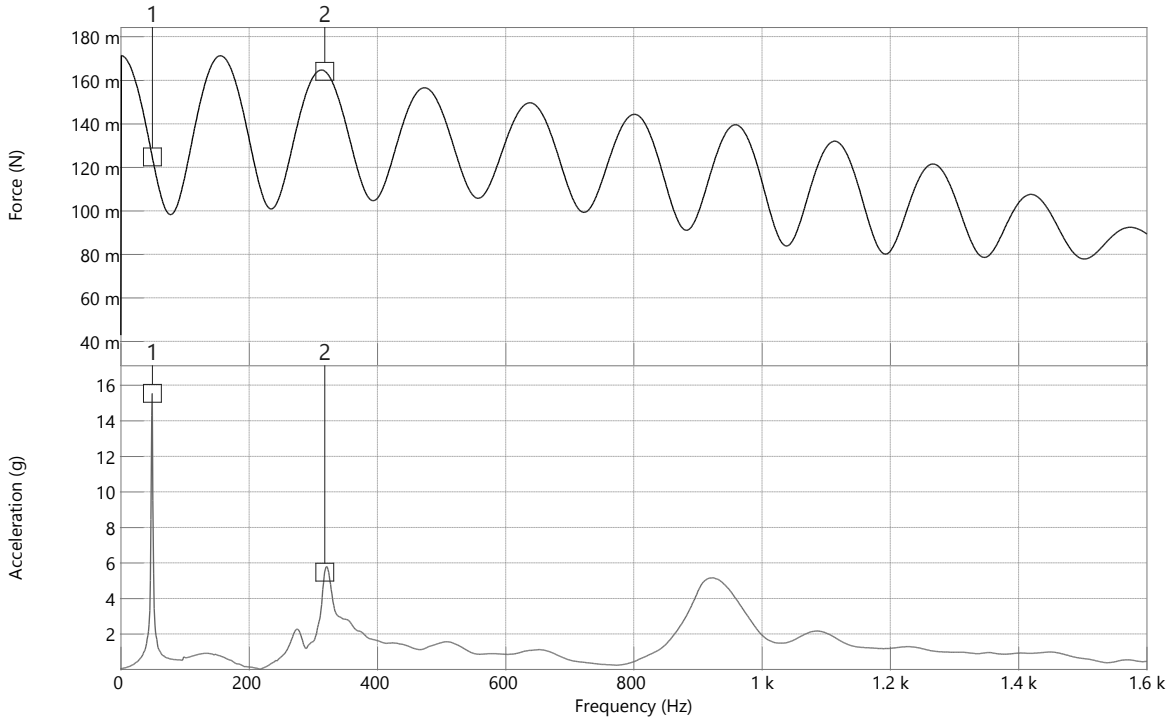

Fig.4.23. Recording Signals for hit at position 1 of cantilever beam

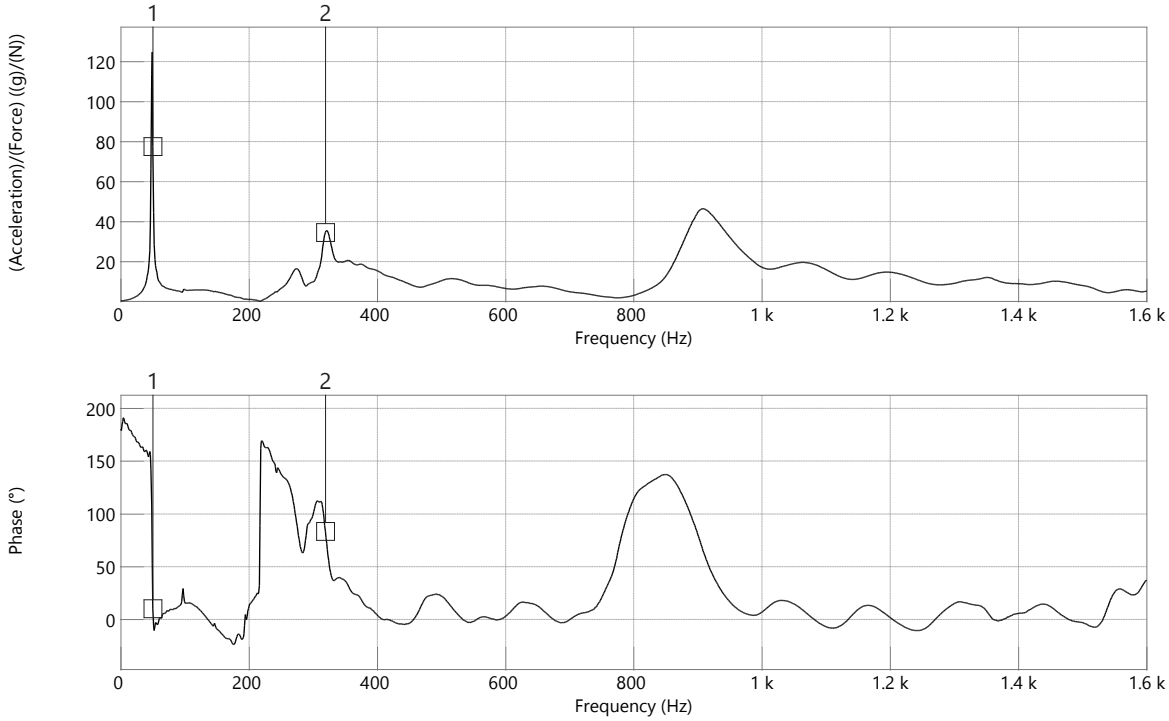

Fig.4.24. FFT obtained for hit at position 1 of cantilever beam

4.4.2. Hit at position 2 of cantilever beam:

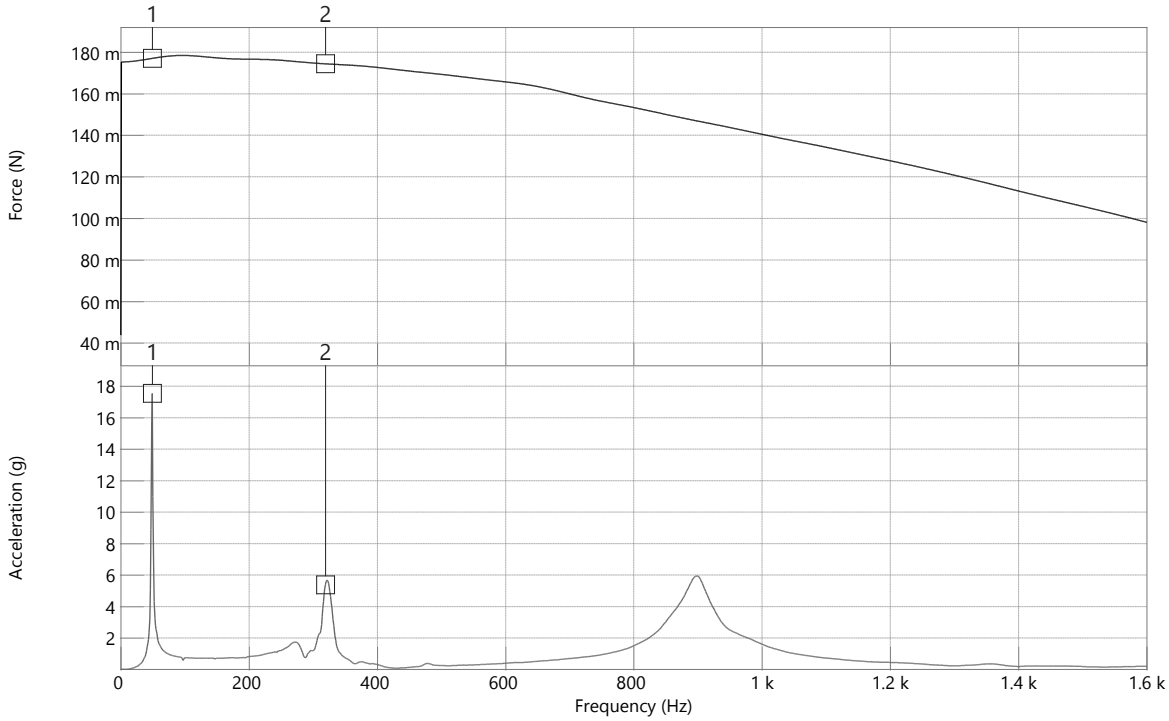

Fig.4.25.Recording Signals for hit at position 2 of cantilever beam

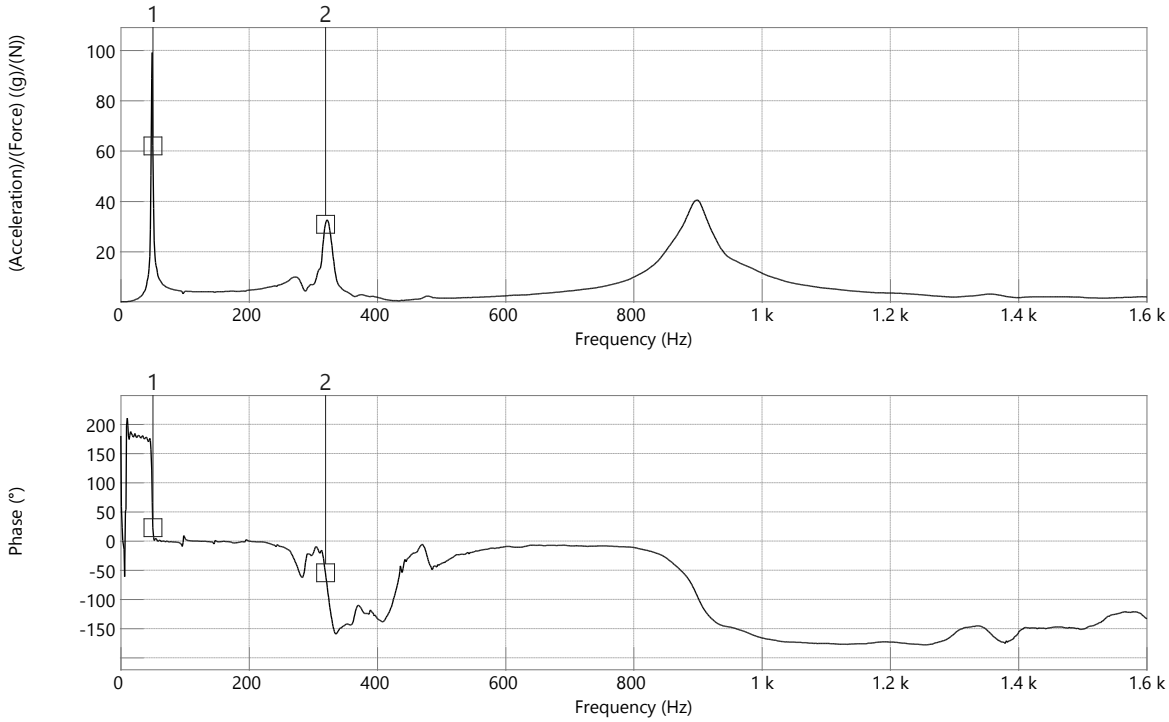

Fig.4.26. FFT obtained for hit at position 2 of cantilever beam

4.4.3. Hit at position 3 of cantilever beam:

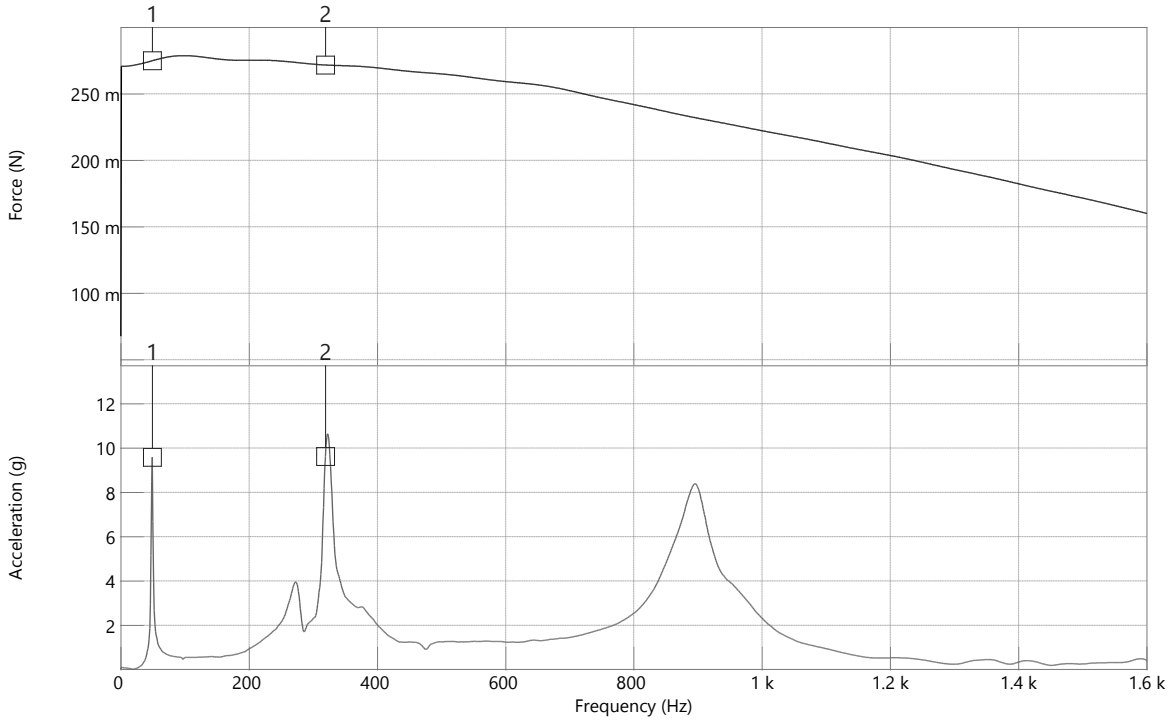

Fig.4.27. Recording Signals for hit at position 3 of cantilever beam

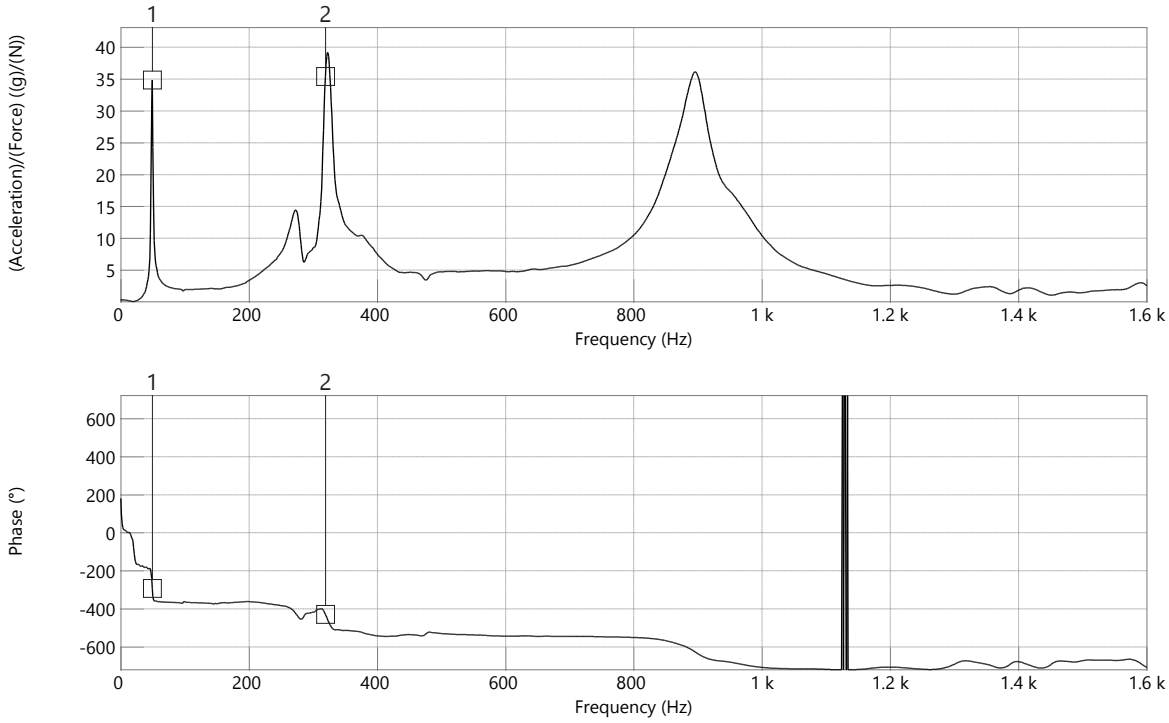

Fig.4.28. FFT obtained for hit at position 3 of cantilever beam

4.4.4. Hit at position 4 of cantilever beam:

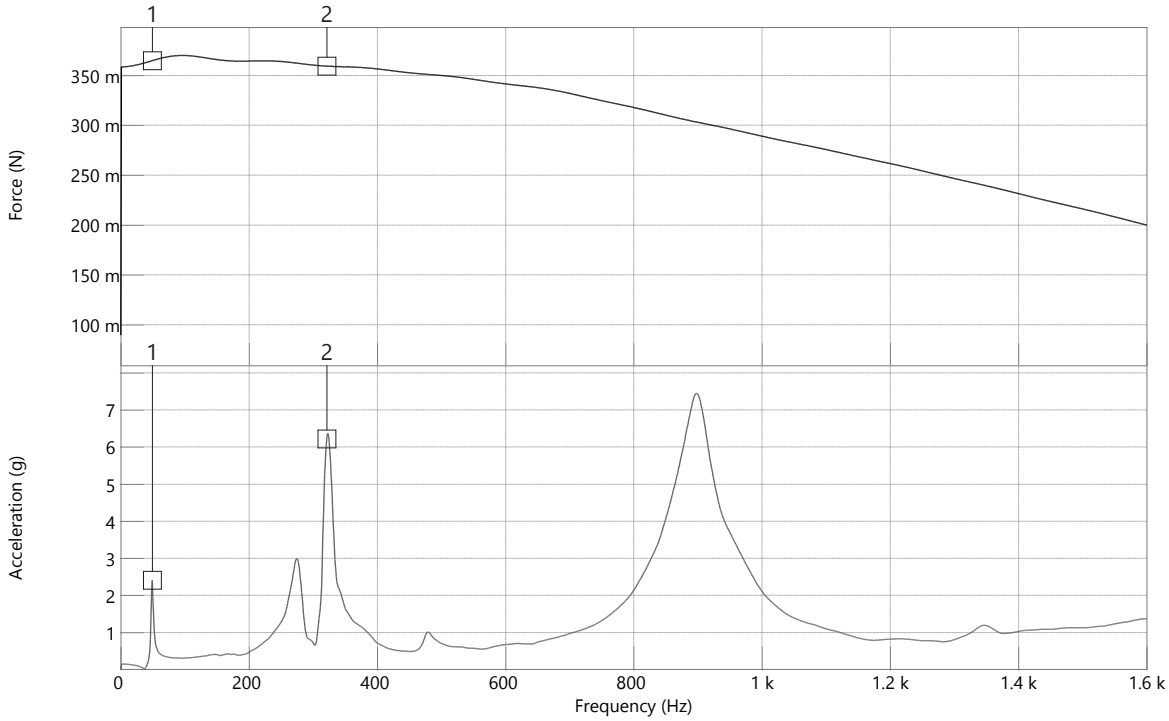

Fig.4.29.Recording Signals for hit at position 4 of cantilever beam

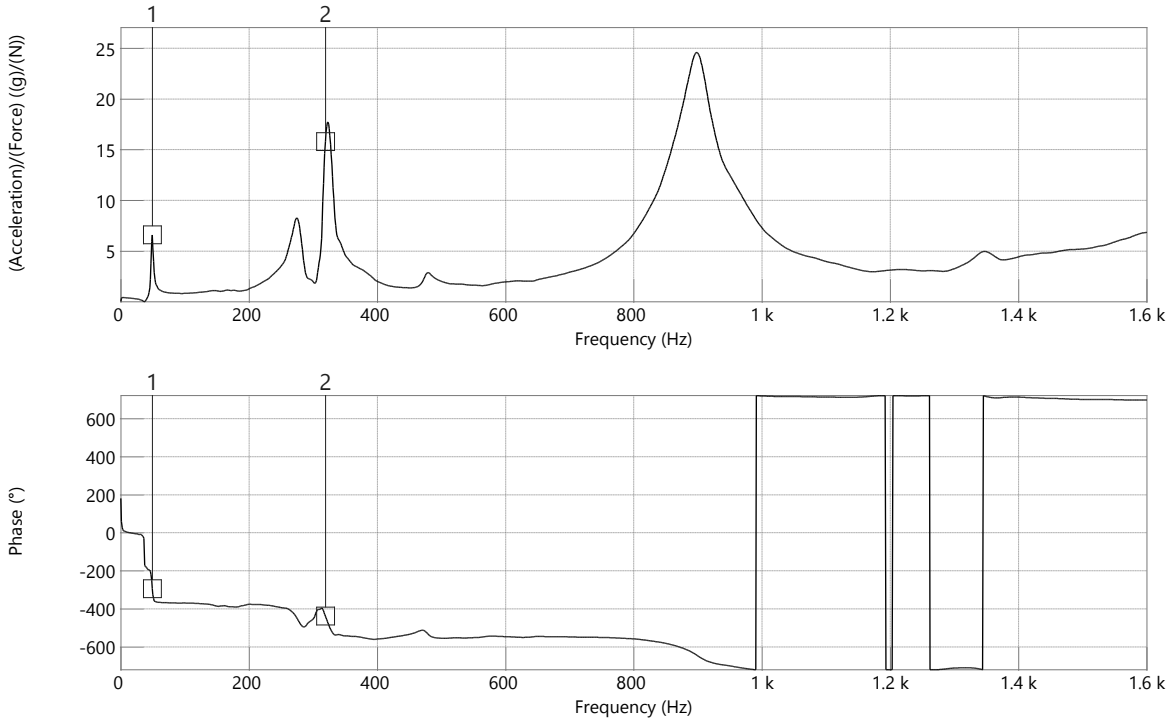

Fig.4.30.FFT obtained for hit at position 4 of cantilever beam

4.4.5. FRF obtained for cantilever beam:

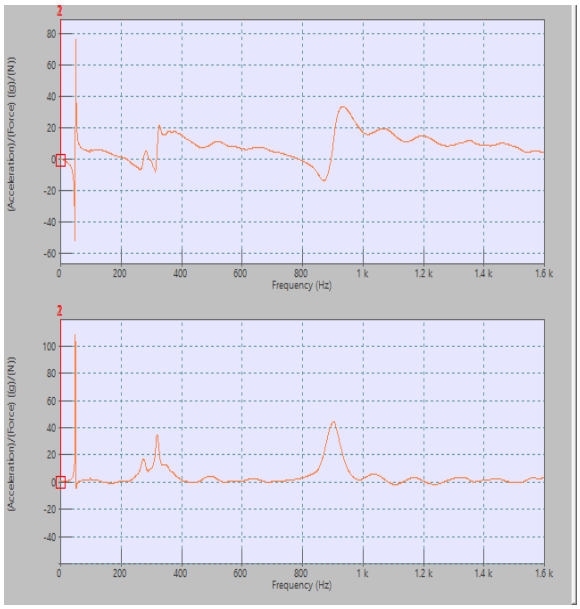

Position 1

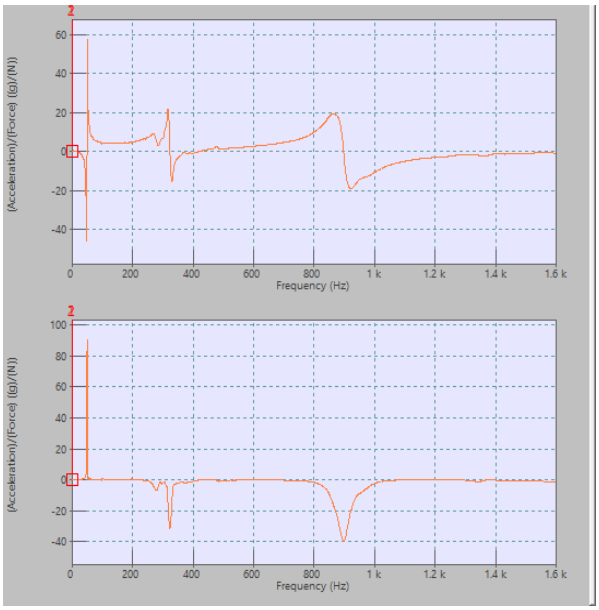

Position 2

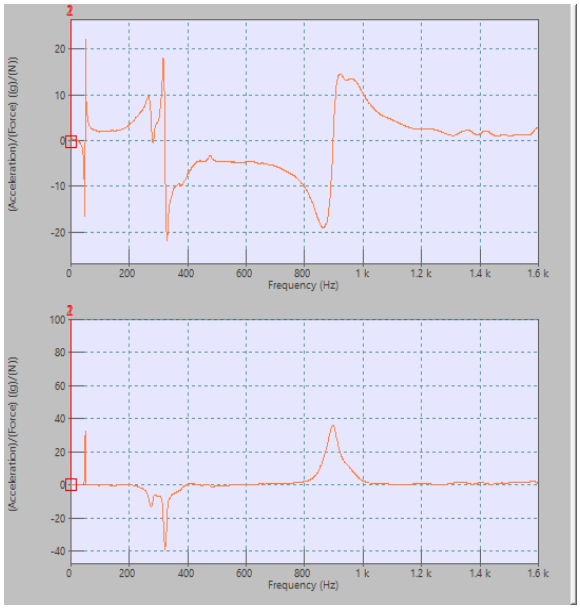

Position 3

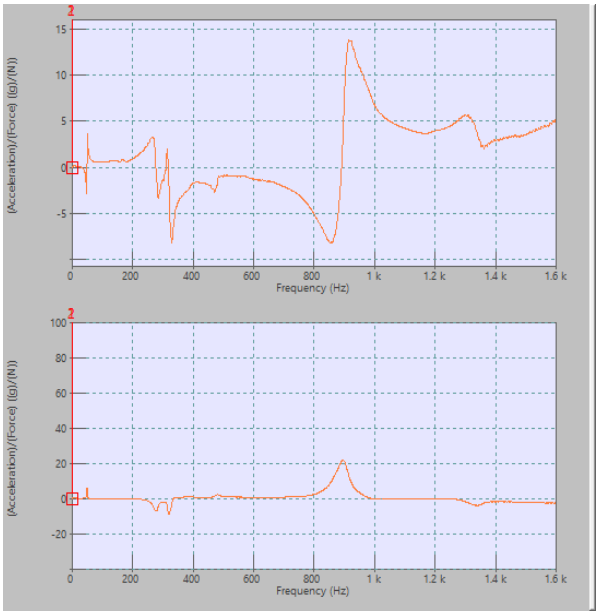

Position 4

Fig.4.31.FRF obtained by hitting at different four positions of cantilever beam.

Now all these four FRF are combined together to obtain the mode shapes of cantilever beam due to bending. And all those peaks will be marked with 180 degree phase difference an those frequencies will give the value for natural frequencies of cantilever beam by joining all those peak of FRF obtained.

4.4.6. Mode shapes obtained from FRFs for cantilever beam:

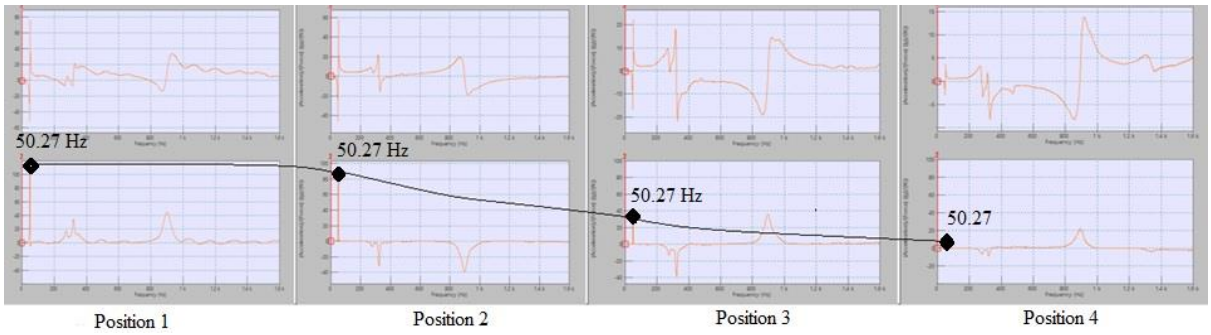

Fig.4.32. Mode Shape-1 obtained at 50.27Hz for cantilever beam

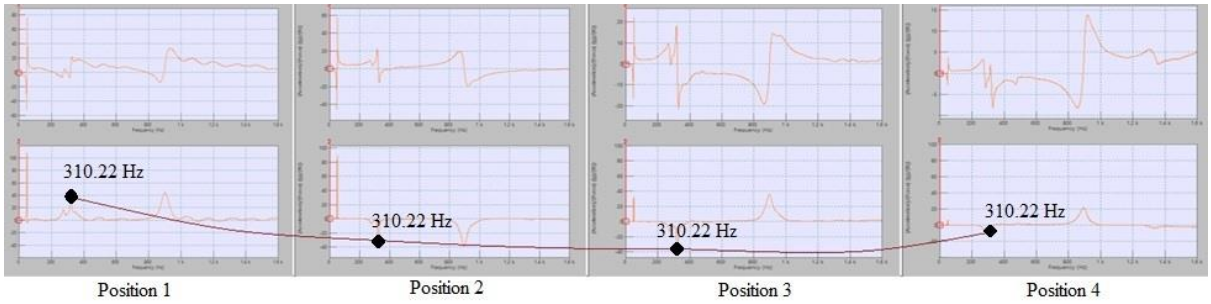

Fig.4.33. Mode Shape-2 obtained at 310.22Hz for cantilever beam

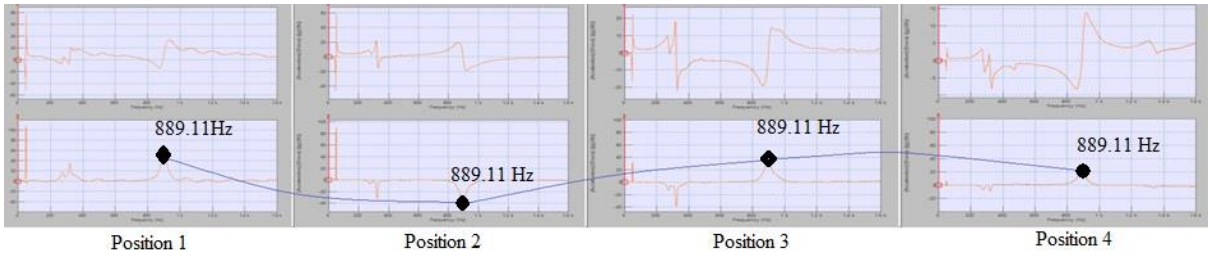

Fig.4.34. Mode Shape-3 obtained at 889.11Hz for cantilever beam

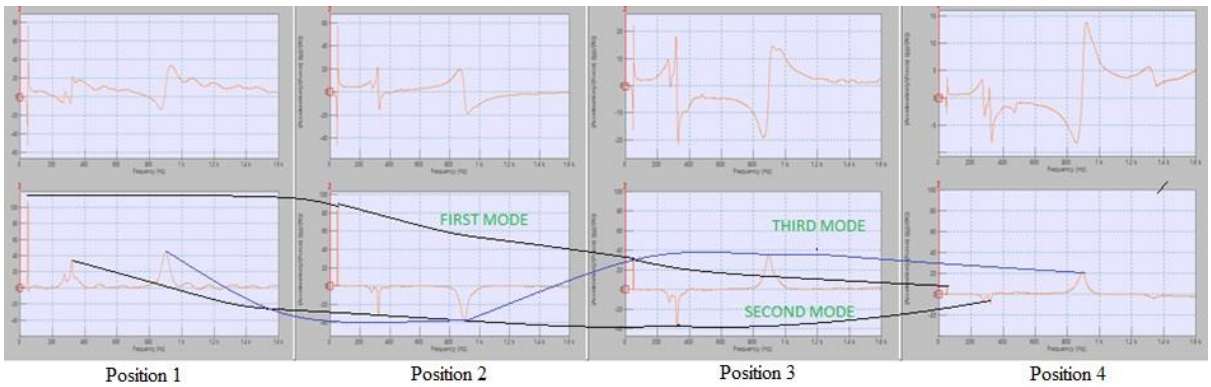

Fig.4.35. All mode shapes obtained from FRFs of cantilever beam

4.5. EMA of IN738 LP-1 gas turbine blade:

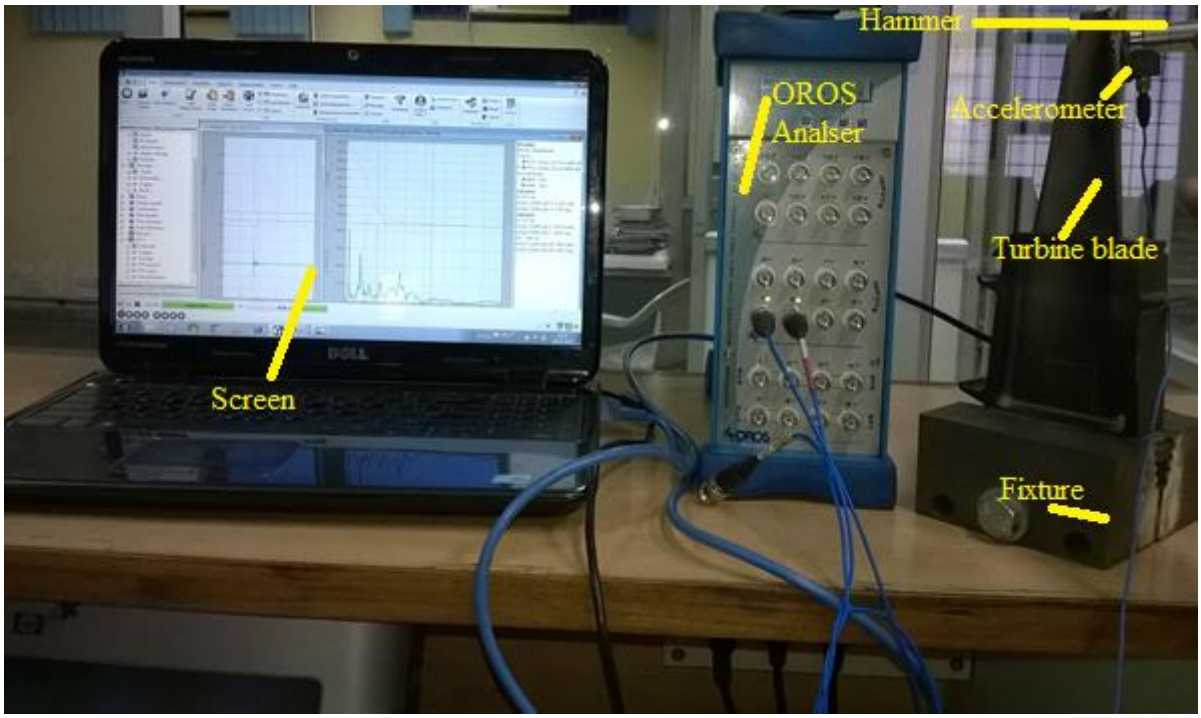

Fig.4.36. Experimental setup for EMA of turbine blade

In this experiment six different positions were marked, three on the turbine blade, two on the base (tang portion) and one at the fitree joint of the turbine blade. Here again the same procedure for cantilever beam is repeated except six observations. Accelerometer is mounted on the tip of the turbine blade and hitting is done at various positions. As cross-section of blade is not uniform hence to get FRF for a single position we hit the same cross-section from different corners and mid which does not shows any variation in the FRF signals, hence this shows that our assumptions of superimposition, homogeneity and reciprocity are validated.

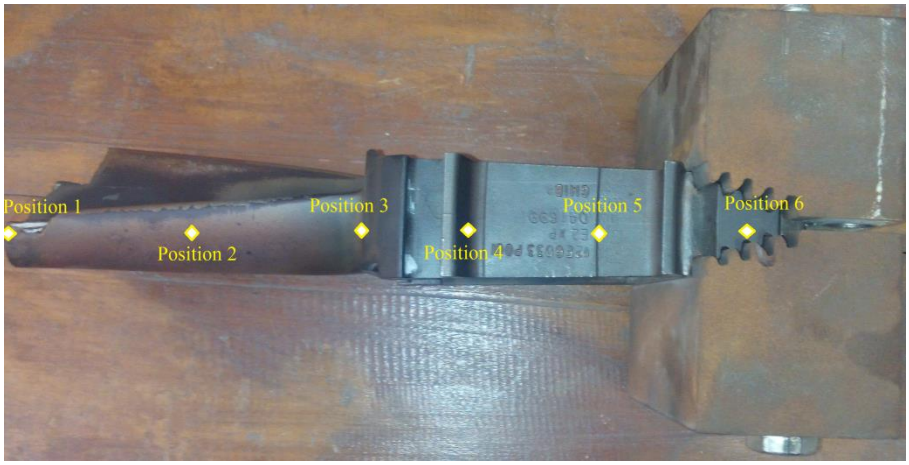

Fig.4.37. Different positions marked on turbine blade

4.5.1. Hit at position 1 of turbine blade:

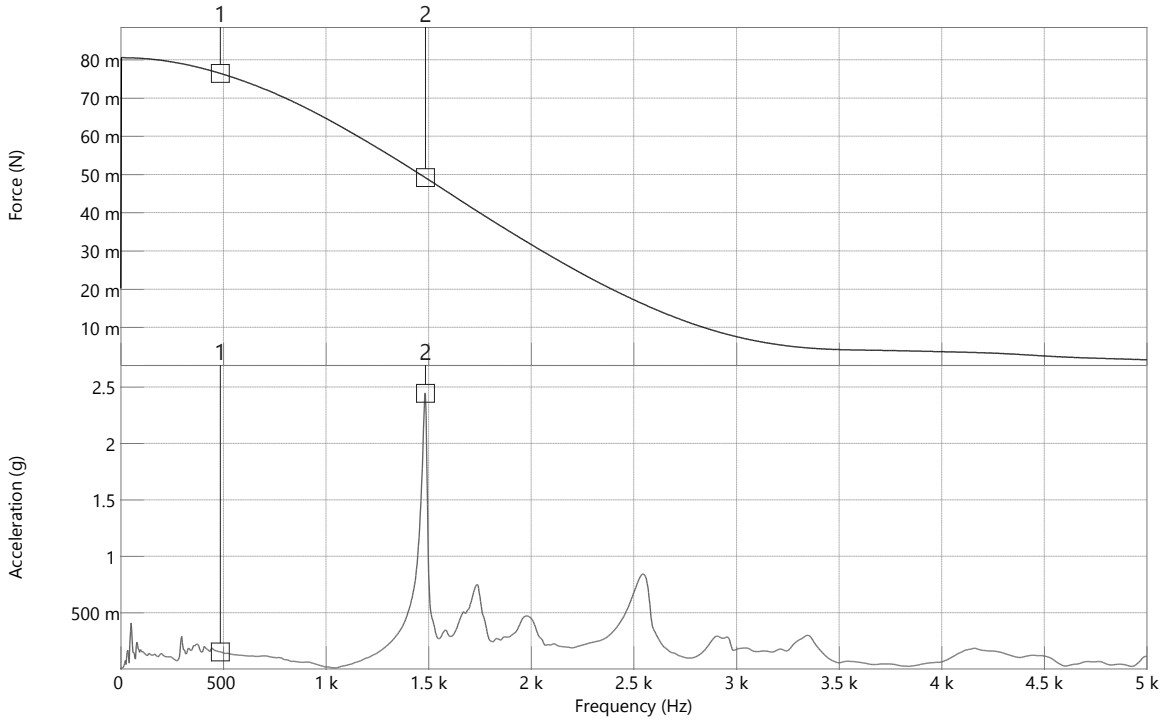

Fig.4.38. Recording Signals for hit at position 1 of turbine blade

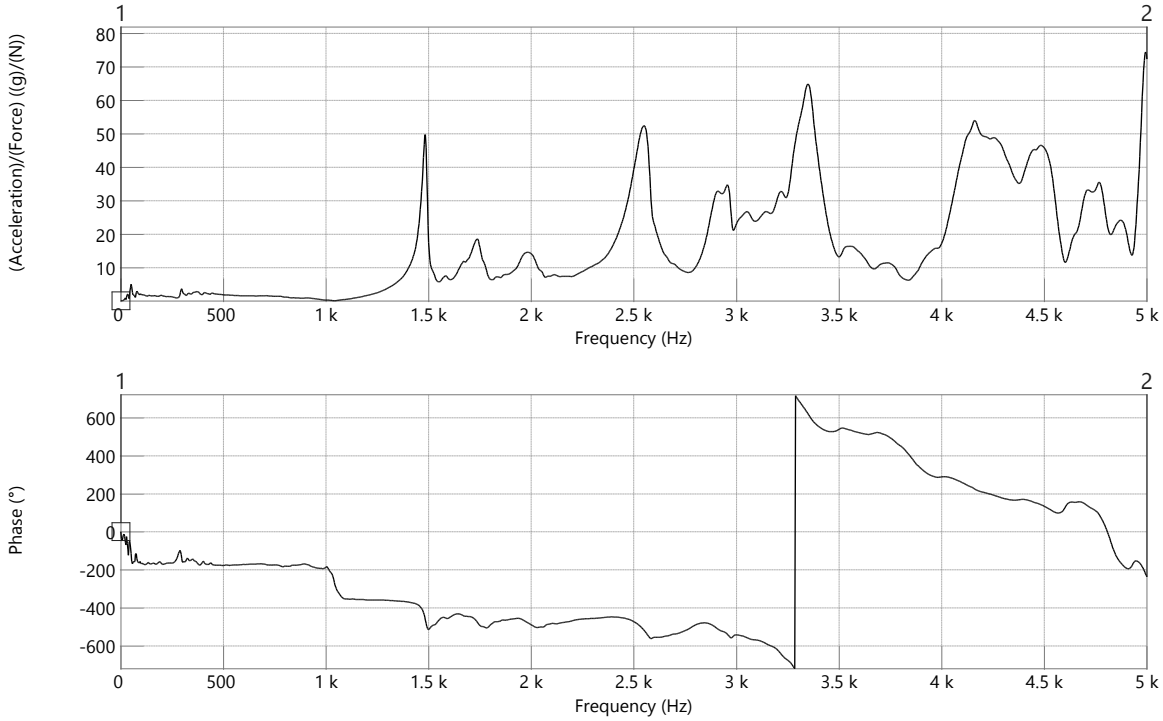

Fig.4.39. FFT obtained for hit at position 1 of turbine blade

4.5.2. Hit at position 2 of turbine blade:

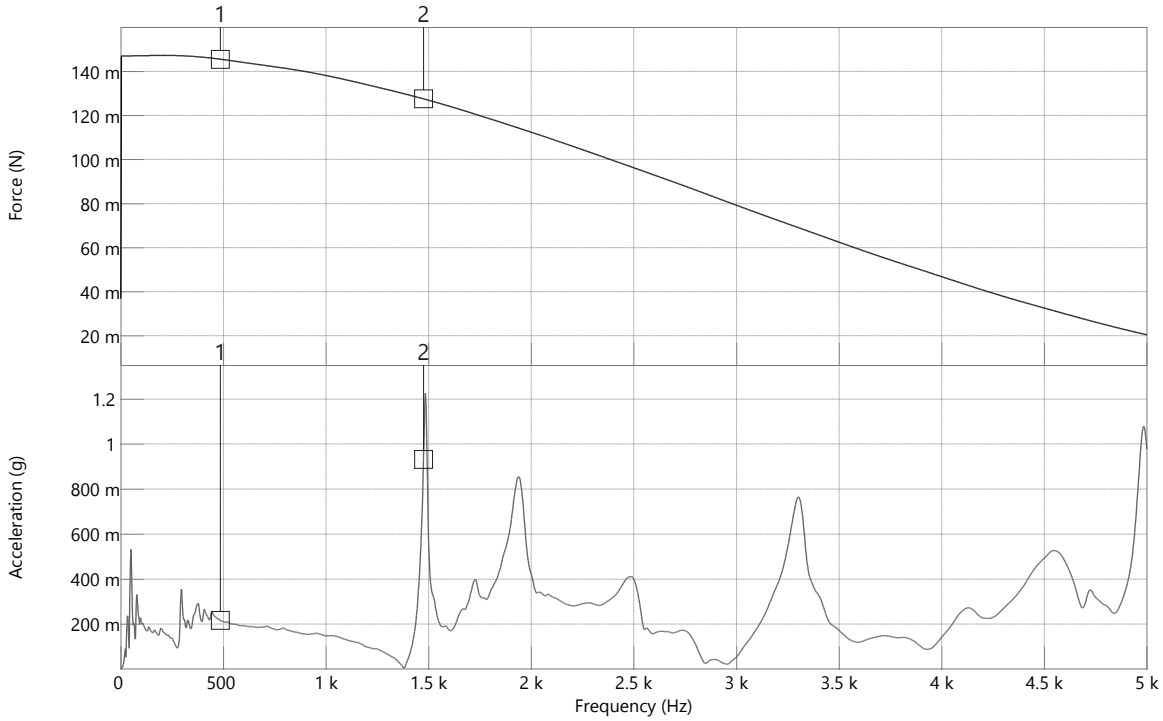

Fig.4.40. Recording Signals for hit at position 2 of turbine blade

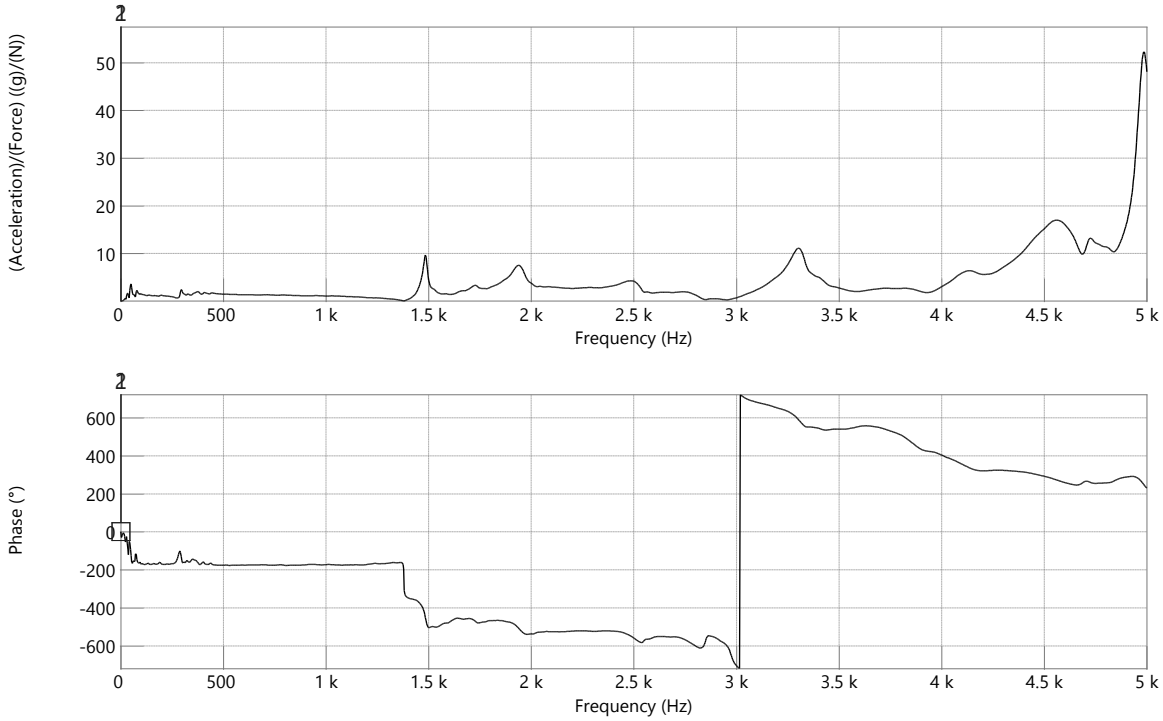

Fig.4.41. FFT obtained for hit at position 2 of turbine blade

4.5.3. Hit at position 3 of turbine blade:

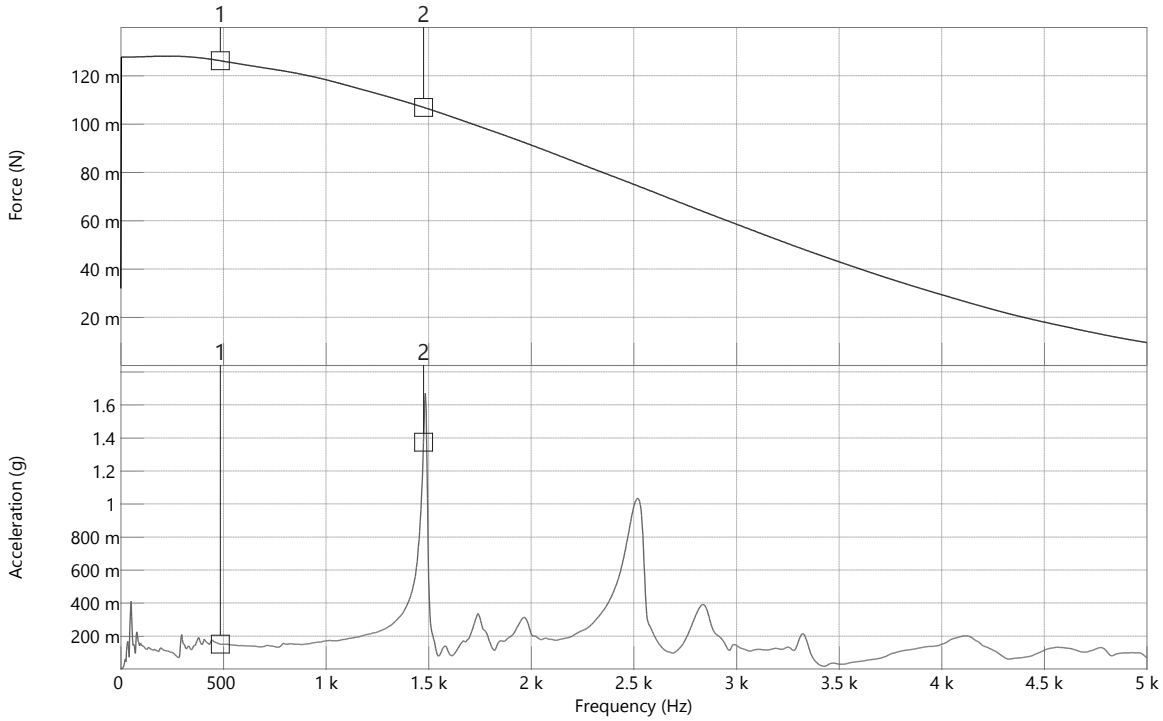

Fig.4.42. Recording Signals for hit at position 3 of turbine blade

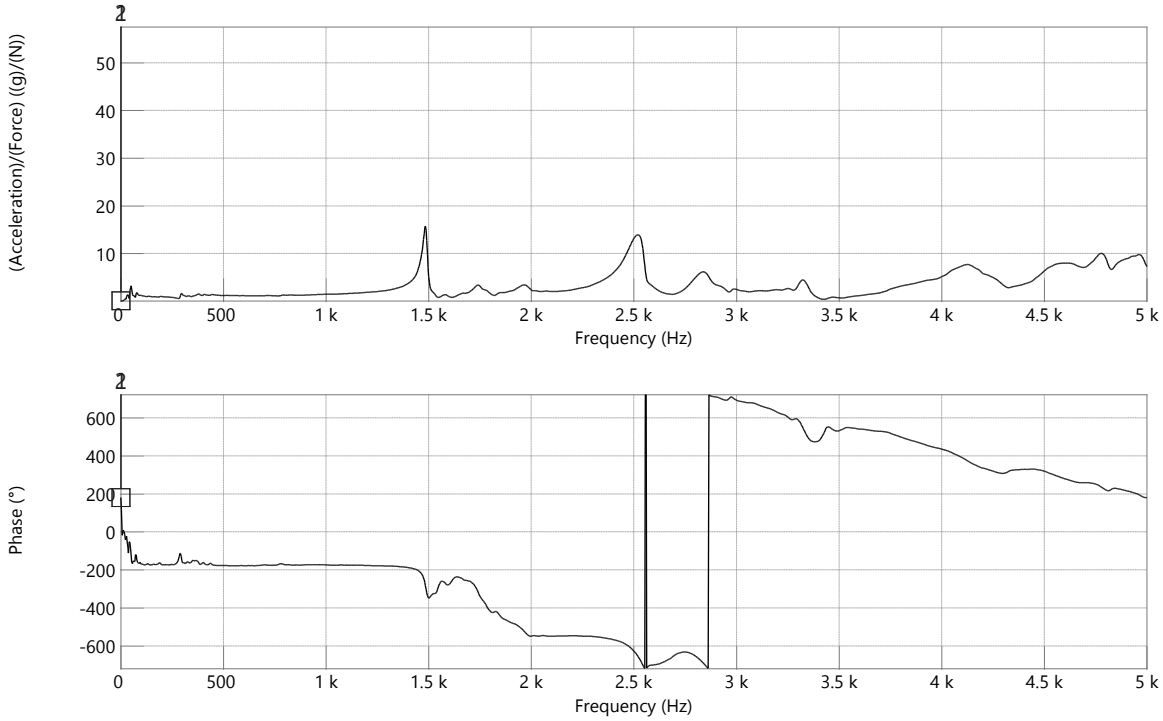

Fig.4.43. FFT obtained for hit at position 3 of turbine blade

4.5.4. Hit at position 4 of turbine blade:

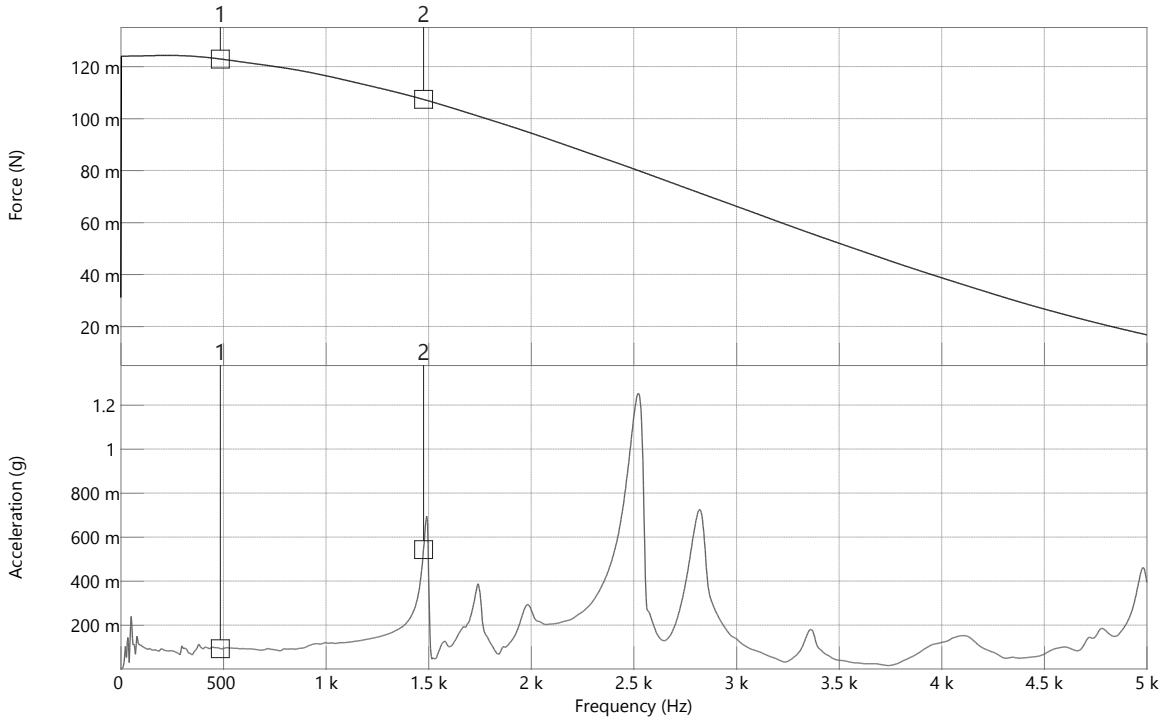

Fig.4.44. Recording Signals for hit at position 4 of turbine blade

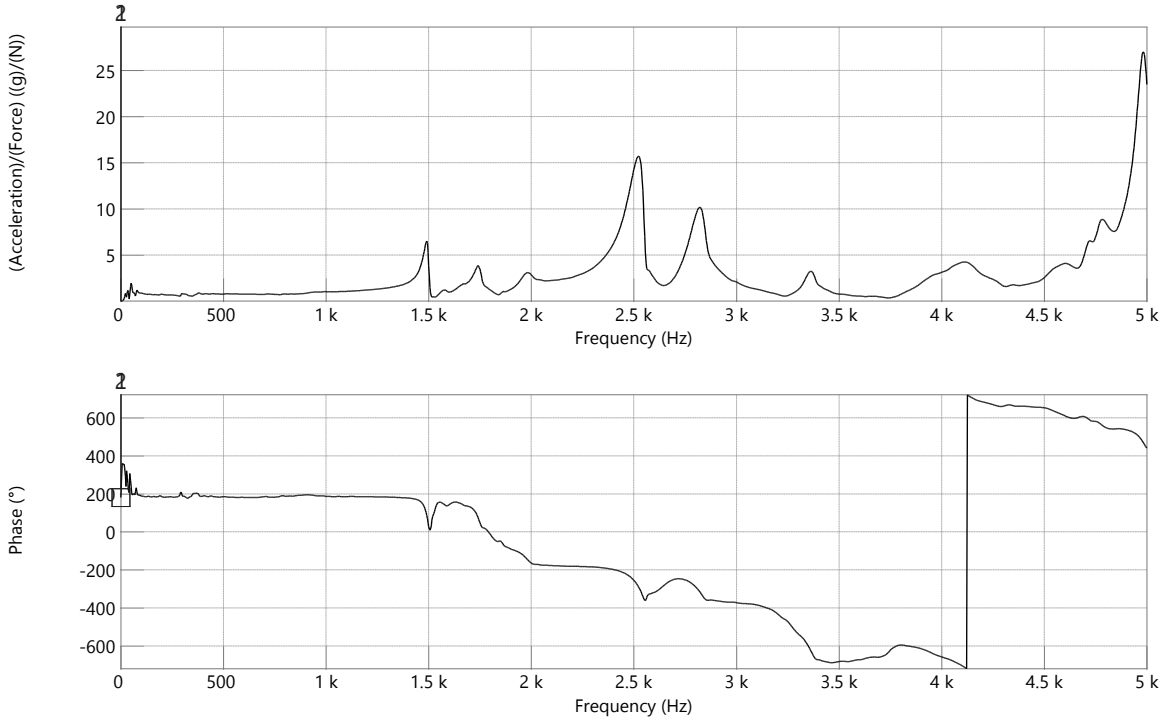

Fig.4.45. FFT obtained for hit at position 4 of turbine blade

4.5.5. Hit at position 5 of turbine blade:

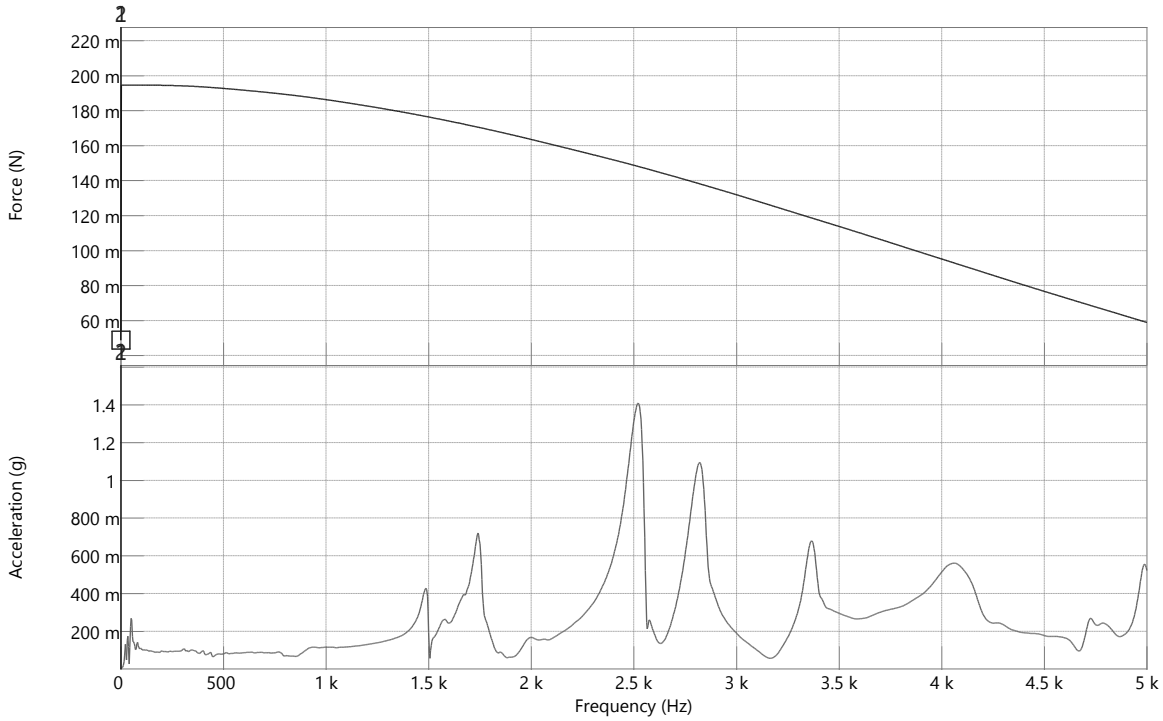

Fig.4.46. Recording Signals for hit at position 5 of turbine blade

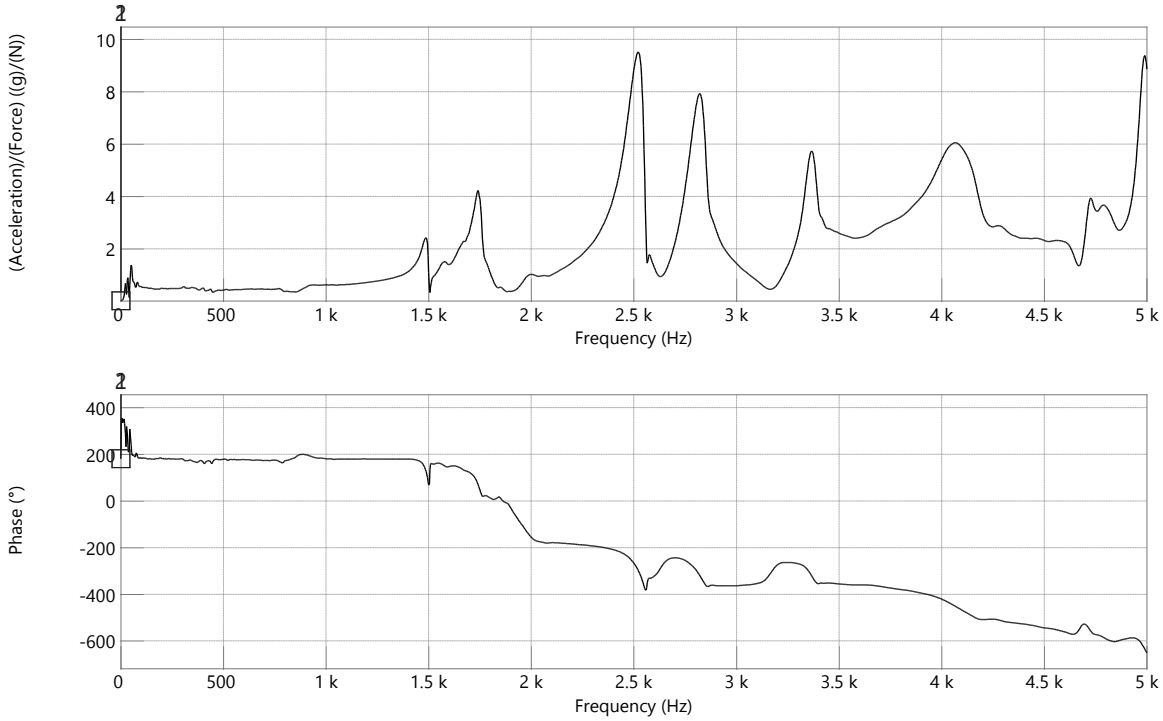

Fig.4.47. FFT obtained for hit at position 5 of turbine blade

4.5.6. Hit at position 6 of turbine blade:

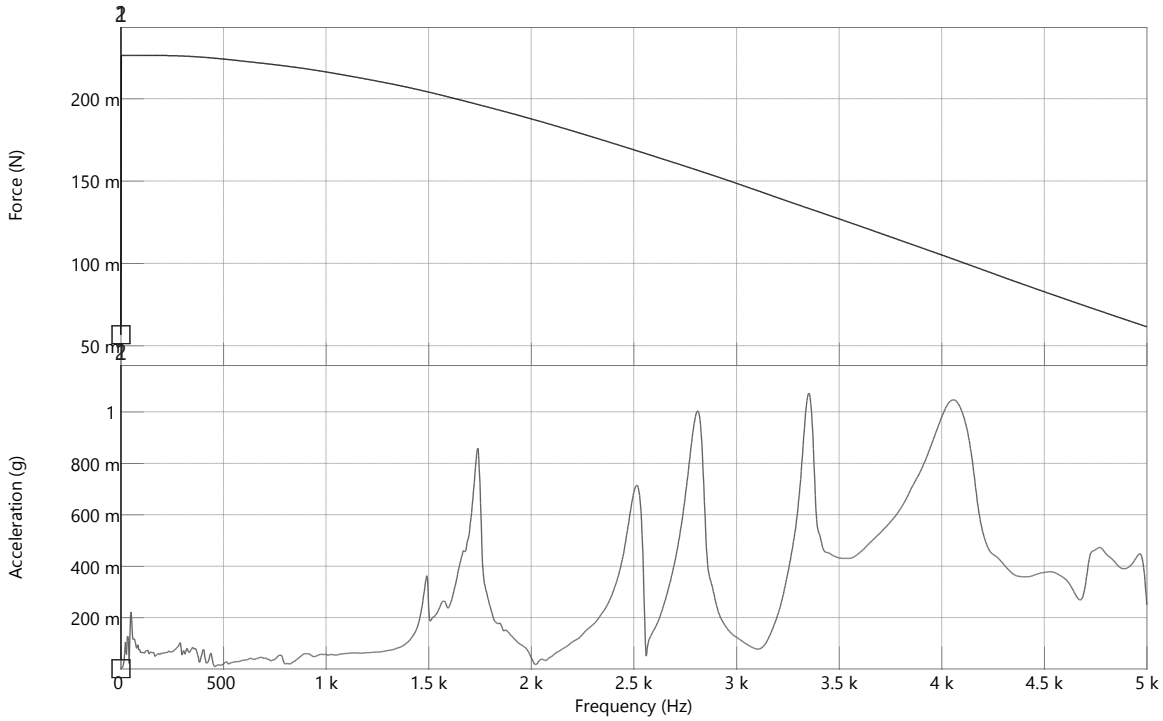

Fig.4.48. Recording Signals for hit at position 6 of turbine blade

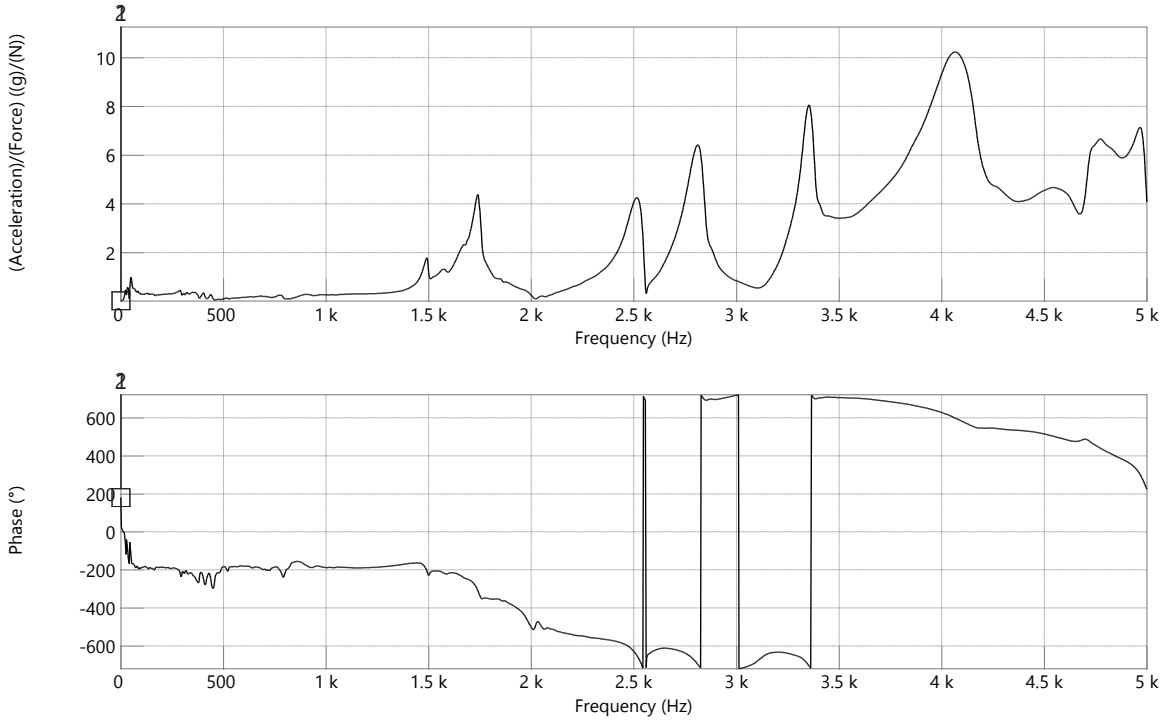

Fig.4.49. FFT obtained for hit at position 6 of turbine blade

4.5.7. FRF imaginary part obtained for turbine blade:

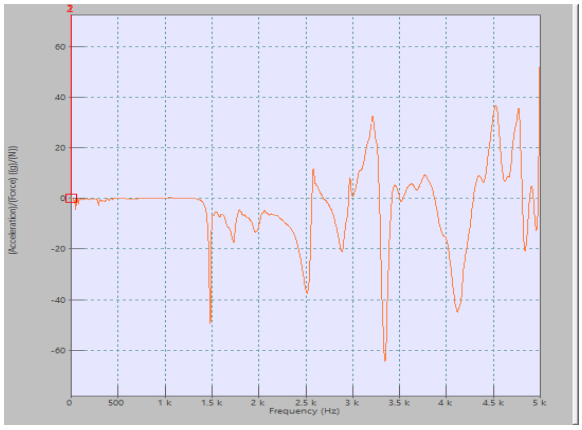

Position 1

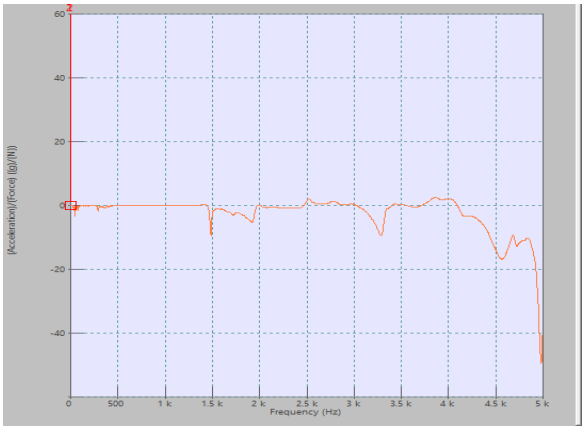

Position 2

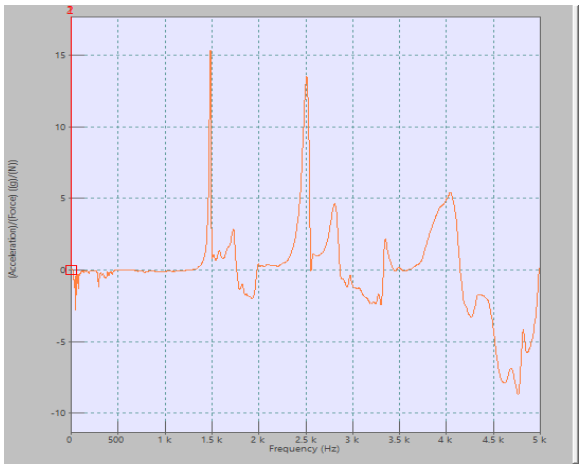

Position 3

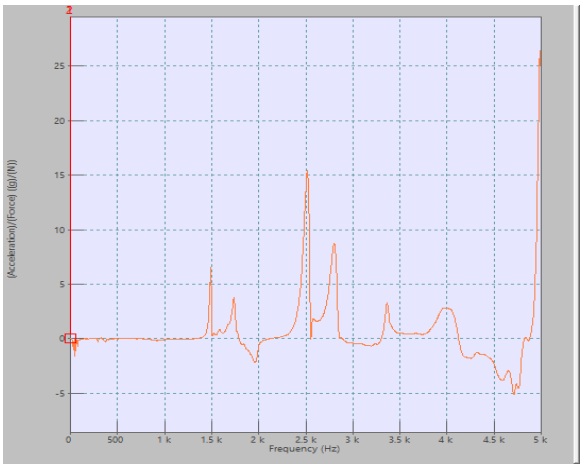

Position 4

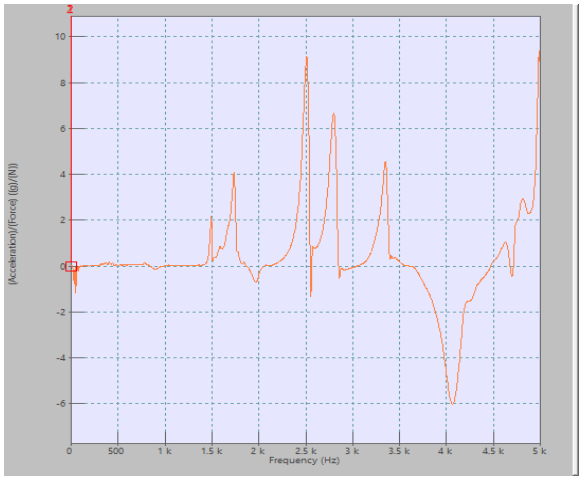

Position 5

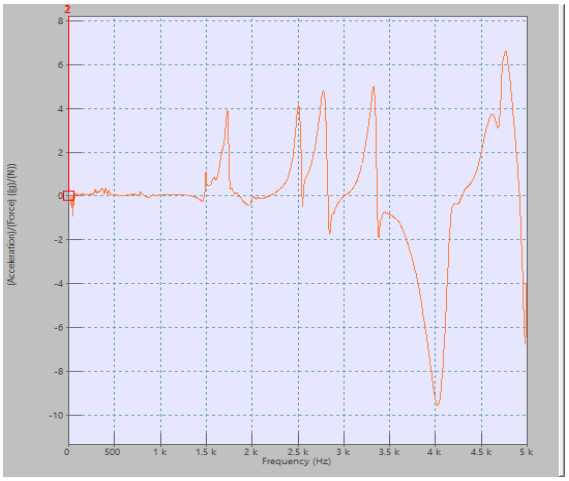

Position 6

Fig.4.50. FRF (Imaginary) obtained by hitting at different four positions of turbine blade

4.5.8. Mode shapes obtained from FRFs for gas turbine blade:

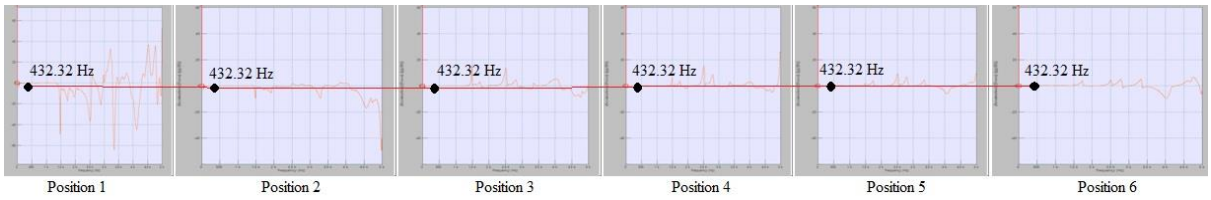

Fig. Mode shape-1obtained at 432.2Hz for gas turbine blade

Fig. Mode shape-2 obtained at 1496.6Hz for gas turbine blade

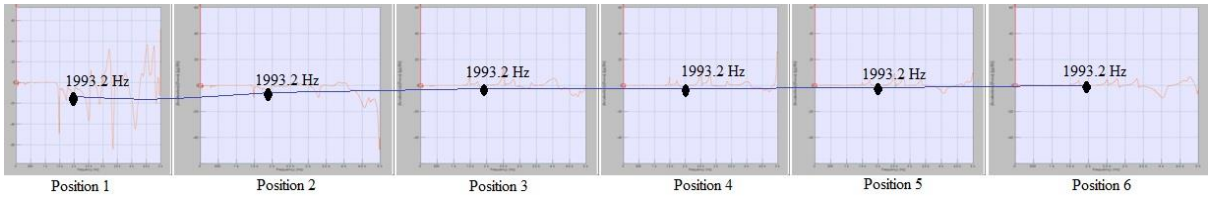

Fig. Mode shape-3 obtained at 1993.2Hz for gas turbine blade

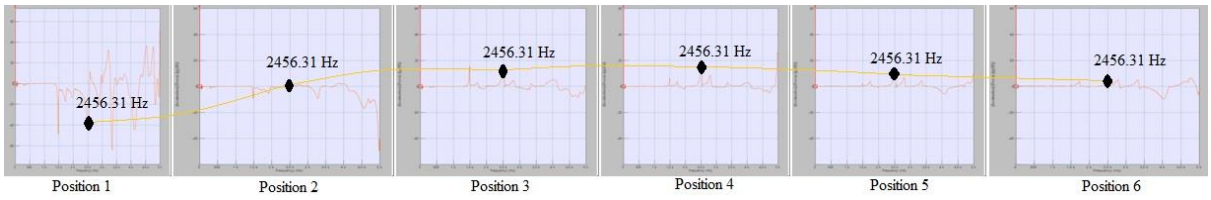

Fig. Mode shape-4 obtained at 2456.31Hz for gas turbine blade

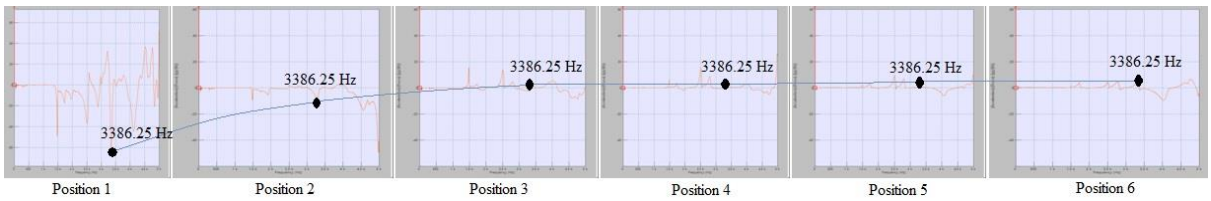

Fig. Mode shape-5 obtained at 3386.25Hz for gas turbine blade

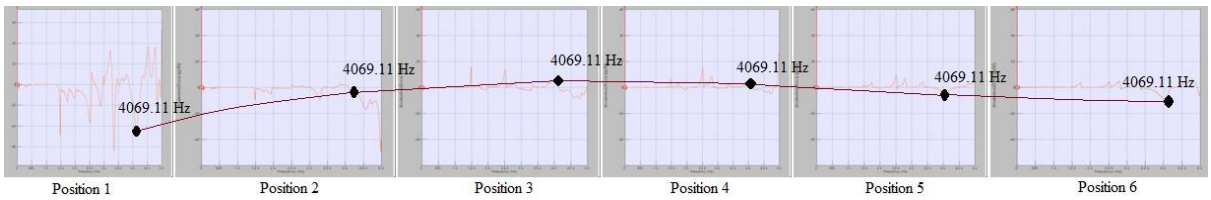

Fig.4.51. Mode shape-6 obtained at 4069.11Hz for gas turbine blade

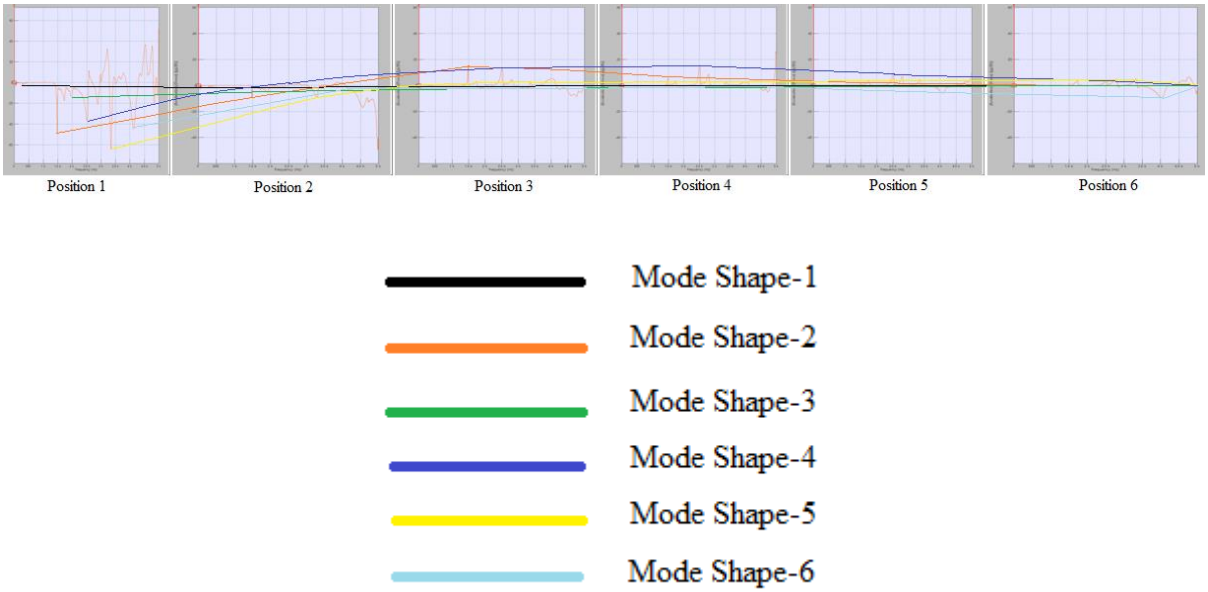

Fig.4.52. All mode shapes obtained from FRFs of gas turbine blade.

4.6. Results of EMA:

4.6.1. Modal frequencies obtained from EMA:

Following results have been obtained from the experimental modal analysis of gas turbine blade and cantilever beam:

Table.4.4. Modal frequencies for cantilever beam obtained from EMA

Modes	Frequency	Factor
Mode-1	50.27	Bending
Mode-2	310.22	Bending
Mode-3	889.11	Bending

Table.4.5. Modal frequencies for gas turbine blade obtained from EMA

Modes	Frequency	Factor
Mode-1	432.2	
Mode-2	1496.6	
Mode-3	1993.2	
Mode-4	2456.31	
Mode-5	3386.25	
Mode-6	4069.11	

4.6.2. Damping factor obtained from resonance peak:

For Cantilever Beam:

Form the highest resonance peak we applying quadrature peak method to obtain the damping factor value for cantilever beam material. Using the following formula:

$$\varepsilon = \frac{w2 - w1}{2w}$$

As, $w_1 = 892$ Hz , $w_2 = 932$ Hz , $w = 910$ Hz

Hence, $\varepsilon = \frac{932-892}{2\times910} = 0.022$

For Gas Turbine Blade:

Same formula we are using in the case of gas turbine to determine the value of damping factor:

Here, $w_1 = 2474.92$ Hz , $w_2 = 2624.08$ Hz , $w = 2538.71$ Hz

Hence, $\varepsilon = \frac{2624.08-2474.92}{2\times2538.71} = 0.029377$

CHAPTER-5

COMPUTATIONAL MODELLING & ANALYSIS

In this exercise Modal and Structural analysis of the same cantilever beam and gas turbine blade is done using ANSYS 15.0 version. Modal analysis is done to identify the natural frequencies of failure and mode shapes under different failure modes, whereas structural analysis gives us the distribution of maximum and minimum stress and strain in cantilever beam and gas turbine blade both.

These results of modal analysis are validated with experimental modal analysis results in order to get the surety. Using ANSYS 15.0 we can determine multiple numbers of modes but here we focusing only on the first six modes of cantilever beam and turbine blade both.

The overall procedure for analysis in ANSYS 15.0 is given below:

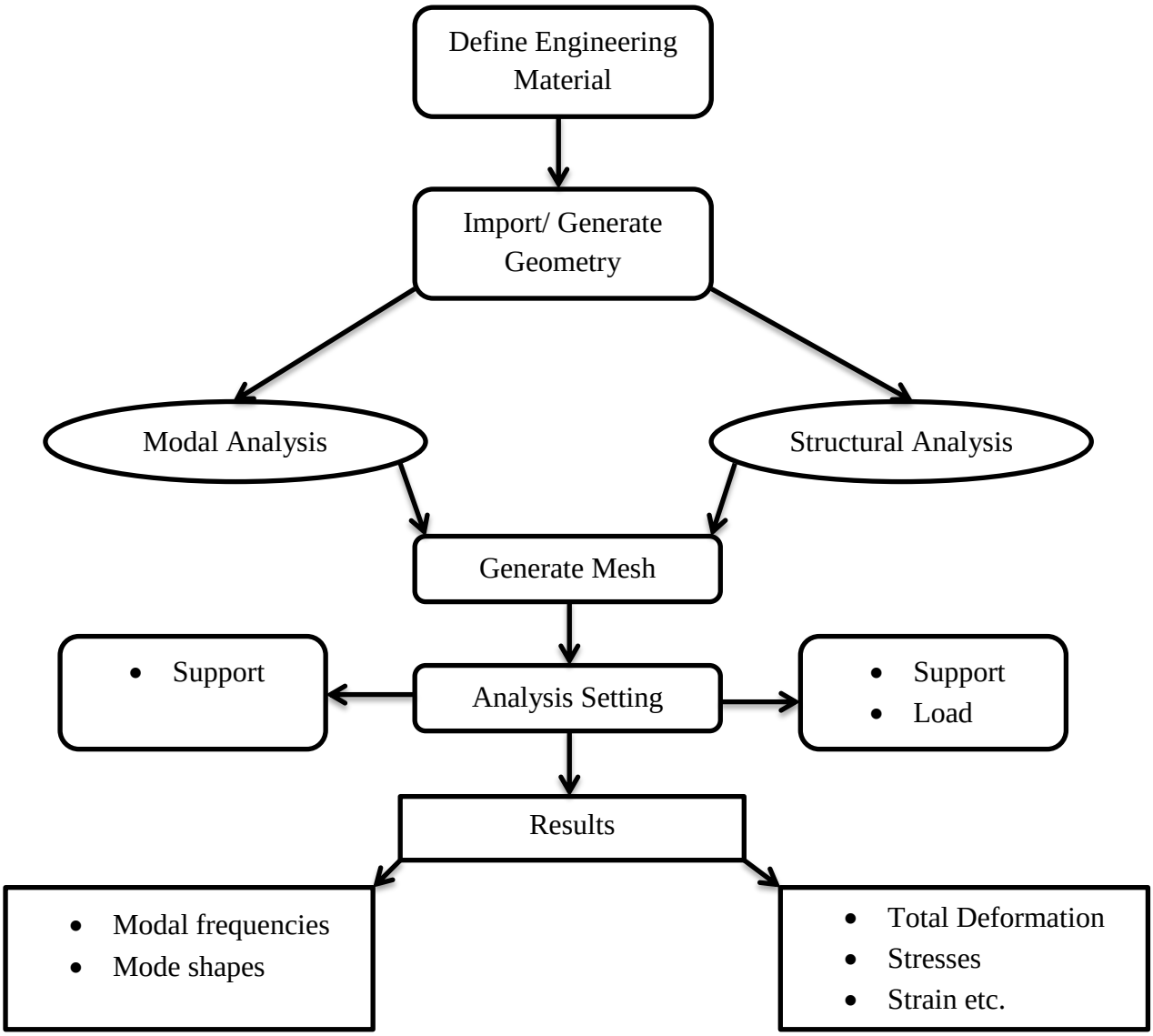

5.1. Modal and Structural analysis of cantilever beam using ANSYS 15.0 Workbench.

Cantilever beam is subjected to modal analysis for validation of OROS experimental modal analysis. In this modal and structural analysis of cantilever beam all dimensions, units, boundary conditions, parameters and results have been shown in tabular form with appropriate graphs and diagrams.

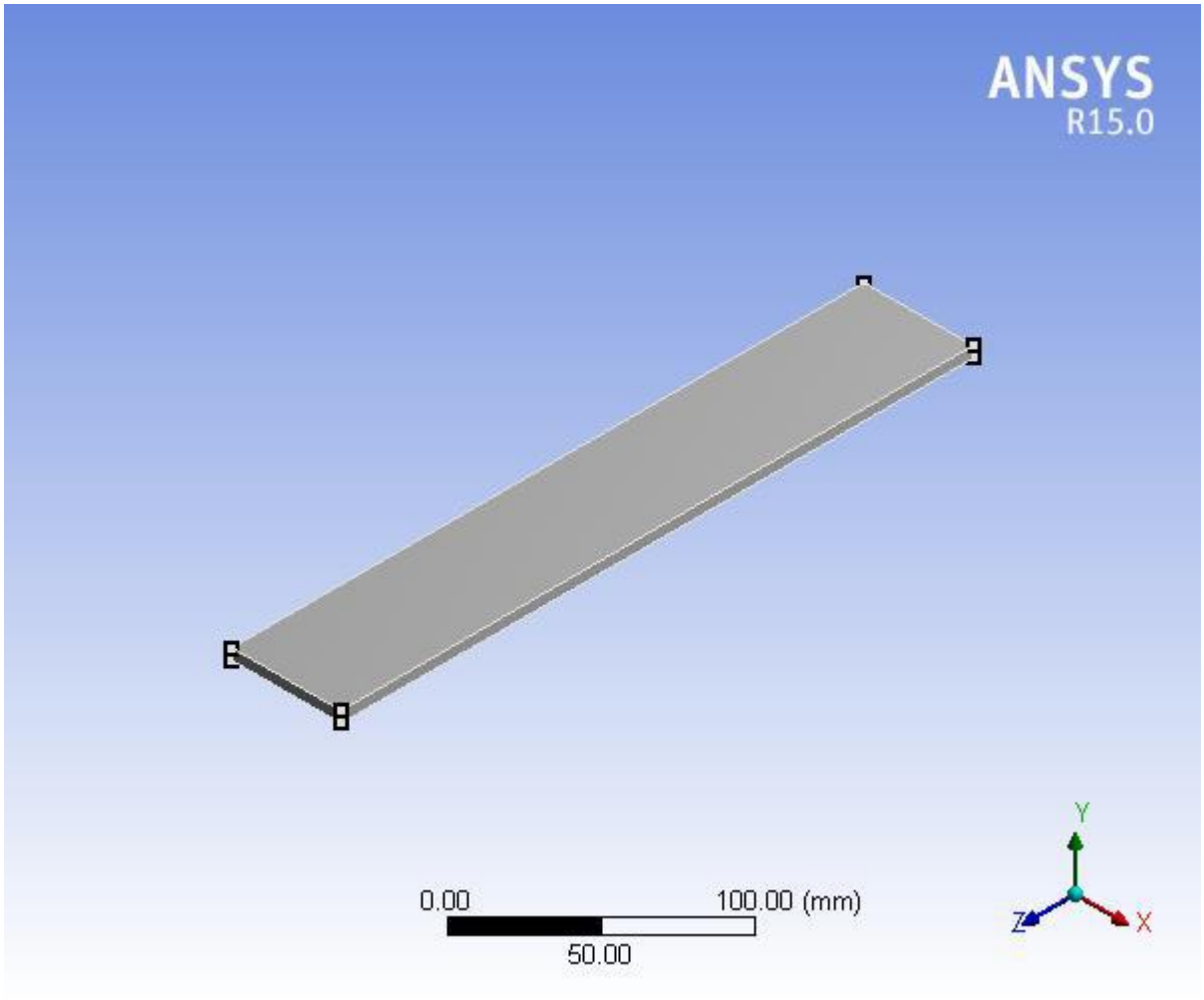

Fig. 5.1. Cantilever beam model

Table 5.1. Units for beam model

Unit System	Metric (mm, kg, N, s, mV, mA) Degrees rad/s Celsius
Angle	Degrees
Rotational Velocity	rad/s
Temperature	Celsius

Table 5.2. Geometry

Object Name	*Geometry*
State	Fully Defined
Definition	
Type	Design Modeller
Display Style	Body Colour
Bounding Box	
Length X	50. mm
Length Y	5. mm
Length Z	290. mm
Properties	
Volume	72500 mm^3
Mass	0.56912 kg
Scale Factor Value	1
Statistics	
Bodies	1
Active Bodies	1
Nodes	78707
Elements	15300
Analysis Type	3-D

In this analysis geometry is created using ANSYS design modeller using metric system of units followed by fine meshing and then boundary conditions will be applied over it according to given physical and environmental conditions. Then after applying appropriate boundary conditions and meshing to the component we will proceed to analysis part for structural and modal analysis.

Table 5.3. Part Specification

Object Name	*Solid*
State	Meshed
Graphics Properties	
Visible	Yes
Transparency	1
Definition	
Suppressed	No
Stiffness Behaviour	Flexible
Coordinate System	Default Coordinate System
Material	
Assignment	Mild Steel
Nonlinear Effects	Yes
Thermal Strain Effects	Yes
Properties	
Centroid X	34.041 mm
Centroid Y	41.535 mm
Centroid Z	145. mm
Moment of Inertia Ip1	3989.8 kg·mm²
Moment of Inertia Ip2	4107.2 kg·mm²
Moment of Inertia Ip3	119.75 kg·mm²

Data obtained from the part specifications of the model also used in the manual calculation for determining modal frequencies and modal parameters of cantilever beam. Hence these parameters are useful in manual and computational analysis both and are correct data as per the specification.

Table 5.4. Coordinate System

Object Name	*Global Coordinate System*
State	Fully Defined
Definition	
Type	Cartesian
Origin	
Origin X	0. mm
Origin Y	0. mm
Origin Z	0. mm
Directional Vectors	
X Axis Data	[1. 0. 0.]
Y Axis Data	[0. 1. 0.]
Z Axis Data	[0. 0. 1.]

Coordinate system plays very important role during modelling and analysis of any component and assembly, hence we generally used to operate from origin in order to get convenience for coordinates. All the work in the graphical interface has been done in Cartesian coordinate system with origin situated at (0,0,0) and directional vectors defined in the Table 5.4.

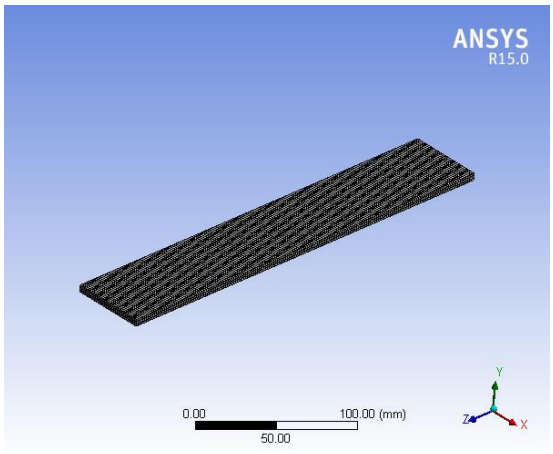

Fig. 5.2. Fully meshed beam

Table 5.5. Meshing

Object Name	*Mesh*
State	Solved
Defaults	
Physics Preference	Mechanical
Relevance	60
Sizing	
Use Advanced Size Function	On: Proximity and Curvature
Relevance Center	Fine
Initial Size Seed	Active Assembly
Smoothing	Medium
Transition	Fast
Span Angle Center	Fine
Curvature Normal Angle	Default (70.3950 °)
Min Size	Default (4.2967e-002 mm)
Proximity Min Size	Default (4.2967e-002 mm)
Max Face Size	Default (4.29670 mm)
Max Size	Default (8.59330 mm)
Growth Rate	Default (1.850)
Minimum Edge Length	5.0 mm
Inflation	
Inflation Option	Smooth Transition
Transition Ratio	0.272
Maximum Layers	5
Growth Rate	1.2

Meshing is done using automatic controlled meshing, in which narrow sections and entities meshed very fine whereas those regular sections comparatively meshed coarse in those regions. Because it is very difficult to provide meshing to narrow sections, that's why we used automatic meshing. In this type on meshing elements are of tetrahedral meshing elements and sweep meshing. As fine as possible will be the mesh finest will the result obtained.

5.1.1. Static structural analysis of cantilever beam:

Table 5.6. Boundary conditions

Object Name	*Fixed Support*	*Force*
State	Fully Defined	
Scope		
Scoping Method	Geometry Selection	
Geometry	1 Face	1 Edge
Definition		
Suppressed	No	
Define By		Components
Coordinate System		Global Coordinate System
X Component		0. N (ramped)
Y Component		-10. N (ramped)
Z Component		0. N (ramped)

One end of the cantilever beam is fixed by fixing one end surface and we applied a 10 N force at opposite edge of the beam as applied in the case of experimental modal analysis. Hence only two boundary conditions have been applied here, one is fixed support and another is load of 10 N (gradually applied load).

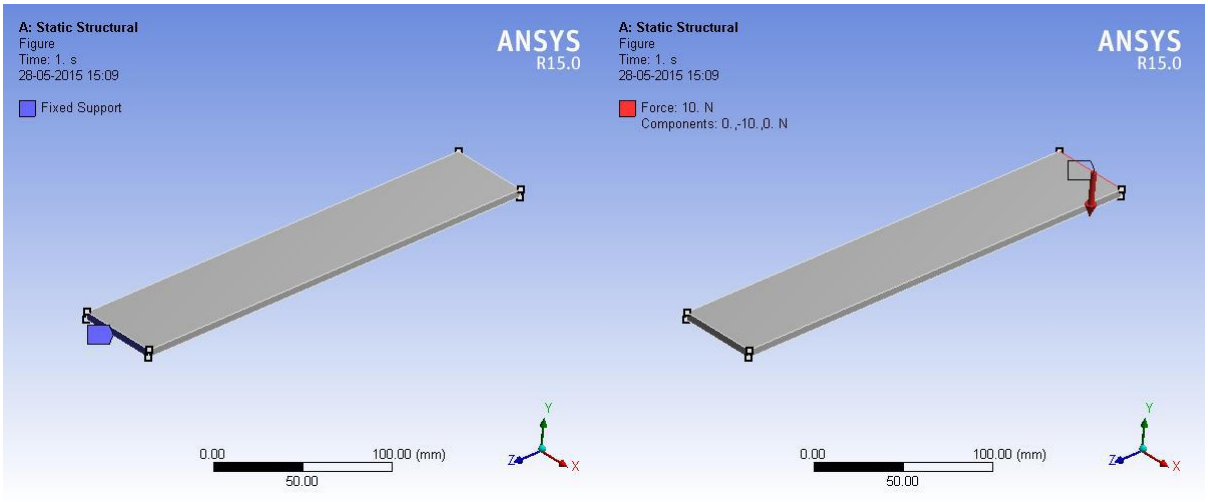

Fig. 5.3. Boundary Conditions applied to beam.

Table 5.7. Structural analysis results of beam

Object Name	*Total Deformation (mm)*	*Equivalent Elastic Strain (mm/mm)*	*Maximum Principal Elastic Strain (mm/mm)*	*Minimum Principal Elastic Strain (mm/mm)*	*Maximum Shear Elastic Strain (mm/mm)*	*Equivalent Stress (MPa)*	*Maximum Principal Stress (MPa)*	*Minimum Principal Stress (MPa)*	*Maximum Shear Stress (MPa)*	*Strain Energy (mJ)*
Results										
Minimum	0.	8.4514e-008	3.5326e-008	-7.4401e-005	8.6352e-008	1.1814e-002	-5.3695	-18.652	6.6425e-003	3.8405e-008
Maximum	0.76836	7.561e-005	7.4358e-005	-2.5763e-008	1.1103e-004	15.08	18.648	5.3803	8.5411	1.3174e-003
Minimum Value Over Time										
Minimum	0.	8.4514e-008	3.5326e-008	-7.4401e-005	8.6352e-008	1.1814e-002	-5.3695	-18.652	6.6425e-003	3.8405e-008

Maximum	0.	8.4514e-008	3.5326e-008	-7.4401e-005	8.6352e-008	1.1814e-002	-5.3695	-18.652	6.6425e-003	3.8405e-008
Maximum Value Over Time										
Minimum	0.76836	7.561e-005	7.4358e-005	-2.5763e-008	1.1103e-004	15.08	18.648	5.3803	8.5411	1.3174e-003
Maximum	0.76836	7.561e-005	7.4358e-005	-2.5763e-008	1.1103e-004	15.08	18.648	5.3803	8.5411	1.3174e-003

From the analysis results of structural analysis of cantilever beam following results has been calculated:

- Total Deformation
- Equivalent elastic strain
- Maximum principle elastic strain
- Minimum principle elastic strain
- Maximum shear elastic strain
- Equivalent stress
- Maximum principle stress
- Minimum principle stress
- Maximum shear stress
- Strain energy.

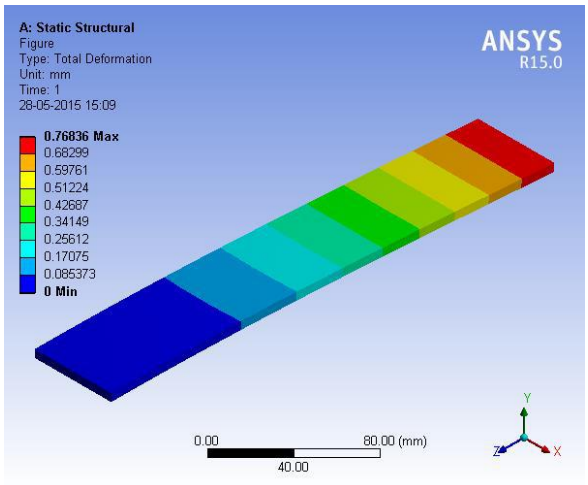

Total deformation

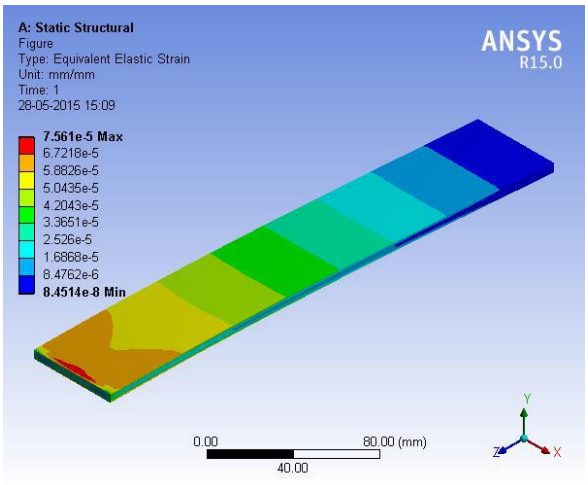

Equivalent elastic strain

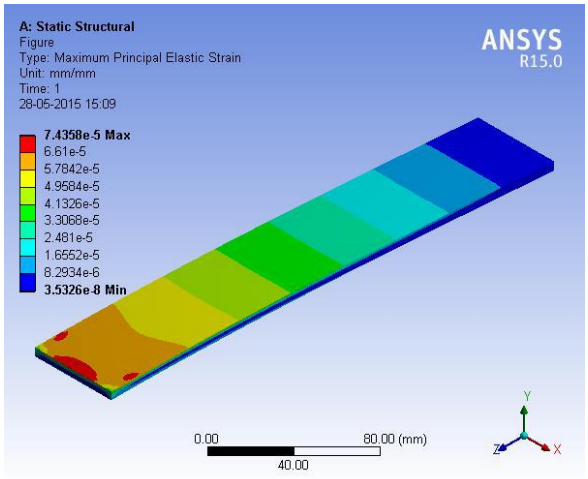

Maximum principle elastic strain

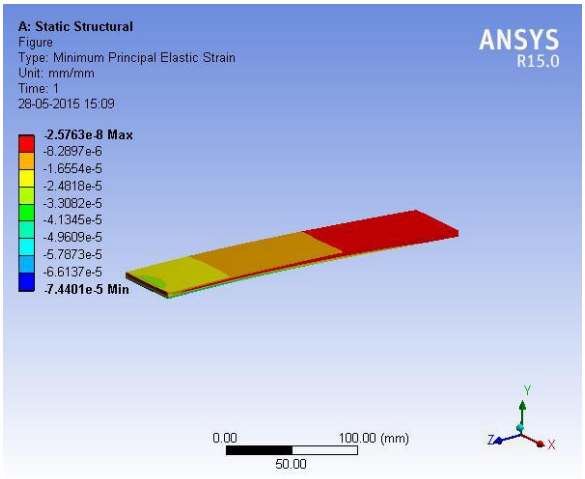

Minimum principle elastic strain

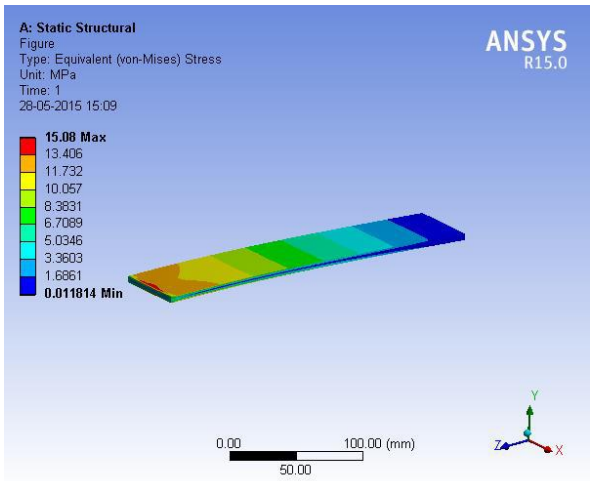

Equivalent Stress

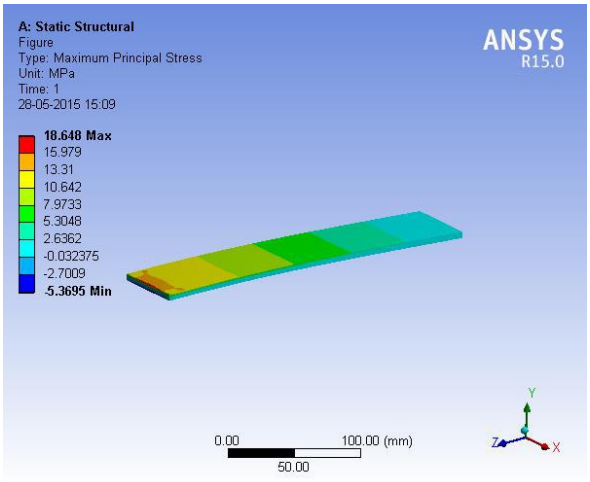

Maximum principle stress

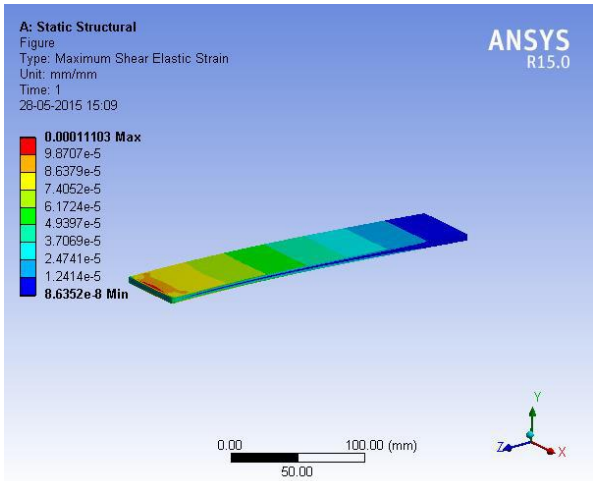

Maximum shear elastic strain

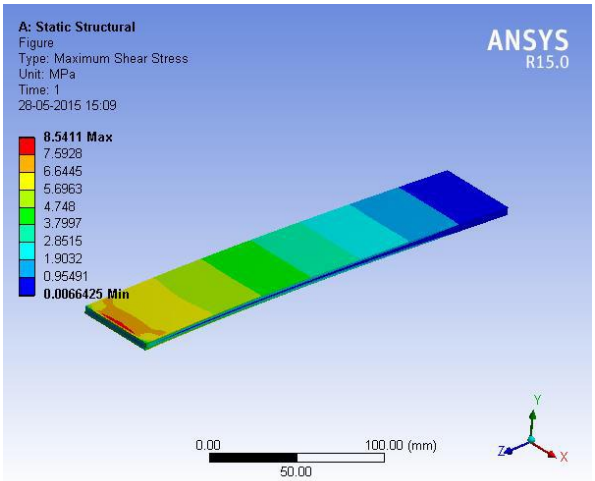

Maximum shear stress

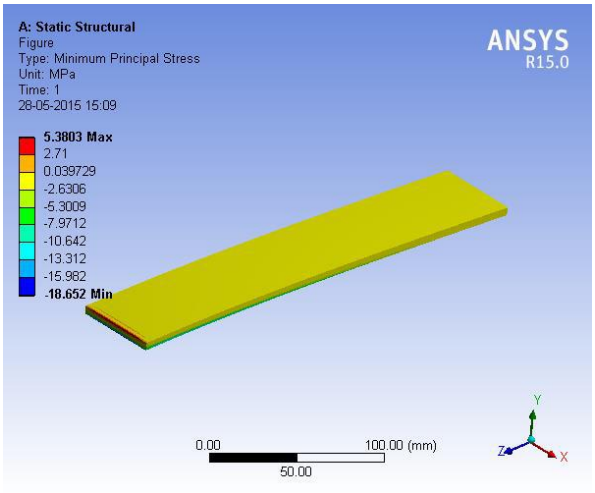

Minimum principle stress

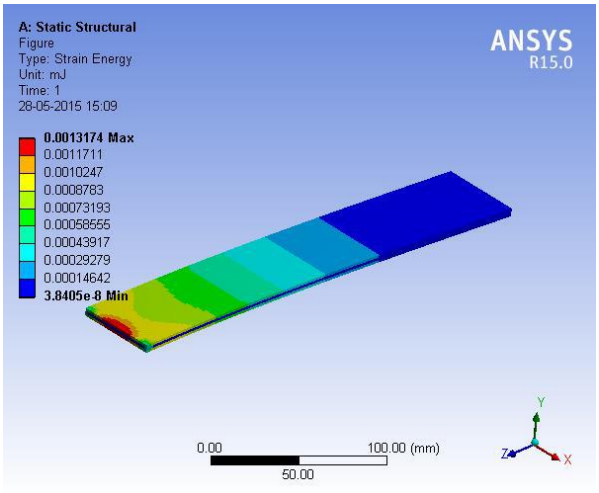

Strain Energy

Fig.5.4. Structural analysis results for beam

Table 5.8. Material Data

Density Kg/mm^3	7.85e-006			
Coefficient of Thermal Expansion	1.2e-005			
Specific Heat mJ/ Kg-C	4.34e+005			
Thermal Conductivity W/mm-C	6.05e-002			
Resistivity Ω-mm	1.7e-004			
Compressive Yield Strength MPa	250			
Tensile Yield Strength MPa	250			
Temperature C	Young's Modulus MPa	Poisson's Ratio	Bulk Modulus MPa	Shear Modulus MPa
22 ^{o}C	2.e+005	0.28	1.6667e+005	76923

5.1.2. Modal analysis of cantilever beam:

In this analysis modal frequencies and mode shapes of cantilever beam determined using ANSYS 15.0 and then these values and mode shapes were compared with experimental modal analysis data.

No. of modes calculated = 6

Table 5.9. Modal frequencies

Mode	Frequency [Hz]
1.	48.966
2.	306.24
3.	475.1
4.	543.01
5.	856.82
6.	1652.4

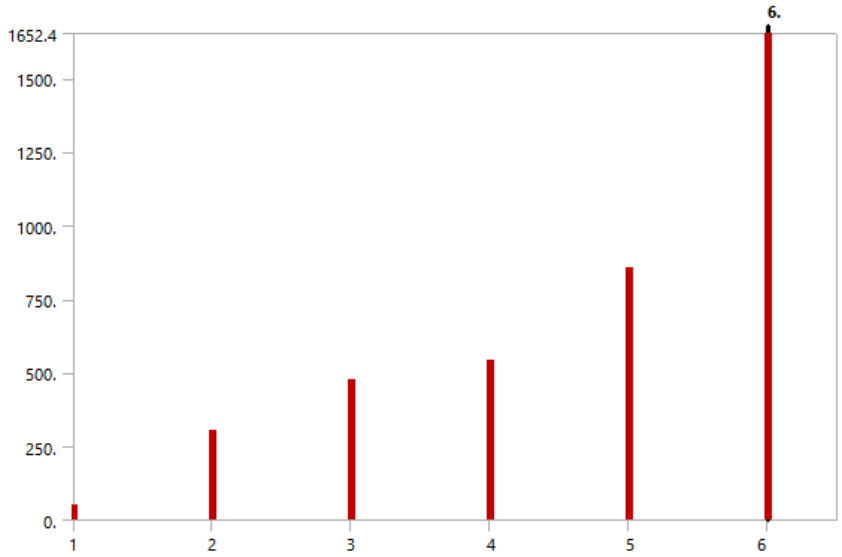

Fig. 5.5. Modal frequencies obtained

Table 5.10. Modal analysis result for beam

Object Name	*Total Deformation 1*	*Total Deformation 2*	*Total Deformation 3*	*Total Deformation 4*	*Total Deformation 5*	*Total Deformation 6*
Mode	1.	2.	3.	4.	5.	6.
Results						
Minimum	0. mm					
Maximum	84.023 mm	84.035 mm	83.332 mm	105.3 mm	84.34 mm	108.74 mm
Frequency	48.966 Hz	306.24 Hz	475.1 Hz	543.01 Hz	856.82 Hz	1652.4 Hz

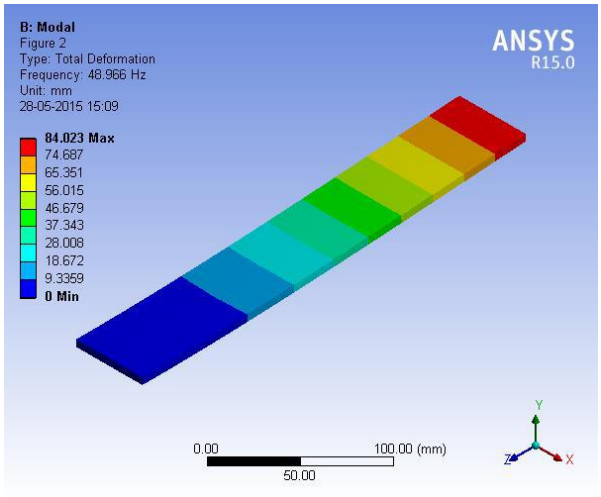

Mode-1

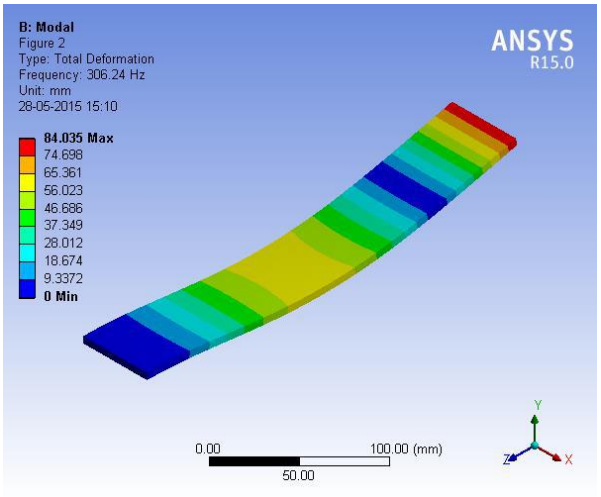

Mode-2

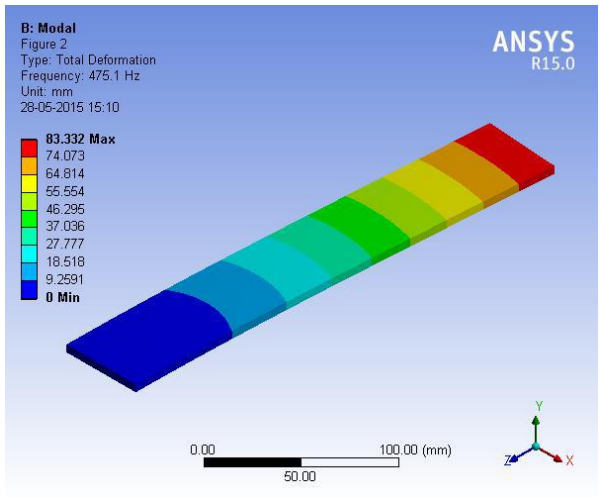

Mode-3

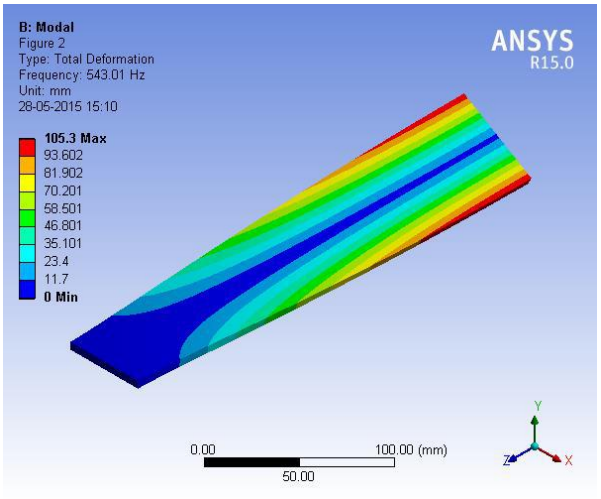

Mode-4

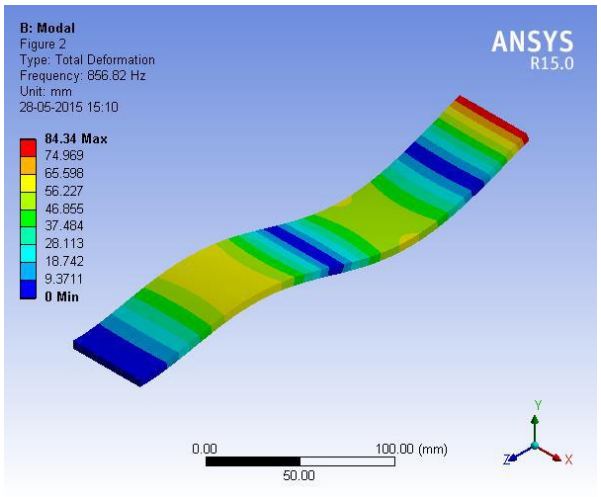

Mode-5

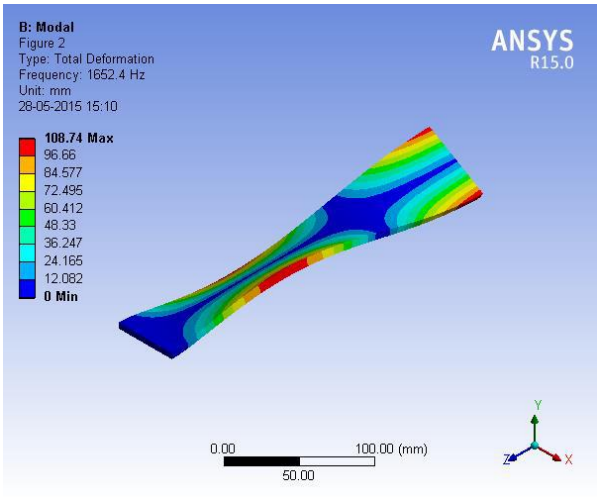

Mode-6

Fig. 5.6. Mode shapes of beam

Different mode shapes are obtained from the modal analysis of cantilever beam provided one end of it is completely fixed as boundary condition for cantilever beam. From these mode shapes it is clear that the failure occurs due to following:

I. Pure bending (Mode-1, Mode-2, Mode-5)
II. Pure twisting (Mode-4)
III. Bending and twisting (Mode-6)
IV. Lateral bending (Mode-3)

Table 5.11. Mode shapes frequencies and possible cause

Mode	Frequency [Hz]	Cause
1.	48.966	Bending
2.	306.24	Bending
3.	475.1	Lateral Bending
4.	543.01	Twisting
5.	856.82	Bending
6.	1652.4	Bending & Twisting

Hence from the analysis of cantilever beam we are able to identify the maximum and minimum value of stress and strain and also their respective location. Also we did modal analysis of the cantilever beam from which we are able to determine modal frequencies which will be compared with the experimental modal analysis data and through which we will validate the results of vibration analyser with ANSYS 15.0.

5.2. Modal and Structural analysis of LP stage-1 gas turbine blade using ANSYS 15.0 Workbench.

A 3D model of gas turbine blade made of IN738 material having special characteristics and termed as Inconel-738 has been scanned using 3D scanner and imported into *.igs* format which will be further imported into design modeller of ANSYS 15.0 for analysis. The actual image of this failed gas turbine blade is shown in fig. 5.7.

Fig. 5.7. IN738 LP-1 failed gas turbine blade

This low pressure stage-1 gas turbine blade has been failed from the upper tip as shown in fig. 5.7. The possible cause of failure has been depicted in chapter-1 within the topic *causes of failure of gas turbine blade.* But the 3D scanned model is not ruptured from anywhere; it is a complete blade on which analysis is done using ANSYS 15.0.

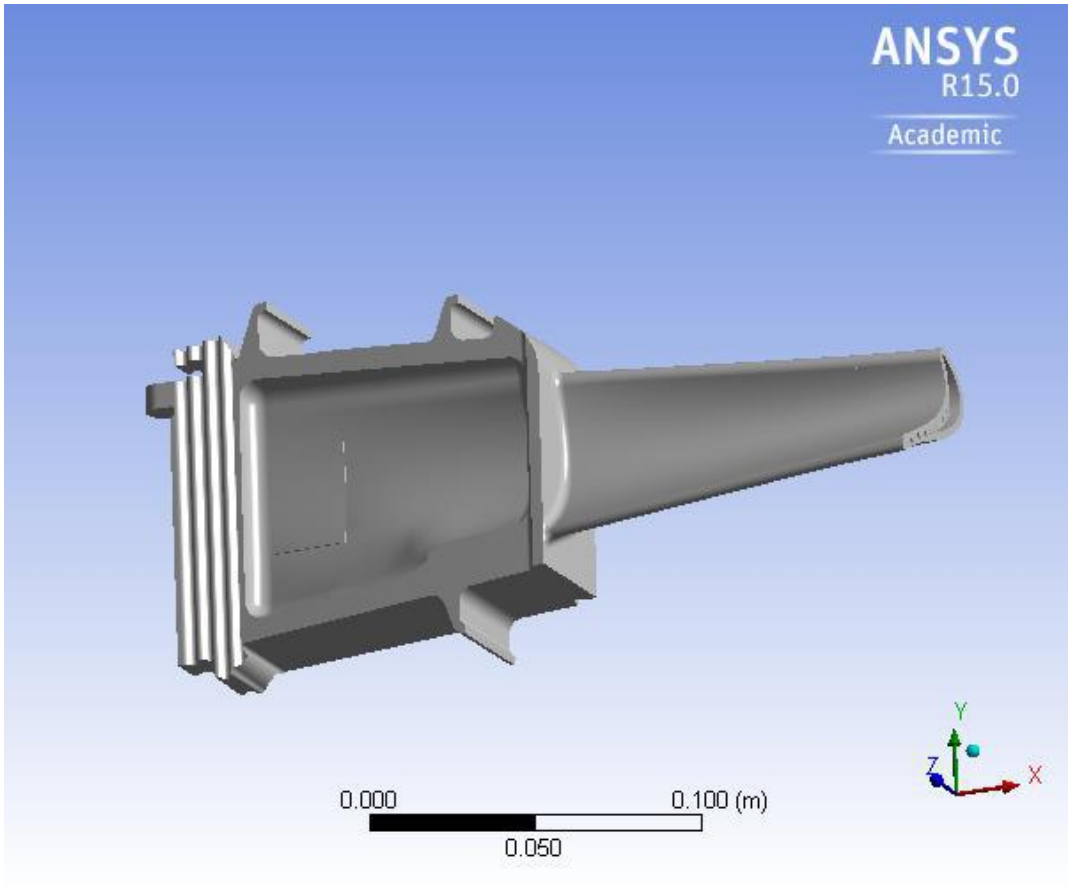

Fig. 5.8. IN738 LP-1 Gas Turbine Blade CAD Model

Table 5.12. Units for turbine blade model

Unit System	Metric (mm, kg, N, s, mV, mA) Degrees rad/s Celsius
Angle	Degrees
Rotational Velocity	rad/s
Temperature	Celsius

Table 5.13. Geometry of turbine blade

Object Name	*Geometry*
State	Fully Defined
Graphics Properties	
Visible	Yes
Transparency	1

Bounding Box	
Length X	.25985 m
Length Y	.11474 m
Length Z	5.4351e-002 m
Properties	
Volume	3.1225e-004 m^3
Mass	2.5323 kg
Scale Factor Value	1
Statistics	
Active Bodies	1
Nodes	136468
Elements	84361
Analysis Type	3-D
Mesh Metric	Aspect Ratio
Min	1.1687
Max	48.783
Average	2.2757
Standard Deviation	1.017
Centroid X	2.7778e-002 m
Centroid Y	4.8283e-003 m
Centroid Z	1.8791e-002 m
Moment of Inertia Ip1	1.6666e-003 kg·m²
Moment of Inertia Ip2	9.8437e-003 kg·m²
Moment of Inertia Ip3	1.1158e-002 kg·m²

Table 5.14. Coordinate system for turbine blade

Object Name	*Global Coordinate System*
State	Fully Defined
Definition	
Type	Cartesian
Origin	
Origin X	0. m
Origin Y	0. m
Origin Z	0. m
Directional Vectors	
X Axis Data	[1. 0. 0.]
Y Axis Data	[0. 1. 0.]
Z Axis Data	[0. 0. 1.]

Table 5.15. Meshing of turbine blade

Relevance	100
Sizing	
Relevance Center	Fine
Smoothing	Medium
Transition	Fast
Span Angle Center	Coarse
Minimum Edge Length	4.3725e-005 m
Transition Ratio	0.272
Maximum Layers	5
Growth Rate	1.2

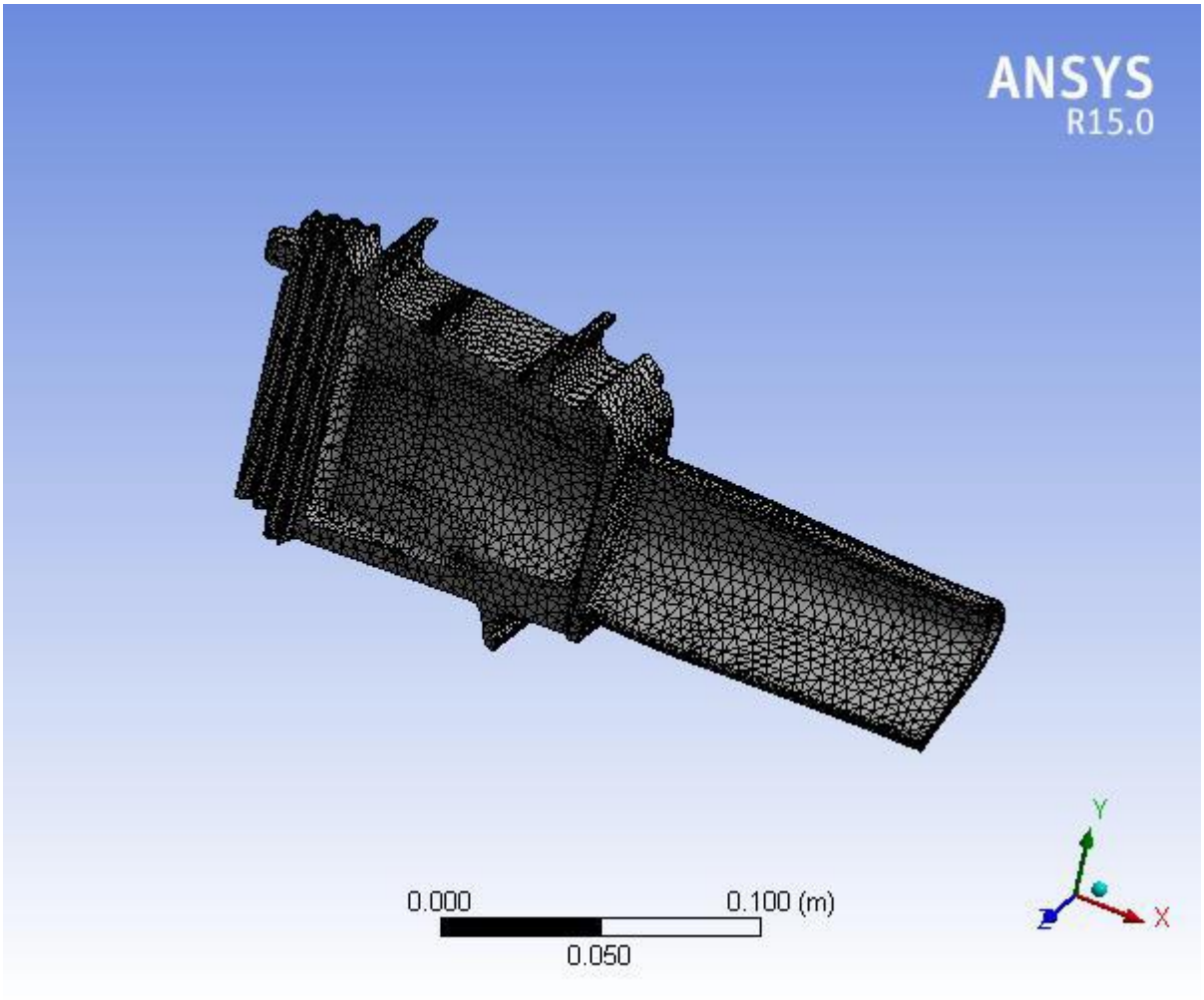

Fig. 5.9. Meshing of IN738 LP-1 Gas Turbine Blade CAD Model

5.2.1. Static Structural Analysis of IN738 LP-1 Gas Turbine Blade:

Static structural analysis of IN738 LP-1 gas turbine blade has been done using ANSYS 15.0 in order to determine the maximum and minimum stress region due application of high pressure fluid. It also gives the result for total deformation of the blade due to pressure application and various stains developed in the blade.

When impact of gas occurs at blade it causes bending and twisting both to the blade and hence blade failed due to fatigue loading. It can be seen clearly from the fig. 5.7 and analysis fig 5.11 that the failure prone area is tip of the turbine blade and in actual failure occurred at the tip of the turbine blade. These similarities in actual and analysis results proves that the data obtained from the analysis of gas turbine blade are true and correct up to maximum extent. Hence from these kind of static structural analysis of components put under highly rigorous operating conditions there failure can be predicted and preventive measures have been taken to improve them for long life.

Table 5.16. Boundary Conditions and load for turbine blade

Object Name	*Pressure*	*Fixed Support*	*Rotational Velocity*
State	Fully Defined		
Scope			
Scoping Method	Geometry Selection		
Geometry	1 Face	68 Faces	Full Body
Definition			
Type	Pressure	Fixed Support	Rotational Velocity
Define By	Components		Components
Coordinate System	Global Coordinate System		Global Coordinate System
X Component	0. Pa (ramped)		537.44 rad/s (ramped)
Y Component	-10017 Pa (ramped)		0. rad/s (ramped)
Z Component	0. Pa (ramped)		0. rad/s (ramped)
Suppressed	No		

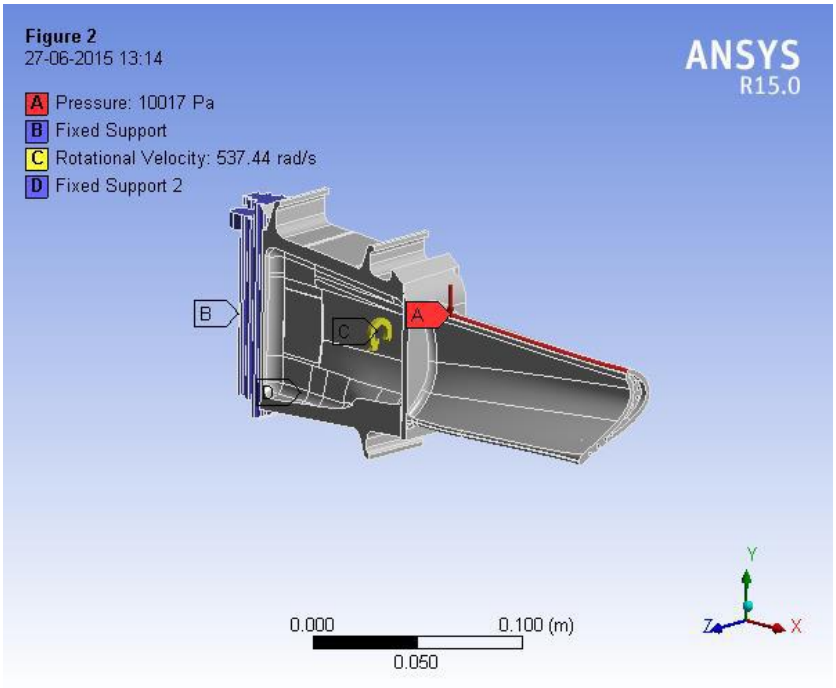

Fig 5.10. Boundary Conditions and load applied to turbine blade

Table 5.17. Static structural analysis results of gas turbine blade

Geometry	All Body				
Definition					
Type	Total Deformation (m)	Equivalent (von-Mises) Stress (Pa)	Equivalent Elastic Strain (m/m)	Strain Energy (J)	Directional Deformation (m)
Suppressed	No				
Results					
Minimum	0	0	0	0	-2.3009e-004
Maximum	1.1934e-003	4.5131e+008	3.2572e-003	1.3443e-003	9.196e-005
Minimum Value Over Time					
Minimum	0	0	0	0	-2.3009e-004
Maximum	0	0	0	0	-2.3009e-004
Maximum Value Over Time					
Minimum	1.1934e-003	4.5131e+008	3.2572e-003	1.3443e-003	9.196e-005
Maximum	1.1934e-003	4.5131e+008	3.2572e-003	1.3443e-003	9.196e-005

Time [s]	Force Reaction (X) [N]	Force Reaction (Y) [N]	Force Reaction (Z) [N]	Force Reaction (Total) [N]
1.	10950	-3317.6	-8667.4	14354

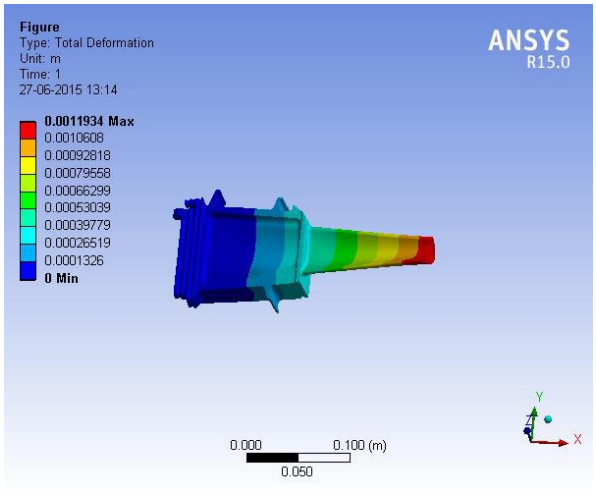

Total Deformation

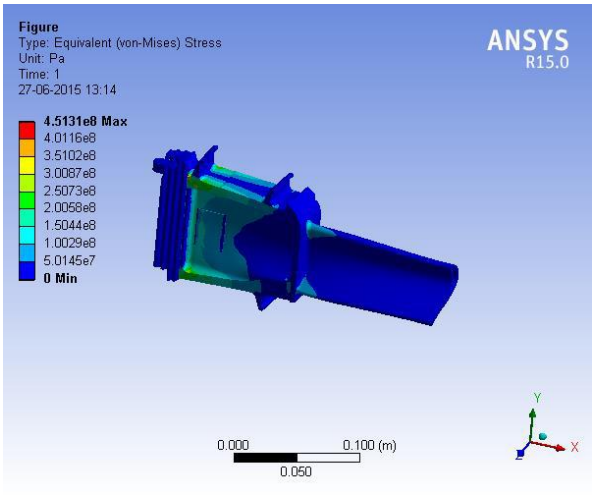

Equivalent Stresses

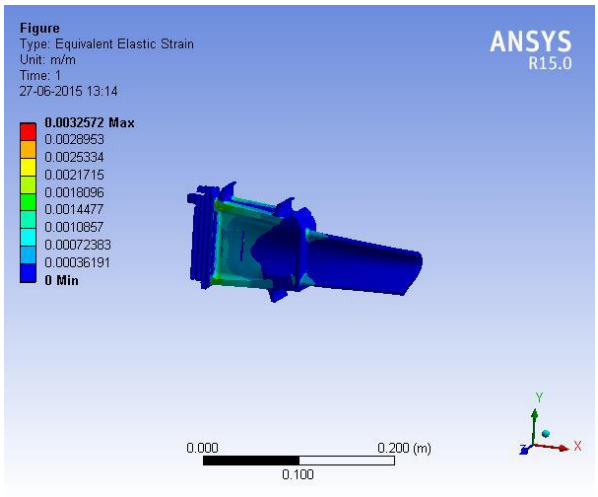

Equivalent Elastic Strain

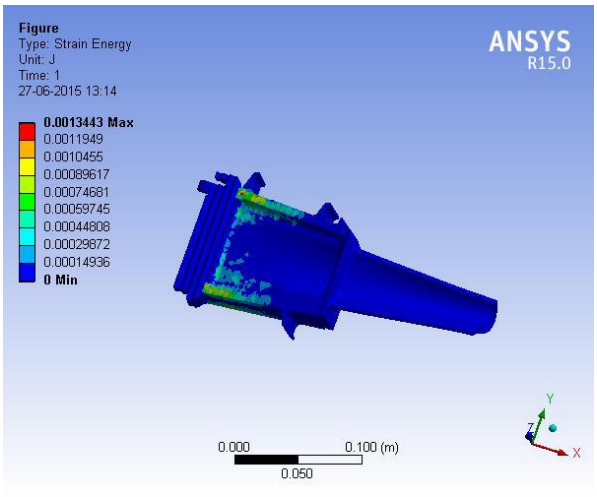

Strain Energy

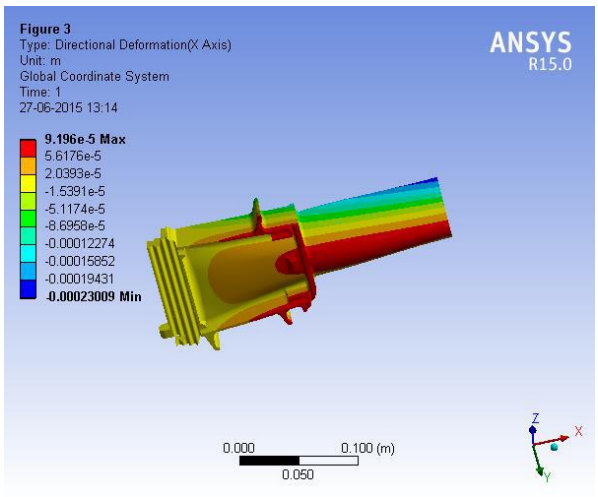

Directional Deformation

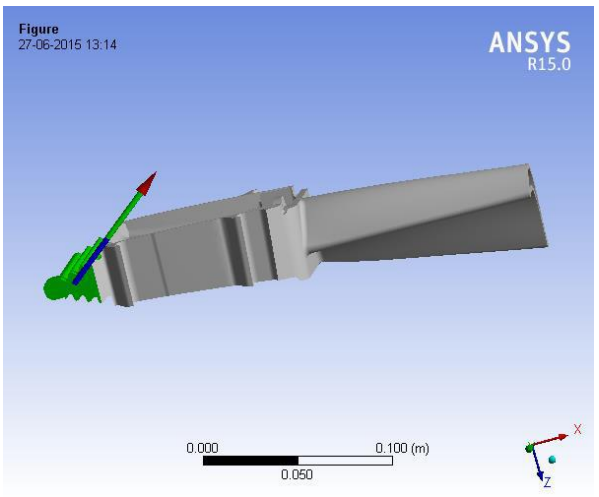

Force Reaction

Fig. 5.11. Static structural analysis of IN738 LP-1 gas turbine blade

5.2.2. Modal Analysis of IN738 LP-1 Gas Turbine Blade:

From this modal analysis of gas turbine blade we are able to determine the mode shapes and modal frequencies for first six modes which will resembles to the mode shapes obtained from the experimental modal analysis of the blade. Hence by obtaining same mode shapes and modal frequencies for first few modes this matches with experimental modal analysis, we will be able to conclude that the further mode shapes and modal frequencies obtained will be approximately correct up to maximum extent.

This modal analysis depicts the failure of gas turbine blade for different number of operating cycles or cyclic loading, which resembles to the actual failure of gas turbine blade.

Actually in our results failure of blade occurs from the blade tip and the failed blade we have also failed from the tip of the blade. This shows that the results we obtained from analytical or computation analysis of model resemble to the actual data.

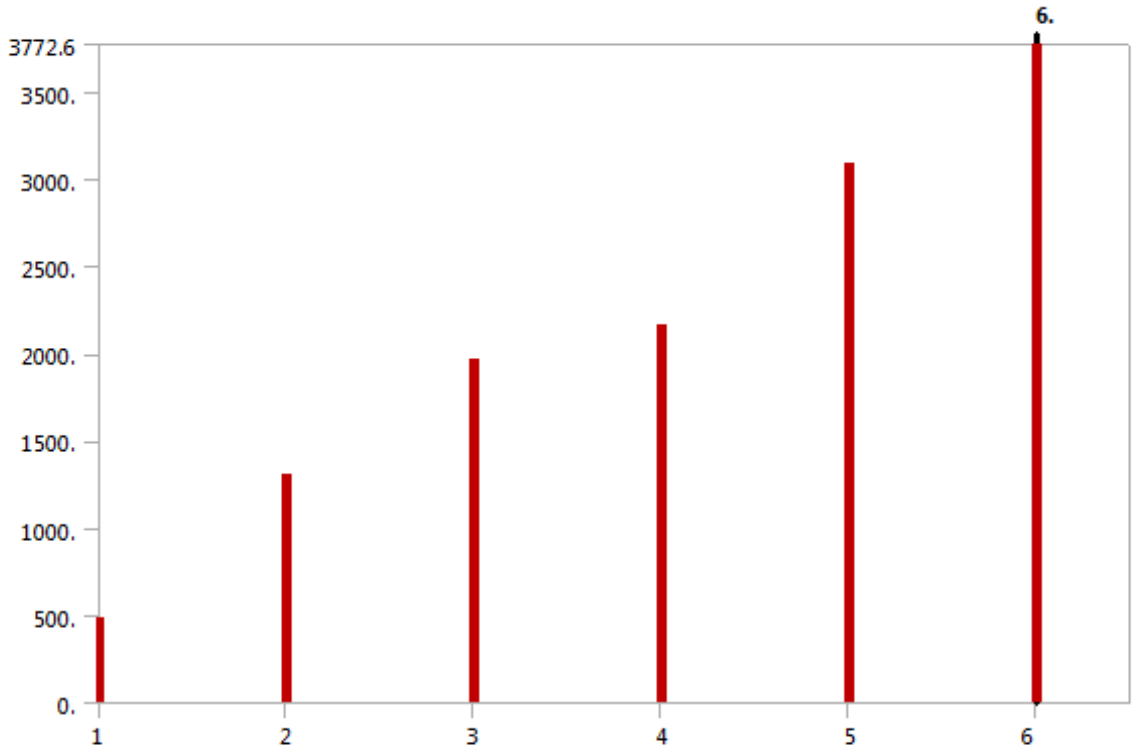

Fig 5.12 Modal frequencies for gas turbine blade

Table 5.18 Modal frequencies of IN738 LP-1 gas turbine blade

Mode	Frequency [Hz]
1.	483.32
2.	1310.2
3.	1969.3
4.	2164.9
5.	3094.9
6.	3772.6

Table 5.19 Modal analysis result of gas turbine blade

Object Name	*Total Deformation 1*	*Total Deformation 2*	*Total Deformation 3*	*Total Deformation 4*	*Total Deformation 5*	*Total Deformation 6*
Definition						
Mode	1.	2.	3.	4.	5.	6.
Frequency	483.32 Hz	1310.2 Hz	1969.3 Hz	2164.9 Hz	3094.9 Hz	3772.6 Hz
Suppressed	No					
Results						
Minimum	0. m					
Maximum	1.9126 m	3.224 m	3.0906 m	3.0008 m	5.6815 m	2.8679 m
Minimum Value Over Time						
Minimum	0. m					
Maximum	0. m					
Maximum Value Over Time						
Minimum	1.9126 m	3.224 m	3.0906 m	3.0008 m	5.6815 m	2.8679 m
Maximum	1.9126 m	3.224 m	3.0906 m	3.0008 m	5.6815 m	2.8679 m

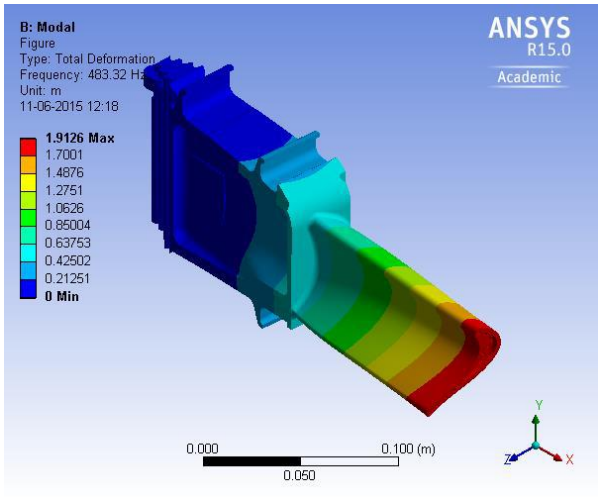

Mode-1

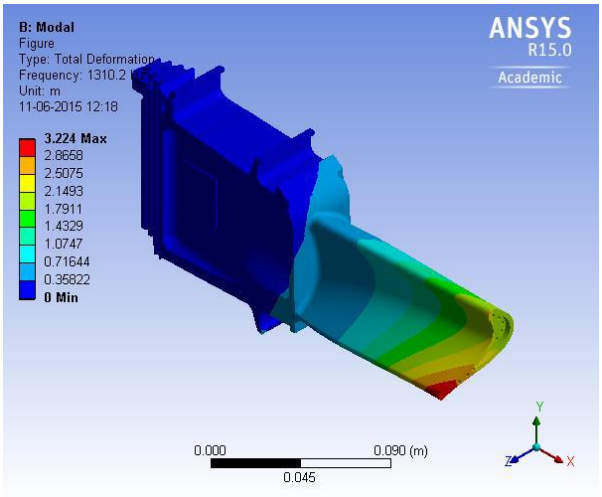

Mode-2

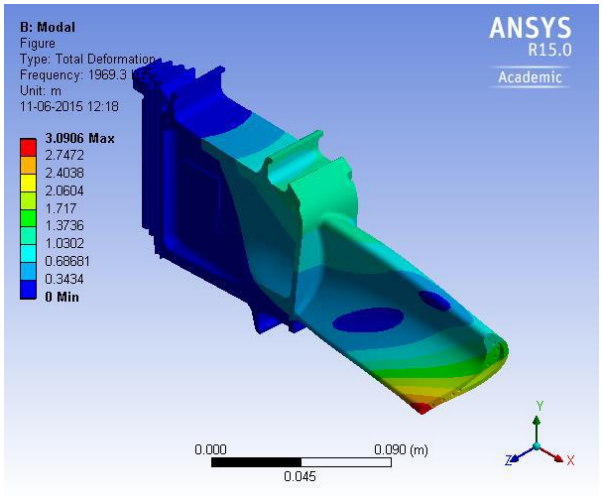

Mode-3

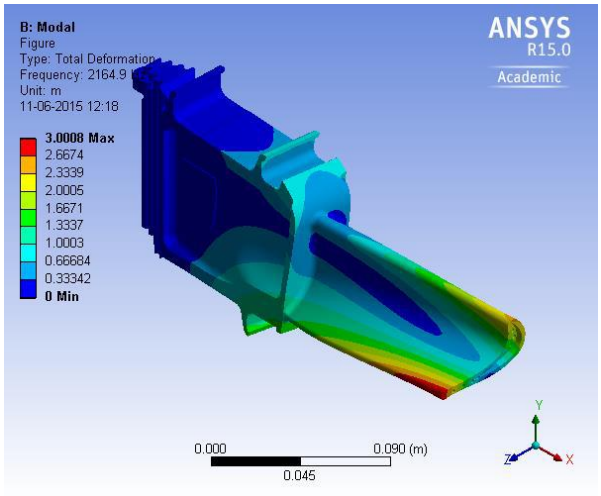

Mode-4

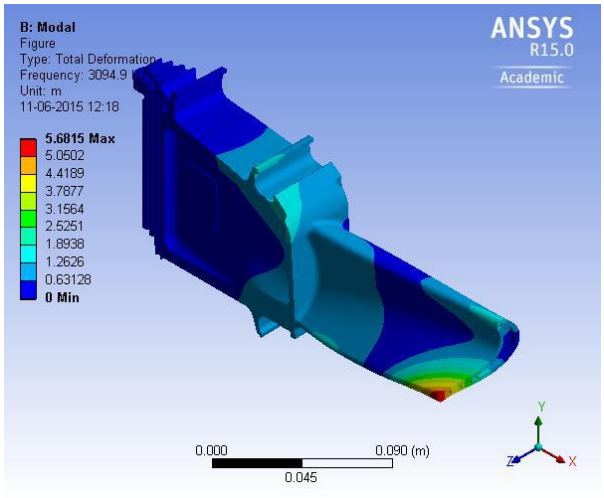

Mode-5

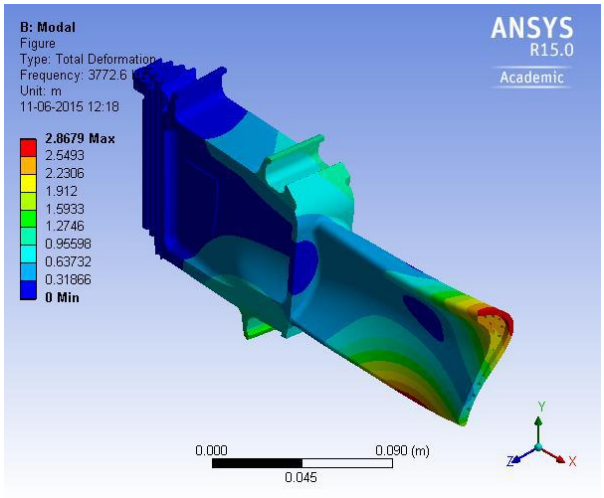

Mode-6

Fig 5.13 Mode shapes of IN738 LP-1 gas turbine blade

Table 5.20 Material data for IN738

Temperature (^{o}C)	Young's Modulus (Pa)	Poisson's Ratio	Bulk Modulus (Pa)	Shear Modulus (Pa)
22	1.3996e+011	0.28	1.1664e+011	5.3832e+010
Density (Kg/m^3)	8110			
Tensile Yield Strength (Pa)	3.4474e+008			

Hence from the static structural and modal analysis of cantilever beam and IN738 LP-1 gas turbine blade following observations perceived:

- Cantilever beam modal frequencies and mode shapes obtained for same boundary conditions as in experimental modal analysis of cantilever beam.
- Here we are able to get all mode shapes due bending or twisting or both, but in EMA we only applying transverse shear load so obtaining only mode shapes due to bending.
- From the static structural analysis of blade it is clear that maximum deformation occurs at blade tip and stresses generates in tang portion of the turbine blade.
- Because tang and fitree portions are inside the rotor disc hence they are not supposed to failure, only blade subjected to external load and environmental factors hence failure of blade occurs first.
- From the modal analysis of gas turbine blade it can be seen that at most of the natural frequencies failure occurs at blade tip, and if we see across our failed blade we will found that failure happens from the blade tip. This implies that the results we are obtaining rely with original data and we are proceeding in correct way.

CHAPTER-6

RESULT AND DISCUSSUION

From the deep study of literature survey we are able to determine the possible cause of failure in any gas turbine and then investigated our own turbine blade to predict the causes of failure. By referring the literature survey we found following possible cause of failure:

- HCF (High cycle fatigue)
- Corrosion
- Erosion wear
- High temperature oxidation

In order identify the root cause and remove them to enhance the life of the blade we selected various methodologies to analyze the component and its characteristics before failure and then possible modifications made to the blade to improve its characteristics.

6.1. Validation of EMA results with CMA results for cantilever beam:

To validate the results of experimental modal analysis with computational modal analysis we did both the processes on cantilever beam made of mild steel. As in case of EMA only bending is possible hence the results of pure bending in CMA of cantilever beam matched with few frequencies of EMA which represents bending only.

And further modal frequencies are also calculated manually as per the formula given by book J.S.Rao of Mechanical Vibrations as following:

$$W_i = (r_i.l)^2.\sqrt{\frac{EI}{\rho Al4}}$$

Where, E = 210GPa, l = 290mm, b = 50mm, h = 5mm, ρ = 7850 g/mm^3

$$I = bh^3/12,\ A = b\times h$$

For cantilever beam,

Modes	1	2	3	4	5
(r_i.l) values	1.875	4.694	7.855	10.996	14.137

Calculating the factor, $\sqrt{\frac{EI}{\rho Al4}} = \sqrt{\frac{210\times10\wedge9\times5\times50\wedge3\times10\wedge4}{7850\times50\times5\times290\wedge4\times12}} = 88.8$

Now calculating modal frequencies,

$$f_1 = \frac{w1}{2\pi} = \frac{(1.875)\wedge2\times88.8}{2\pi} = 49.69 \text{ Hz}$$

$$f_2 = \frac{w2}{2\pi} = \frac{(4.694)\wedge2\times88.8}{2\pi} = 311.40 \text{ Hz}$$

$$f_3 = \frac{w3}{2\pi} = \frac{(7.855)\wedge2\times88.8}{2\pi} = 872.01 \text{ Hz}$$

$$f_4 = \frac{w4}{2\pi} = \frac{(10.996)\wedge2\times88.8}{2\pi} = 1708.84 \text{ Hz}$$

$$f_5 = \frac{w5}{2\pi} = \frac{(14.137)\wedge2\times88.8}{2\pi} = 2824.54 \text{ Hz}$$

As only first three modal frequencies lies in the range of our interest and f_1, f_2 *and* f_3 a frequency matching with the three modal frequencies due to bending only approximately. Hence we are able to conclude that modal frequencies obtained through EMA, CMA and analytically are approximately same and hence our result for cantilever is validated in all these three cases.

Also the mode shapes obtained from the EMA resembles with mode shapes obtained from CMA due to bending.

Table.6.1. Validation of EMA and CMA modal frequencies for cantilever beam

Modes	Frequency (Hz)			Cause
	EMA	Analytical	CMA	
1	50.27	49.69	48.966	Bending
2	310.22	311.40	306.24	Bending
3	-	-	475.1	Lateral Bending
4	-	-	543.01	Twisting
5	889.11	872.01	856.82	Bending
6	-	-	1652.4	Bending & Twisting

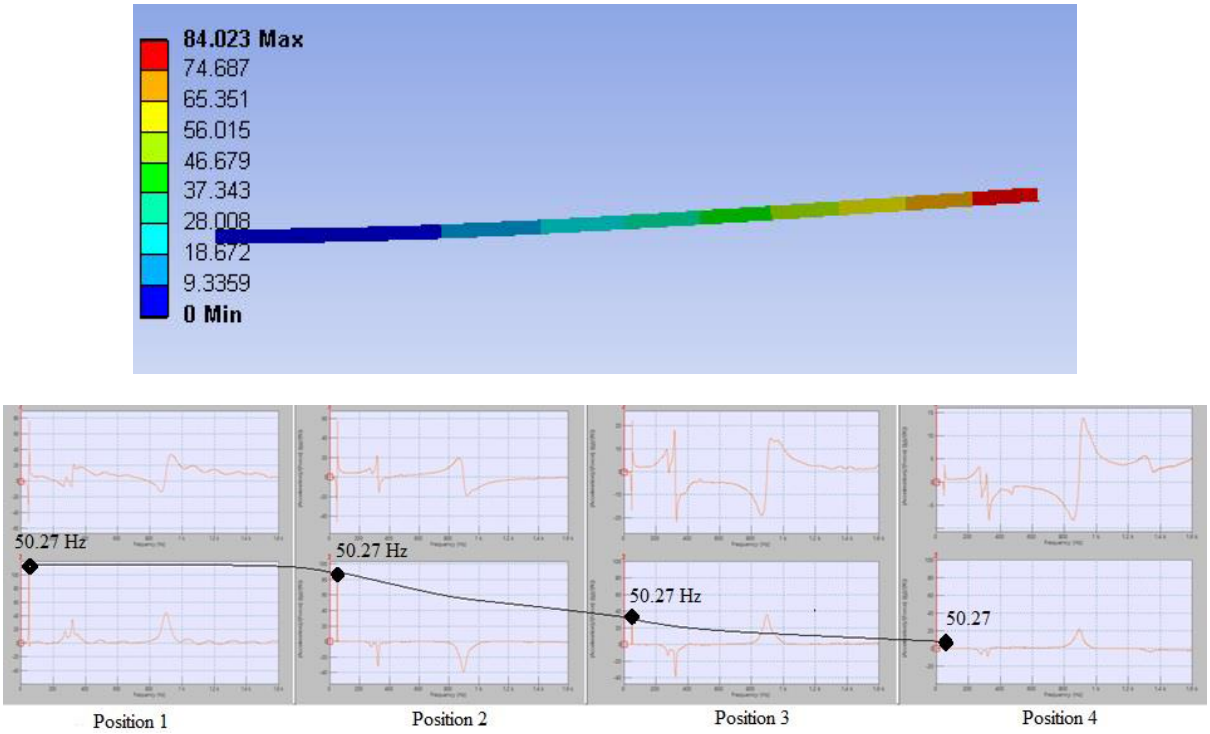

Fig.6.1. Resemblance of mode -1 of CMA with EMA of cantilever beam

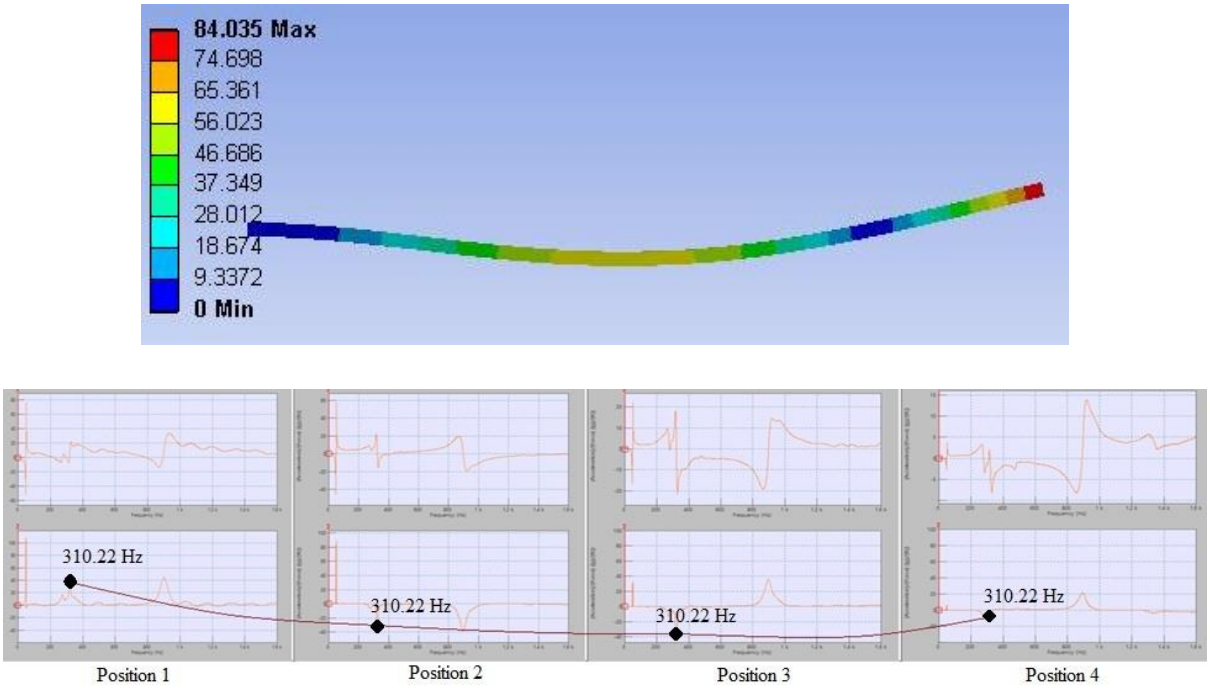

Fig.6.2. Resemblance of mode -2 of CMA with EMA of cantilever beam

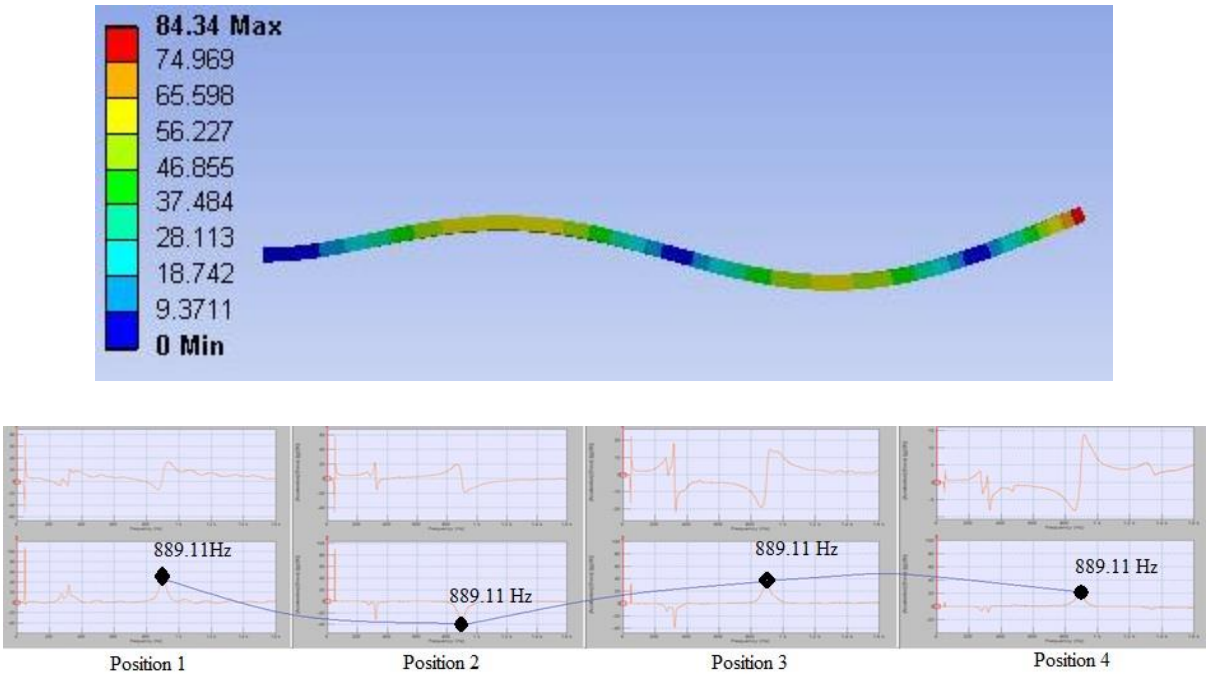

Fig.6.3. Resemblance of mode -5 of CMA with EMA of cantilever beam

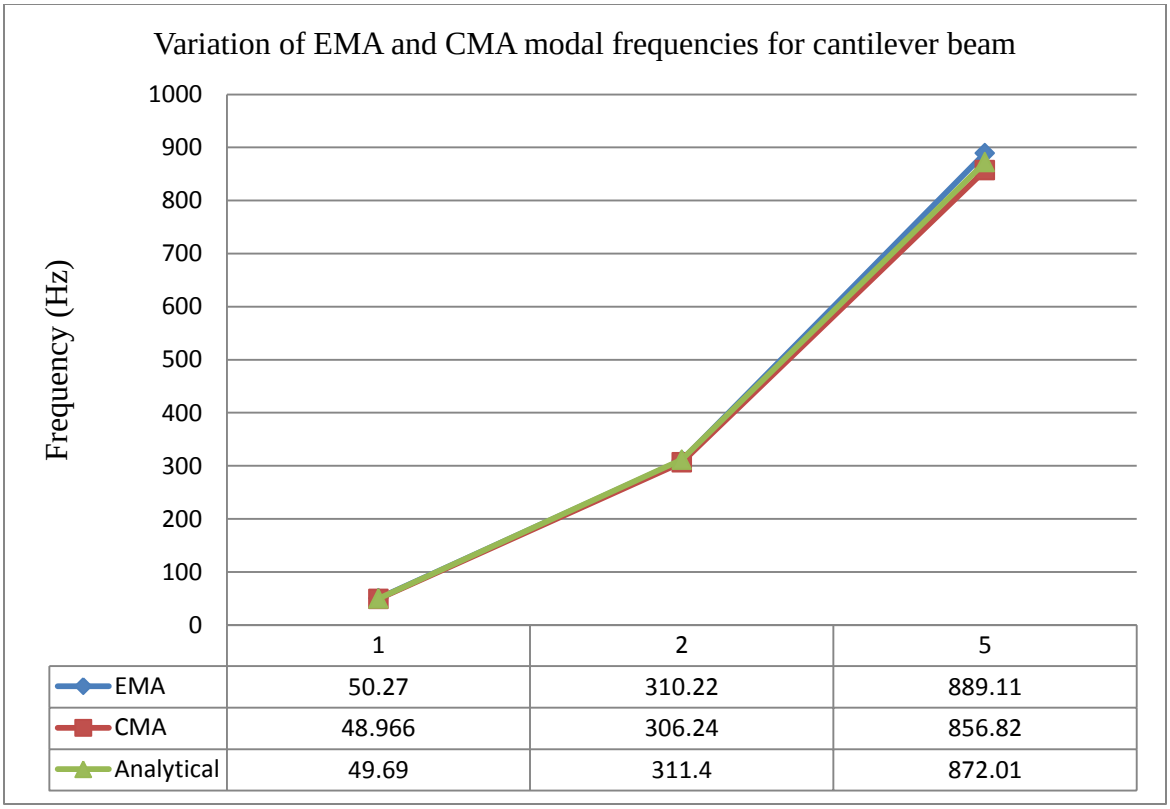

Fig.6.4. Graph showing the variation of EMA and CMA results for cantilever beam

6.2. Analysis and validation of EMA and CMA results for gas turbine blade:

For the experimental modal analysis of IN738 LP-1 gas turbine blade the major issue was fixing the base during analysis from fitree joint. For which we designed a fixture as shown in fig.5.4. to make it stable during hammer impact testing.

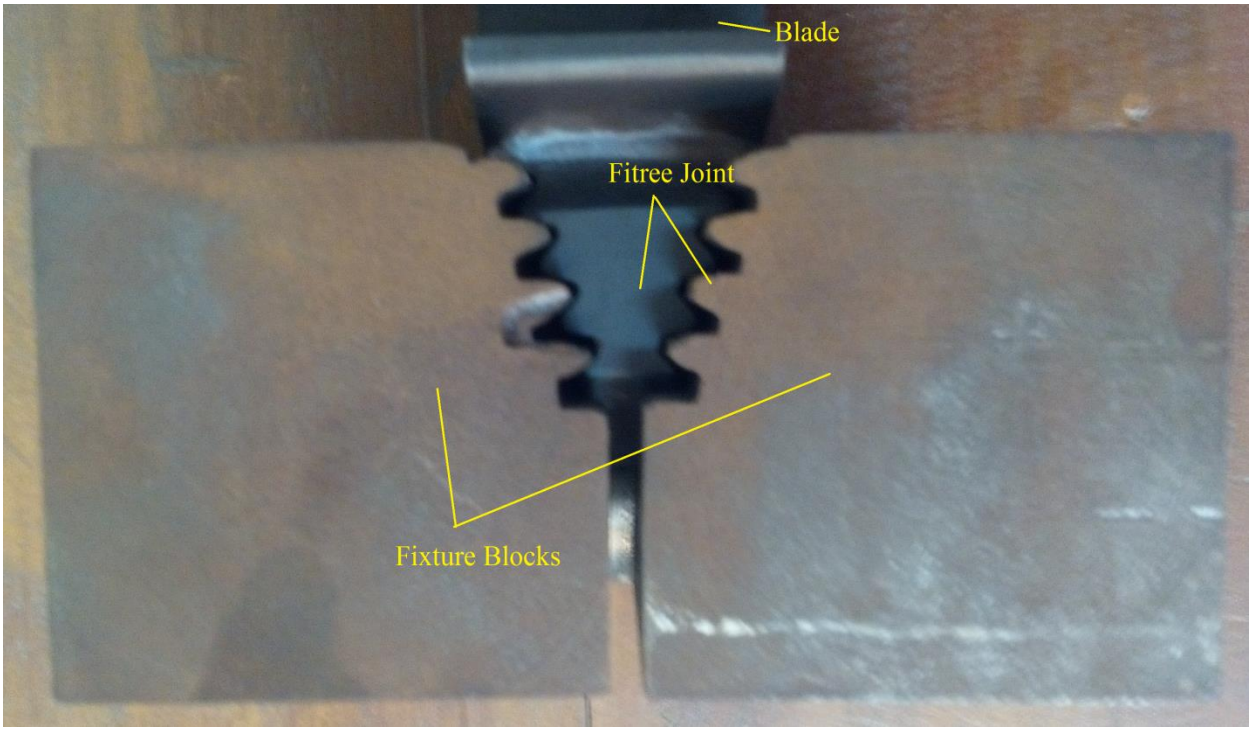

Fig. 6.5. Fixture Blocks for fitree joint.

Table.6.2. Validation of EMA and CMA modal frequencies for gas turbine blade

Modes	Frequency	
	EMA	CMA
1	432.2	483.32
2	1496.6	1310.2
3	1993.2	1969.3
4	2456.31	2164.9
5	3386.25	3094.9
6	4069.11	3772.6

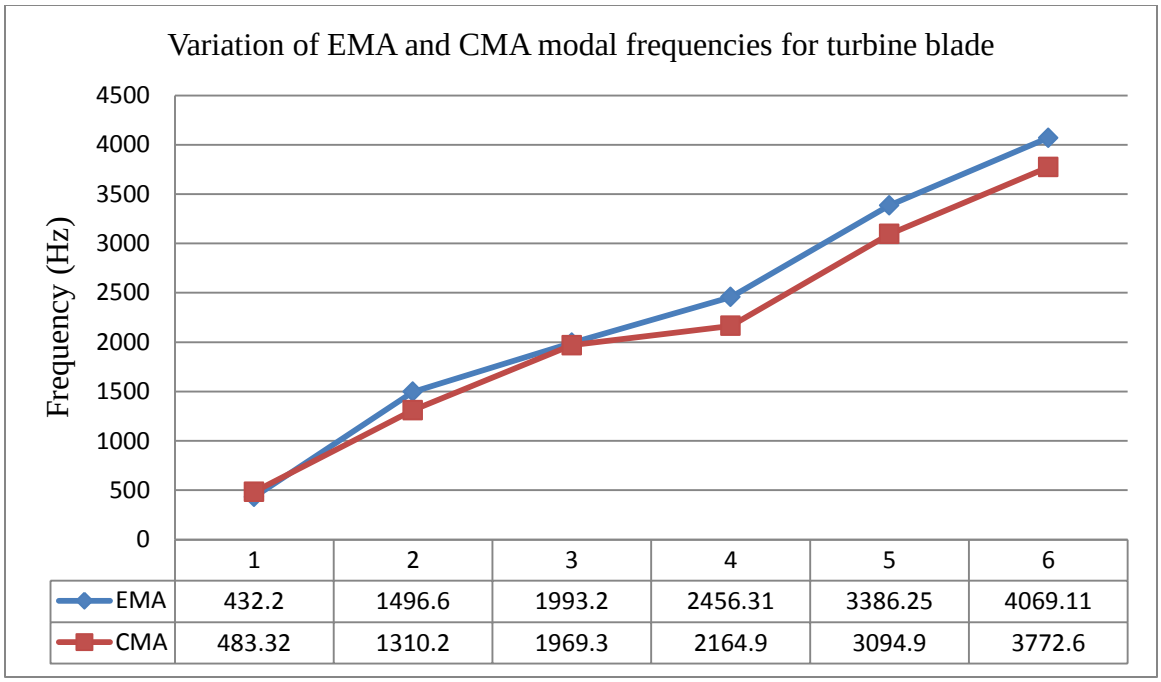

Fig.6.6. Graph showing the variation of EMA and CMA results for gas turbine blade

As compare to variation in the modal frequencies of cantilever beam, variation in the frequencies of turbine blade is more, it is because of following reasons:

- Instability of the base during impact testing.
- Non-uniform cross section of the turbine blade.
- Damaged turbine blade may result inappropriate data.
- Non-uniform environmental conditions may affect sensitivity of sensors.
- Repeatability, precision or accuracy of sensor is low.
- Unknown value of force given by force hammer manually.

Form the experimental modal analysis damping factor was calculated from resonance peak as, For gas turbine blade, $\varepsilon = 0.0294$

For cantilever beam, $\varepsilon = 0.022$

Not exactly but somehow we are able to draw similar mode shapes obtained as obtained from EMA and CMA of gas turbine blade.

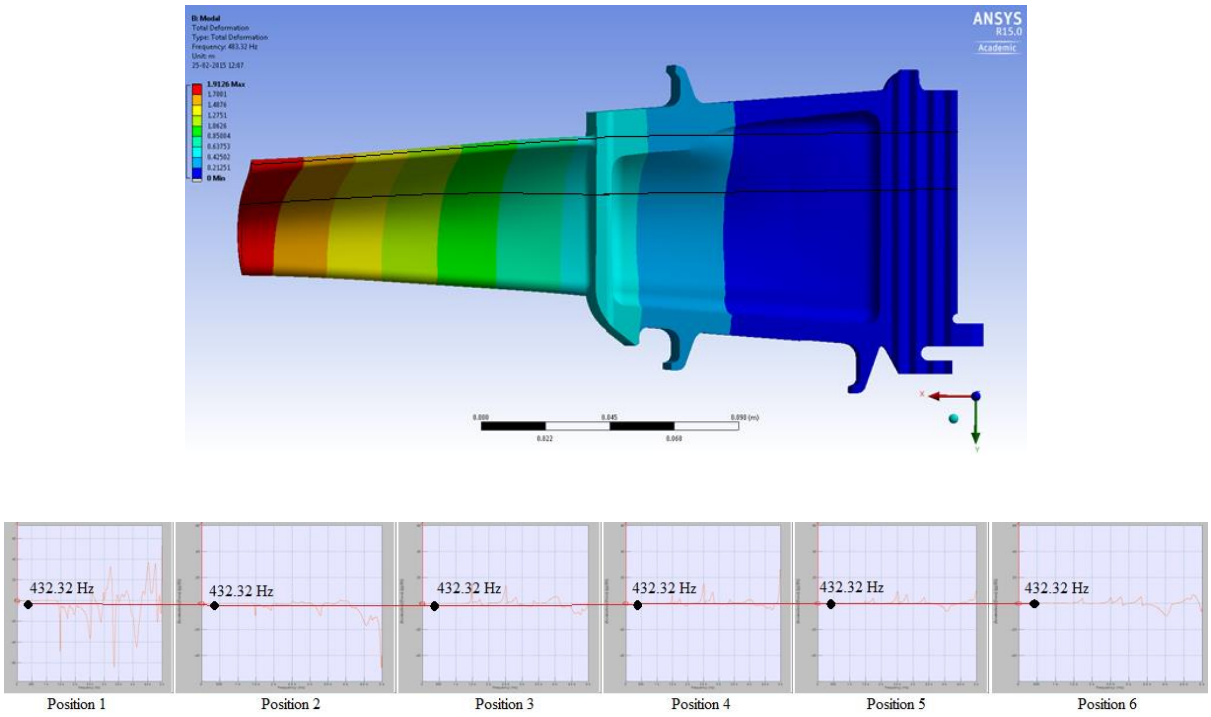

Fig.6.7. Resemblance of mode -1 of CMA with EMA of gas turbine blade

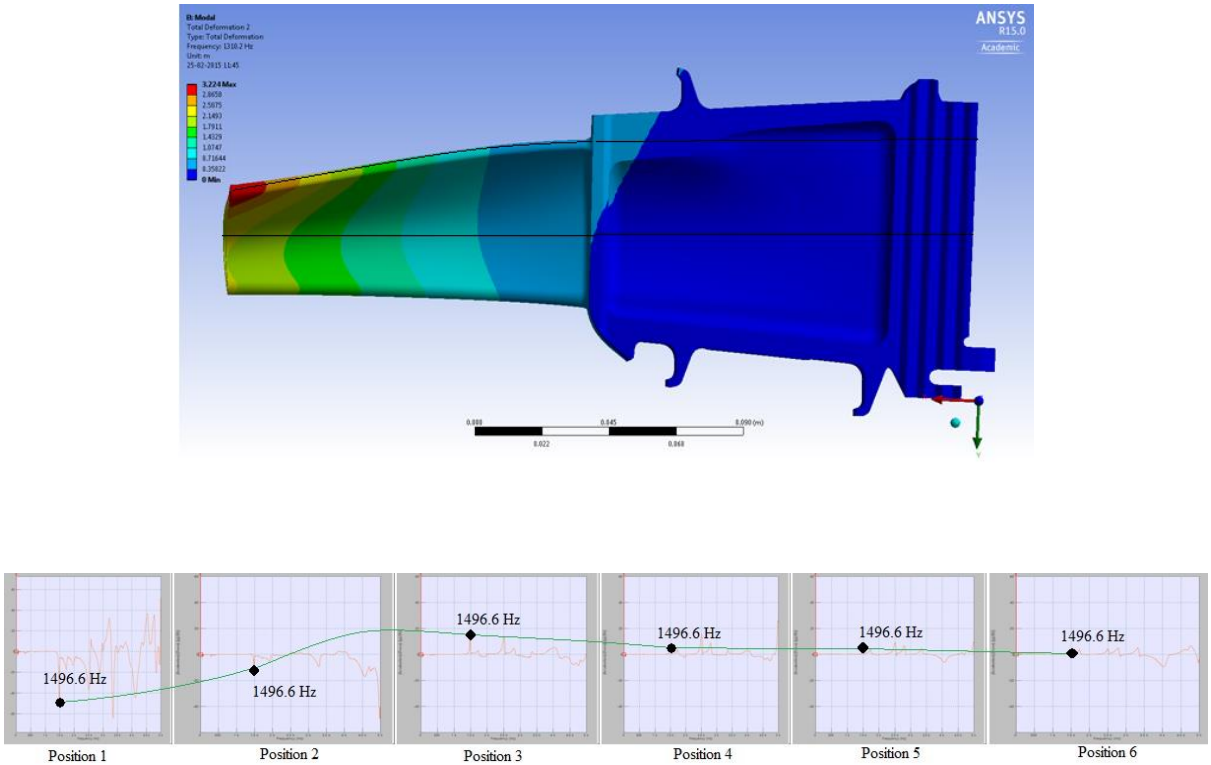

Fig.6.8. Resemblance of mode -2 of CMA with EMA of gas turbine blade

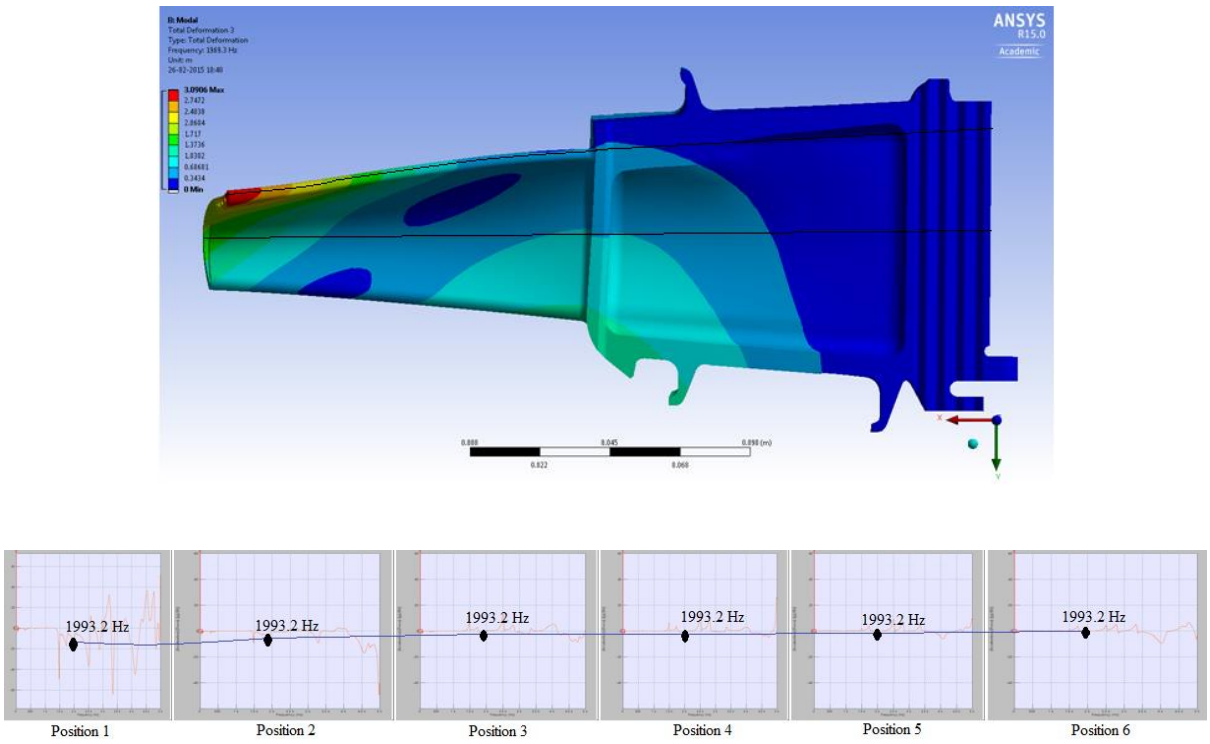

Fig.6.9. Resemblance of mode -3 of CMA with EMA of gas turbine blade

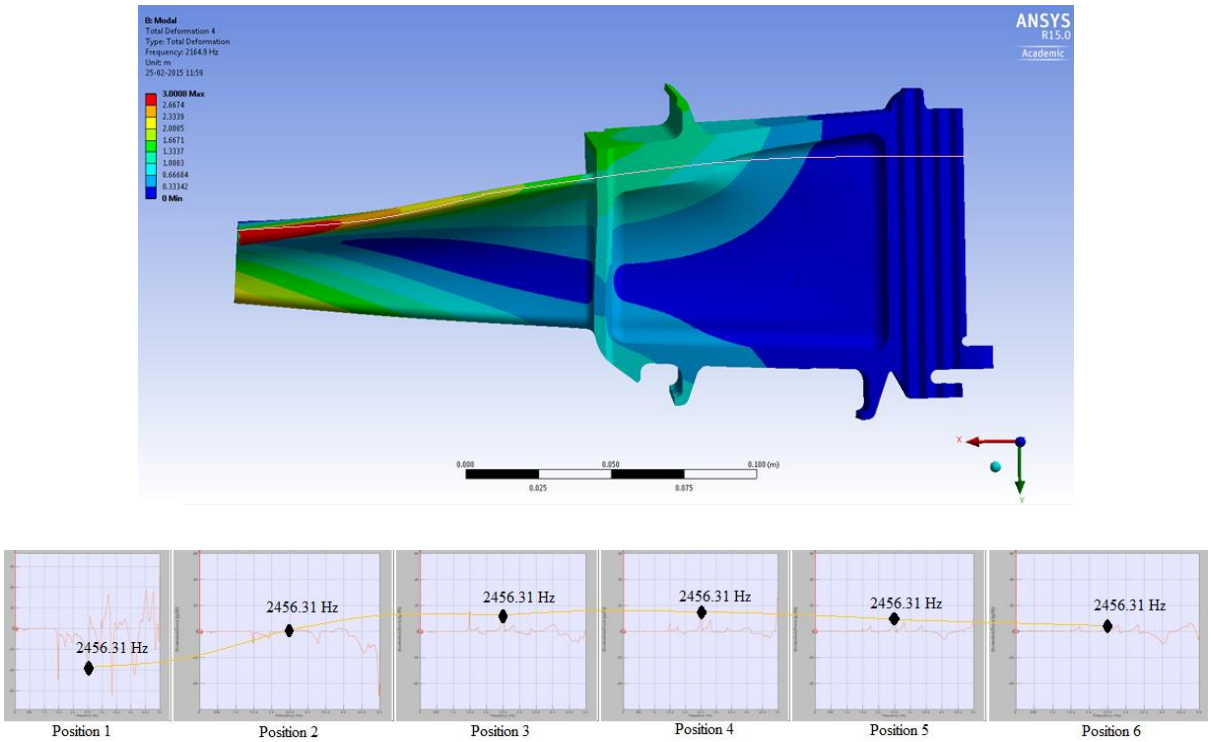

Fig.6.10. Resemblance of mode -4 of CMA with EMA of gas turbine blade

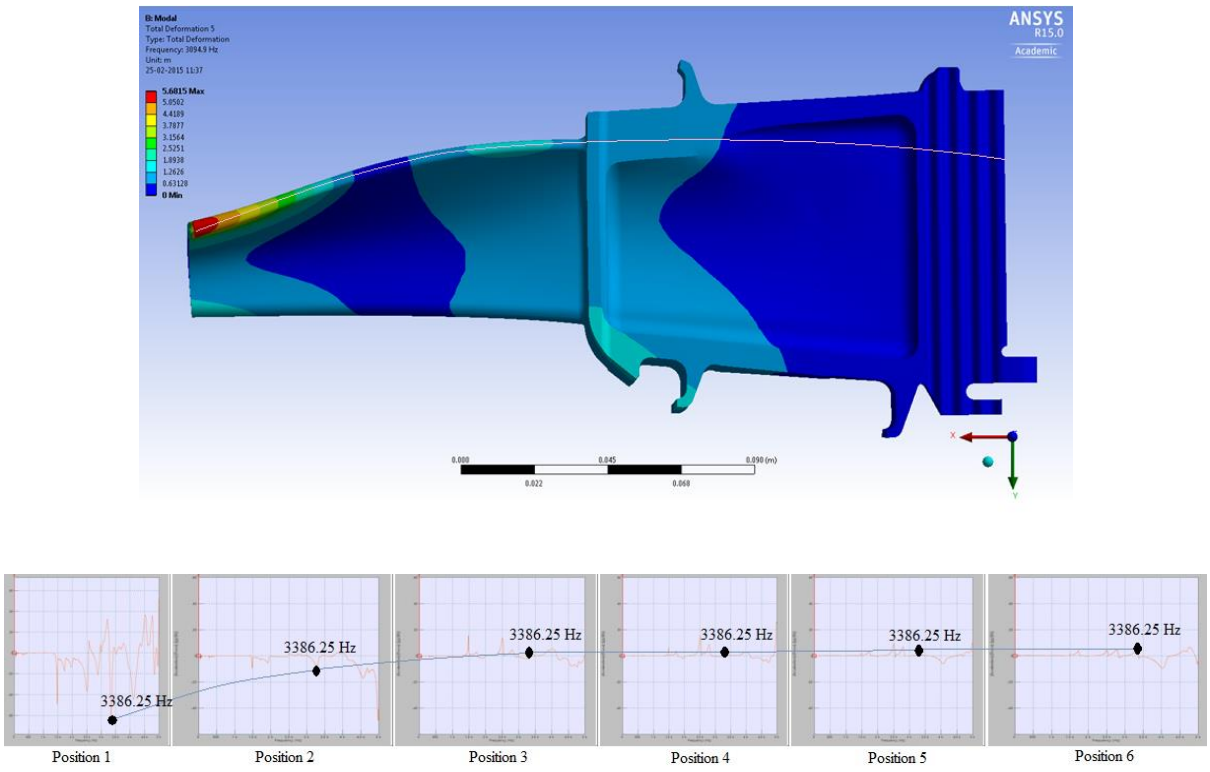

Fig.6.11. Resemblance of mode -5 of CMA with EMA of gas turbine blade

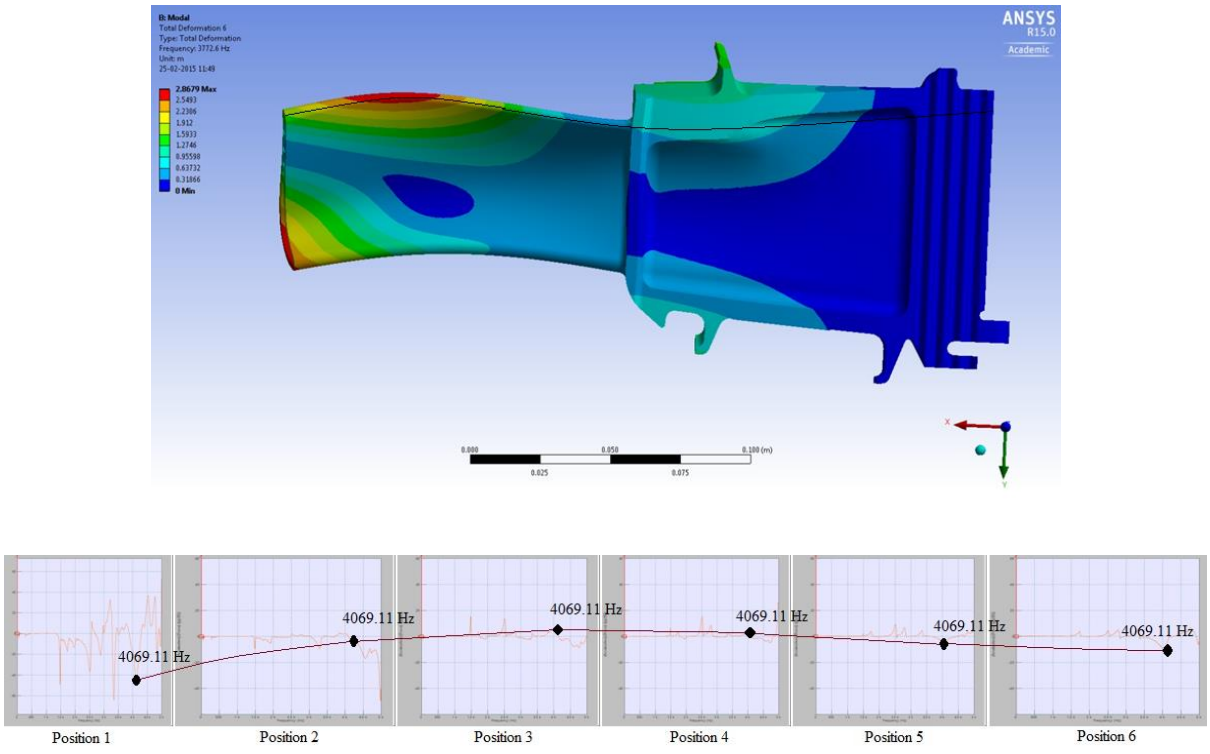

Fig.6.12. Resemblance of mode -6 of CMA with EMA of gas turbine blade

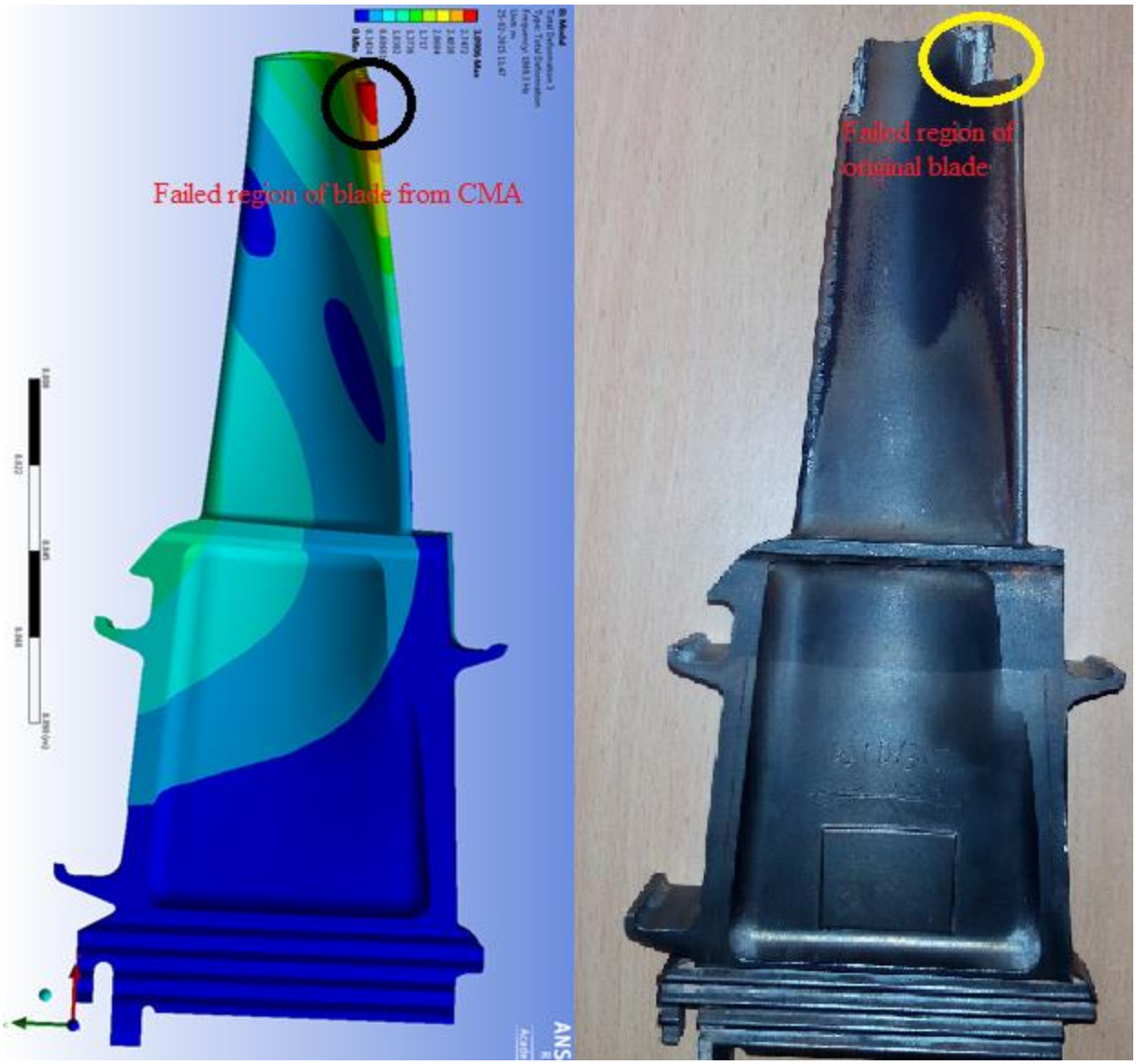

Fig.6.13. Correct prediction of CMA for blade failure.

Hence from the overall analysis and simulation it is clear that cantilever beam analysis was introduced just only to validate the experimental, computational and analytical results, and all three are validated successfully with less variation. Because the results obtained from these analysis for gas turbine blade supposed to be correct on behalf of the validated results for cantilever beam. Finally we obtained the natural frequencies of failure for gas turbine blade by EMA and CMA and these results correlates with each other with small variation, also damping factor for blade is computed and it is proved that failure results predict the correct failure location and failure frequencies.

REFERENCES

[1]. Hassan FARHANGI and Ali Asghar FOULADI MOGHADAM "*Fractographic investigation of the failure of second stage gas turbine blades*". Prooceedings of 8th International Fracture Conference 7 – 9 November 2007 Istanbul/TURKEY.

[2]. Loveleen Kumar Bhagi, Pardeep Gupta, Vikas Rastogi "*Fractographic investigations of the failure of L-1 low pressure steam turbine blade*". Case Studies in Engineering Failure Analysis, 2013.

[3]. M. Attarian, R. Khoshmanesh, S. Nategh, P. Davami "*Microstructural evaluation and fracture mechanisms of failed IN-738LC gas turbine blades*". Case Studies in Engineering Failure Analysis 1 (2013) 85–94.

[4]. J. R. Nicholls, N. J. Simms, W. Y. Chan and H. E. Evans "*Smart Overlay Coatings – Concept and Practice*". Surface and Coatings Technology, Vol. 149, Issues 2-3, 15 January 2002, Pages 236-244.

[5]. Bruce M. Warnes and David C. Punola "*Clean diffusion coatings by chemical vapor deposition*". Surface and Coating Technology 94-95 (1997) I-6.

[6]. N. S. Vyas & J. S. Rao "*Fatigue Life Estimation Procedure for a turbine blade under transient loads*". Transactions of the ASME Vol. 116, JANUARY 1994.

[7]. J.A. Loyaa, L. Rubiob, J. Fernandez-Saez "*Natural frequencies for bending vibrations of Timoshenko cracked beams*". Journal of Sound and Vibration 290 (2006) 640–653.

[8]. Craig P. Lawson and Paul C. Ivey "*Turbomachinery blade vibration amplitude measurement through tip timing with capacitance tip clearance probes*". Sensors and Actuators A 118 (2005) 14–24.

[9]. S. Zucca, D. Di-Maio, D.J. Ewins "*Measuring the performance of under platform dampers for turbine blades by rotating laser Doppler Vibrometer".* Mechanical Systems and Signal Processing 32 (2012) 269–281.

[10]. S. Narasimha, G. Venkata Rao and S. Ramakrishna "*Stress and vibration analysis of a gas turbine blade with a cottage-roof friction damper using finite element method*". 14th National Conference on Machines and Mechanisms (NaCoMM-09).

[11]. Cyrus B. Meher-Homji and George Gabriles "G*as turbine blade failures-causes, avoidance, and troubleshooting".* Proceedings of the 27th Turbomachinery symposium.

[12]. Dundas, R. E., June 1 3 - 1 6, 1 994, "*A Statistical Study of Gas Turbine Losses and Analysis of Causes and Optimum Methods of Prevention*". ASME International Gas Turbine and Aero engine Congress, The Hague, Netherlands, ASME Paper Number: 94-GT-279.

[13]. Rao, J. S . , 1 992, "*Turbomachinery Blade Vibration*". New York, New York: John Wiley and Sons.

[14]. Zaba, T. 1980, "*Losses in Gas Turbines Due to Deposits on the Blading".* Brown Boveri Review, 1 2-80, pp. 7 1 5-722.

[15]. Trumpler, W. E. and Owens, H. M., 1953, "*Turbine Blade Vibration and Strength*". American Society of Mechanical Engineers, ASME Paper 53A-98.

[16]. Sohre, J. S . , 1975, "*Steam Turbine Blade Failures, Causes and Corrections*", Proceedings of the Fourth Turbomachinery Symposium, Turbomachinery Laboratory, Texas A&M University, College Station, Texas, pp. 9-30.

[17]. S. Narasimha , G. Venkata rao and S. Ramakrishna, "*Dynamic analysis of a turbine blade without and with damping plate using finite element method*", proceedings of the National Conference on Emerging Trends in Mechanical Engineering, July 1-2, 2009, SNIST, PP.99-102.

[18]. P.V. Ramaiah and Dr. G. Krishnaiah , "*Modelling and Analysis of contact region of the friction damper used for gas turbine blade vibration control-A microslip approach*", IE (I) Journal-MC.

[19]. Csaba G., "*Friction Damping of Turbine Blade Vibrations Using a Microslip Model*", Journal of Machine Vibration, 1995, Vol. 4, pp. 2-7and LiU-Tek-Lic-1995:09, ISBN 91-7871-507-5.

[20]. Vyas, N. S., 1986, "*Vibratory Stress Analysis Stress and Fatigue Life Estimation of Turbine Blade*". Ph.D. Thesis, I.I.T., New Delhi, India.

[21]. Rao, J. S., and Vyas, N. S., 1990, "*Transient Stress Response of a Turbine Blade under Non Linear Damping Effects*". ASME Paper No. 90-GT-269.

[22]. M. Shen, C. Pierre, "*Natural modes of Bernoulli–Euler beams with symmetric cracks*". Journal of Sound and Vibration 138 (1990) 115–134.

[23]. H.P. Lee, T.Y. Ng, "*Natural frequencies and modes for the flexural vibration of a cracked beam*". Applied Acoustics 42 (1994) 151–163.